DISSERTATION

submitted to the
Combined Faculties for the Natural Sciences and for Mathematics
of the Ruperto - Carola University of Heidelberg, Germany
for the degree of
Doctor of Natural Sciences

presented by
Diplom - Biologist Andrea Giordano
born in L'Aquila, Italy

Oral examination:

Title:

Cell-Permeant Fluorescently-labelled Peptides

Referees: Dr. Lars Steinmetz (EMBL, Heidelberg)

Prof. Andres Jäschke (University of Heidelberg)

“Let’s go fishing for a dream,
let’s find some place new
somewhere we can be ourselves...”
Turin Brakes (english acoustic duo)

A Roberto e Katia,
Tommaso, Ida, Laura, Marisa e Settimio

Table of contents

Abstract

Peptide-based fluorescent reporters of enzyme activity in living cells have been proposed to complement, or provide alternatives to, genetically-encoded probes, such as those based on the Green Fluorescent Protein and its colourful variants. The use of well-established chemical methodologies – especially solid phase synthesis – and the vast array of fluorescent dyes available allow the preparation and the evaluation of compounds with different specificities, making a wide range of investigations possible. However, cell uptake of these compounds is generally poor, and normally requires invasive methods such as microinjection or electroporation. In these conditions, the usefulness of these probes can be severely limited.

The discovery of the so-called cell-penetrating peptides (CPPs), more than ten years ago, has actually revealed that some of these compounds can cross efficiently the cell membranes and are able to deliver hydrophilic cargoes, such as DNA, proteins or even nanoparticles inside the cell. Unfortunately, much of the initial enthusiasm dissipated when it was found that endocytosis plays a major role in the uptake process. The entrapment in endosomal vesicles may in fact impose strict limits in terms of modification and degradation of the cargo of interest.

This thesis describes the synthesis of fluorescent peptides and focuses on the problem of their delivery into the cytoplasm of living cells. A negatively charged peptide corresponding to one of the autophosphorylation sequences of the epithelial grow factor receptor (EGFR), namely DADEY^{992}L, was taken as an example to investigate the possibility of creating a cell-permeable fluorescent sensor for the EGFR kinase activity in living cells. The use of a conjugate of the cell-penetrating peptide Penetratin and the probe revealed an endosomal localization in one cell type, and surprisingly no uptake in a second cell line tested. Different fluorescent derivatives of Penetratin demonstrated variations in cell uptake under different experimental conditions. During this study, red fluorescent derivatives of the cell-penetrating TAT peptide were also assessed. Although they also showed predominantly accumulation in membrane-bound compartments, these appeared to be different from the endosomal vesicles. One TAT variant in particular, namely TAT(K-LRh), may be potentially exploited as a novel vector, provided that further studies will clarify unambiguously the compartment of its accumulation.

To overcome the limits inherent in the use of Penetratin conjugates, a different strategy was implemented, which relied on the chemical modification of the probe with bioactivatable protecting groups. The rationale behind these modifications was to increase the hydrophobic character of the peptide and allow its diffusion into the cells. In particular, acetoxymethyl (AM) esters were used to temporarily mask the negative charges of the aspartate and glutamate residues present in the peptide sequence. These biodegradable esters are promptly removed by ubiquitous non-specific esterases present in cells. The modified fluorescent peptide was able to penetrate easily and distribute homogeneously into the cytoplasm and the nucleus of several cell lines, with a mechanism resembling passive diffusion. Unfortunately, FRET-based assays did not measure any interaction with the EGFR. *In vitro* analyses showed unmasking of the carboxylate groups, albeit with modifications to the peptide backbone, which may have resulted from intramolecular condensations and formation of aspartimide residues. In particular, mass spectrometry data support this model. A loss of substrate specificity may be expected to result from such modifications, which may explain why the fluorescent peptide did not appear to interact with its enzyme target despite intracellular delivery having been achieved.

This work highlights the feasibility of a tailored modification of peptides, either by masking negatively charged groups as, for example, AM esters, or by conjugating to variant of the TAT peptide, for the intracellular delivery of peptidic cargoes. Further refinements may solve the problems of poor endosomal escape or backbone modifications, and may yet offer small-molecule alternatives to genetically encoded probes.

Zusammenfassung

Fluoreszente Reporterkonstrukte zum Nachweis von Enzymaktivität in lebenden Zellen, die auf Peptiden basieren sind eine ideale Ergänzung und Alternative zu genetisch kodierten Konstrukten auf der Grundlage von fluoreszierenden Proteinen, wie das Grün-Fluoreszierende-Protein oder eine der vielen anderen Farbvarianten. Die etablierten chemischen Verfahren, wie vor allem die Festphasensynthese und eine große Außwahl fluoreszenter Farbstoffe, erlauben die Herstellung von Verbindungen mit den unterschiedlichsten Eigenschaften. Dies macht sie für den Einsatz in einer Vielzahl von Untersuchungen interessant. Das Einbringen dieser Verbindungen in lebende Zellen ist sehr schwierig und nur mit langandauernden und invasiven Methoden wie der Mikroinjektion möglich, was bisher die Anwendbarkeit stark eingeschränkt hat.

Die Entdeckung von sogenannten zell-penetrierenden Peptiden (CCPs, ***c****ell-****p****enetrating* ***p****eptide****s***) vor mehr als zehn Jahren, hat gezeigt, dass einige dieser Verbindungen die Zellmembran effizient durchdringen können. Zusätzlich konnten diese, auch angehängte hydrophile Moleküle wie DNA, Proteine oder sogar Nanopartikel mitnehmen. Von dem anfänglichen Enthusiasmus blieb wenig übrig, als man feststellte, dass Endozytose einen Grossteil dieses Effekts ausmachte. Der Einschluss in endosomale Vesikel stellt eine starke Einschränkung, vor allem in Bezug auf Modifikation und Zersetzung der einzubringenden Verbindung, dar.

Die Synthese fluoreszenter Peptide und vor allem das Problem deren Einbringung in das Zytosol lebender Zellen, stehen im Mittelpunkt dieser Arbeit. An dem Beispiel des der Autophosphorylierungssequenz des Rezeptors für den epithelialen Wachstumsfaktor (EGFR, ***e****pithelial* ***g****rowth* ***f****actor* ***r****eceptor*) entsprechenden, negativ geladenen Peptids, DADEY^{299}L, sollte die Möglichkeit, eine membrangängigen fluoreszenten Sensor für die Aktivität der EGFR-Kinase in lebenden Zellen herzustellen, geprüft werden. Die Verwendung eines Konjungats aus dem zell-penetrierenden Peptid Penetratin und der Sonde, führte zur Aufnahme in Endosomen in einem Zelltyp, während in einem weiteren getesteten Zelltyp überhaupt keine Aufnahme nachzuweisen war. Auch konnte mit verschiedenen fluoreszenten Penetratinderivaten gezeigt werden, wie die Aufnahme in Zellen unter verschiedenen experimentellen Bedingungen variierte. Während dieser Untersuchung, wurden auch rot-fluoreszierende Derivate des zell-penetrierenden

TAT-Peptids analysiert. Obwohl diese auch eine Akkumulation in vorwiegend membrangebundenen Kompartimenten aufwiesen, erschienen diese jedoch anders als endosomale Vesikel. Speziell die TAT-Variante TAT(K-LRh) könnte sich als neuer Vektor erweisen, wenn aufgeklärt werden kann in welchen Zellkompartimenten dieses Peptid akkumuliert.

Um die, bei der Verwendung von Penetratin, auftretenden Einschränkungen zu überwinden, wurde eine Strategie verfolgt, die auf einer chemischen Modifikation der Sonde mit bioaktivierbaren Schutzgruppen basiert. Das Grundprinzip war, den hydrophoben Charakter des Peptids zu verstärken, um so die Diffusion durch die Zellmembran zu ermöglichen. Insbesondere wurden Azetoxymethylester (AM) verwendet um die negativen Ladungen der in dem Peptid vorkommenden Aspartat- und Glutamatreste zu maskieren. Diese bioaktivierbaren Ester werden sofort durch unspezifische Esterasen, die in allen Zellen vorkommen, abgespaltet. Die fluoreszent markierten Peptide durchdrangen leicht die Plasmamembran, vergleichbar mit passiver Diffusion, und verteilten sich homogen im Zytosol und Nukleus in verschiedenen getesteten Zelllinien. Leider konnte durch FRET keine Interaktion der Peptide mit dem EGFR nachgewiesen werden. *In vitro* Analysen ergaben, dass die Karbonatgruppen entschützt werden konnten, wenngleich dieses zu Modifikationen des Peptidrückgrats durch intramolekulare Kondensation und die Bildung von Aspartimidresten geführt haben könnte. Durch diese Modifikationen ließe sich der Verlust der Substratspzifität und somit die fehlende Interaktion mit der Kinase erklären, obwohl das Peptid in die Zelle eingebracht werden konnte.

Diese Arbeit hebt die Machbarkeit der Einbringung Peptiden in lebende Zellen durch massgeschneiderte Modifikationen, entweder indem negativ geladenen Gruppen durch AM oder andere hydrolisierbare Ester maskiert werden, oder indem sie mit einem der TAT-Peptide konjugiert werden, hervor. Durch weitere Verfeinerung der Verfahren könnten die auftretenden Probleme, wie Einschluß in Vesikel oder das Auftreten von Modifikationen des Peptidrückgrats, gelöst werden und so eine Alternative zu den viel größeren genetisch Kodierten Sonden bieten.

Abbreviations

Chemicals:

5(6)-TAMRA SE		5(6)-carboxytetramethylrhodamine, succinimidyl ester
Ac_2O		acetic anhydride
ACN		acetonitrile
AcOH		acetic acid
ActPEN		activated Penetratin peptide
AEEAc		aminoethoxyethoxy acetic acid
Ahx		aminohexanoic acid
AM		acetoxymethyl
Boc		*tert*-butyloxycarbonyl
BSA		bovine serum albumine
Cl-Trt		2-chlorotrityl
DCI		4,5-dicyanoimidazole
DCM		dichloromethane
DIC		diisopropylcarbodiimide
DIPEA		diisopropylethylamine
DMF		N,N-dimethylformamide
DVB		divinylbenzene
EDTA		ethylenediaminetetraacetic acid
Fmoc		9-fluorenylmethoxycarbonyl
H_2CO		formaldehyde
HBTU		2-(1H-benzotriazol-1-yl)-1,1,3,3-tetramethyluronium hexafluorophosphate
HEPES		4-(2-hydroxyethyl)-1-piperazineethanesulfonic acid
HOBt		1-hydroxybenzotriazole
iPrOH		isopropanol
LRh		Lissamine™-rhodamine B
LRh-SO_2Cl		Lissamine™-rhodamine B sulfonylchloride
LTG		LysoTracker™ Green
LTR		LysoTracker™ Red
Mtt		4-methyltrityl
NMP		1-methyl-2-pyrrolidinone
Pbf		2,2,4,6,7-pentamethyldihydrobenzofuran-5-sulfonyl
PEG		polyethylene glycol
PFA		paraformaldehyde
PI		propidium iodide
PLE		porcine liver esterase
PP		polypropylene
PS		polystyrene
*t*Bu		*tert*-butyl
tBuOMe		*tert*-butyl-O-methyl ether
tBuOOH		*tert*-butyl hydroperoxide

TCEP		tris(2-carboxyethyl)phosphine
TEA		triethylamine
TFA		trifluoroacetic acid
TIS		trisopropylsilane
TNBS		2,4,6-trinitrobenzenesulfonic acid
Trt		trityl

Other abbreviations:

(E)GFP		(enhanced) Green Fluorescent Protein
(E)YFP		(enhanced) Yellow Fluorescent Protein
a.a.		amino acid(s)
a.m.u.		atomic mass unit(s)
DMEM		Dulbecco's modified Eagle medium
EGFR		epithelial grow factor receptor
eq		equivalent(s)
ER		endoplasmic reticulum
ESI-MS		Electrospray Ionization – Mass Spectrometry
FBS		fetal bovine serum
HPLC		High Performance Liquid Chromatography
m/z		mass to charge ratio
NA		numerical aperture
PMT		photo multiplier tube
PTP1B		Protein Tyrosine Phosphatase 1B
RP		reverse phase
SPE-RP		solid phase extraction-reverse phase
UV-VIS		ultraviolet-visible

1. Introduction

1.1 Peptides and other small molecule-based fluorescent reporters of enzymatic activity

Synthetic peptides that mimic natural substrates represent often a good starting point for the design of probes aimed at the study of enzyme activities, due to their natural high specificity. In particular, when equipped with fluorogenic or fluorescent molecules, they enable high-sensitive, fluorescence-based *in vitro* assays, to be conveniently performed on crude cell extracts *in vitro*, without the need for time-consuming purification procedures. Reporters of this kind have been developed, for instance, for the measurement of the *in vitro* activity of the apoptotic caspase-3 enzyme [1] or those of various protein tyrosine phosphatases (PTPs) [2] (Fig. 1.1.1). In depth studies, such as those aimed at understanding the complex phenomena of signalling networks, require reporting from inside living cells, where the contribution of the physiological components of the intact system can be assessed and possibly regulated, thus helping to provide a more comprehensive and accurate model than the "artificial" environment of a cuvette [3].

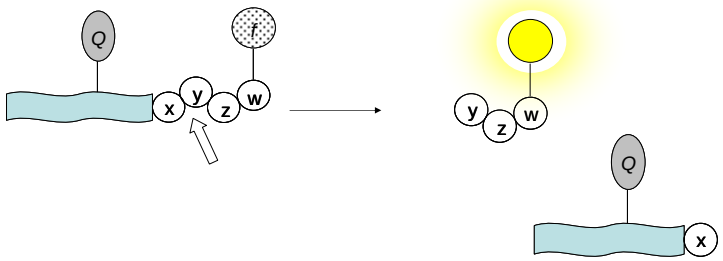

Fig. 1.1.1 A generic probe for proteases based on a fluorogenic peptide. The design of the substrate includes a quencher (Q) for the fluorochrome (*f*), separated by an hypothetical consensus sequence for the protease (xyzw). Upon cleavage, the fluorescent signal can be recorded. This kind of probes are often used in *in vitro* assays [1, 2] (adapted from [3]).

Nevertheless, the *in vivo* application of fluorescent peptides as *non*-genetically encoded probes for monitoring enzyme activity is usually a demanding task. In fact, the progress in this field has notably lagged behind the use of the Green Fluorescent Protein (GFP) and its genetically-encoded variants [4]. If extracellular activity can be investigated – as in the case of different matrix-degrading enzymes [5-7] – on the other hand one is faced immediately with the non trivial task of delivering the reporter molecules inside the cell, in suitable ways to preserve both integrity and viability of the system. Ideally, the reporter should freely permeate biological membranes, in order to reach the compartment(s) where the specific

activity needs to be monitored. Moreover, the fluorophore itself should have negligible influence on the localization of the probe. Due to the nature of polar and charged molecules, peptide-based reporters – except rare cases [8-10] – are notoriously reluctant to diffuse through a lipid bilayer. Indeed, several fluorescent probes for the detection of enzyme activity *in vivo* are not based on peptides, yet they demand a certain grade of chemical modification to meet all the requirements for cell permeability. Of this kind, for instance, is the reporter PENN/SATE for the detection of phospholipase A_2 (PLA_2) activity [11], a class of phospholipid hydrolases involved in intracellular signalling and inflammation as initiators of the arachidonic acid cascade [12, 13]. This probe is built upon a phosphatidylethanolamine molecule chemically modified to achieve the highest specificity toward PLA_2 enzymes (Fig. 1.1.2). The charges on the head group are masked by bioactivatable S-acetyl-2-thioethyl (SATE) moieties, which are promptly released in the cell upon action of non-specific esterases. The fluorescent part of the molecule is composed of two dyes, each sitting at the ends of the fatty acid chains and forming a Förster resonance energy transfer (FRET) pair [14]: the 7-nitrobenzo-2-oxa-1,3-diazole amine (NBD) and the 2-hydroxy derivative of 9-diethylamino-5H-benzo[a]phenoxazin-5-one (Nile red). Generally, two fluorophores form a FRET pair when the emission spectrum of one (termed *donor*) overlaps with the excitation spectrum of the second (termed *acceptor*). When certain criteria are met, such as the proximal position of the fluorophores (2 – 10 nm) and a favourable dipole-dipole orientation [15], a non-radiative transfer of energy occurs to the acceptor upon donor excitation. Under these circumstances, light emission from the acceptor is obtained with a concomitant decrease in the donor emission. Variations of FRET within a fluorescent reporter provide a direct readout of the enzymatic activity since the acceptor/donor intensity ratio can be monitored over time and quantified, both *in vitro* and *in vivo* [16, 17]. Direct excitation of NBD (435 – 485 nm) in the PENN/SATE probe leads to Nile red fluorescence (600 – 660 nm) as long as the molecule remains intact, but upon cleavage of the fatty acid chain by PLA_2, only emission from NBD is obtained (515 – 555 nm), because of the spatial separation of the fluorophores and disruption of the FRET pair (Fig. 1.1.2).

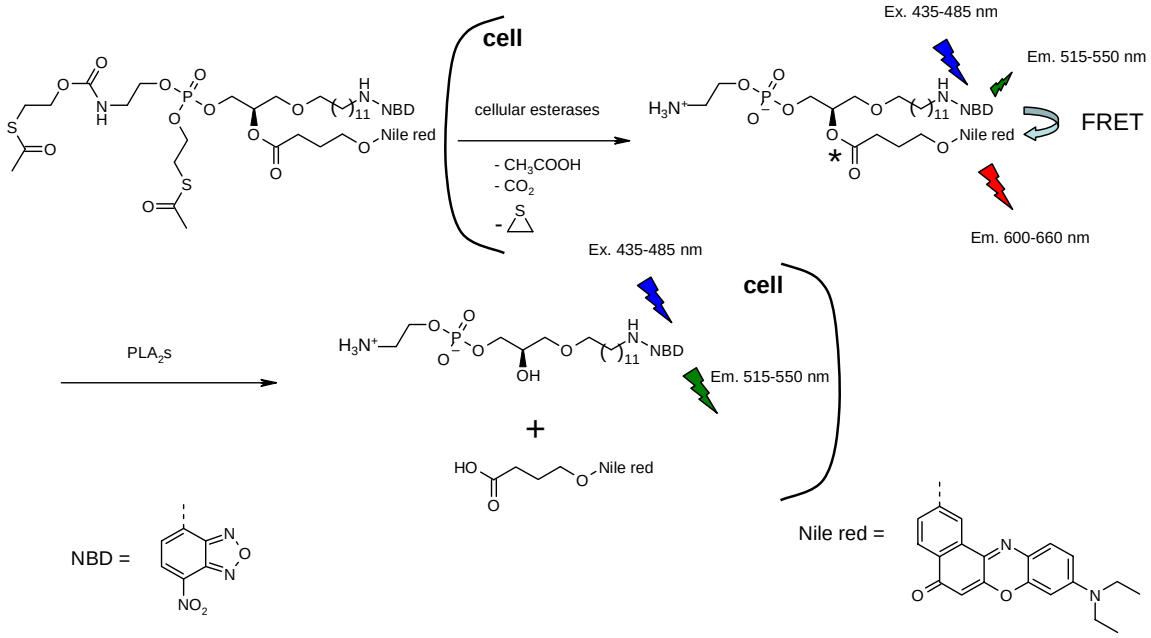

Fig. 1.1.2. The PENN/SATE FRET reporter for PLA_2 activity *in vivo*. The probe is built upon a modified phosphatidylethanolamine backbone featuring the FRET pair NBD/Nile red at the tip of the fatty acid chains. The asterisk illustrates the hydrolysable bond by PLA_2. To ensure cell permeability, the polar head of the lipid is equipped with bioactivatable S-acetyl-2-thioethyl (SATE) groups which are removed upon the action of intracellular non-specific esterases. Restoration of charges on the molecule entraps the probe inside the cell. Upon hydrolysis of the fatty acid chain, a 20 – 30 fold increase in the emission ratio NBD/Nile red was observed in living cells due to disruption of the FRET pair. The probe was able to monitor the onset of PLA_2 activity in the whole body of a developing *Medaka* fish embrio (adapted from [11]).

This behaviour was confirmed both *in vitro* and in various living cell lines, in which the probe could easily diffuse in and accumulate at the sites of PLA_2 action. Upon hydrolysis of the fatty acid chain, 20 – 30-fold changes in emission ratio were recorded. More remarkably, the probe could be administered to a developing *Medaka* fish embryo (age 3 h), where it reported the onset of PLA_2 activity (between 37 and 48 h of development). The probe remained visible until the fish hatched (eight days), indicating also the lack of induced toxicity.

A similar concept was applied in an earlier study for the design of the CCF2/AM reporter of gene expression, based on a fluorogenic substrate for the bacterial β-lactamase [18]. This enzyme catalyzes the hydrolysis of the β-lactam ring in cephalosporins. A FRET sensor was designed by incorporating a 6-chloro-7-hydroxycoumarin and a fluorescein dyes in the scaffold of a cephalosporin molecule. To ensure cell permeability the construct was equipped with bioactivatable acetyl (Ac), butyryl (Bt) and acetoxymethyl (AM) esters (Fig. 1.1.3). The construct, initially non-fluorescent due to the chemical modifications, penetrated into the cells and exhibited FRET (ex. 409 nm, em. 520 nm), indicating successful removal of

the masking groups by cellular esterases. The cells, additionally transfected with a β-lactamase plasmid, produced the enzyme. As a result of the hydrolysis of the β-lactam ring, the probe molecule underwent β-elimination to loose the fluorescein moiety. FRET was then impossible and the emission of the coumarin fluorophore became prominent. The authors could correlate the expression of the β-lactamase with the coumarine/fluorescein emission ratios, which were up to 70-fold the initial value. Due to the high sensitivity detection of the blue/green fluorescence pattern, the assay demonstrated its utility in the selection, by means of flow cytometry, of specific cellular clones co-expressing the β-lactamase enzyme along with a gene of interest.

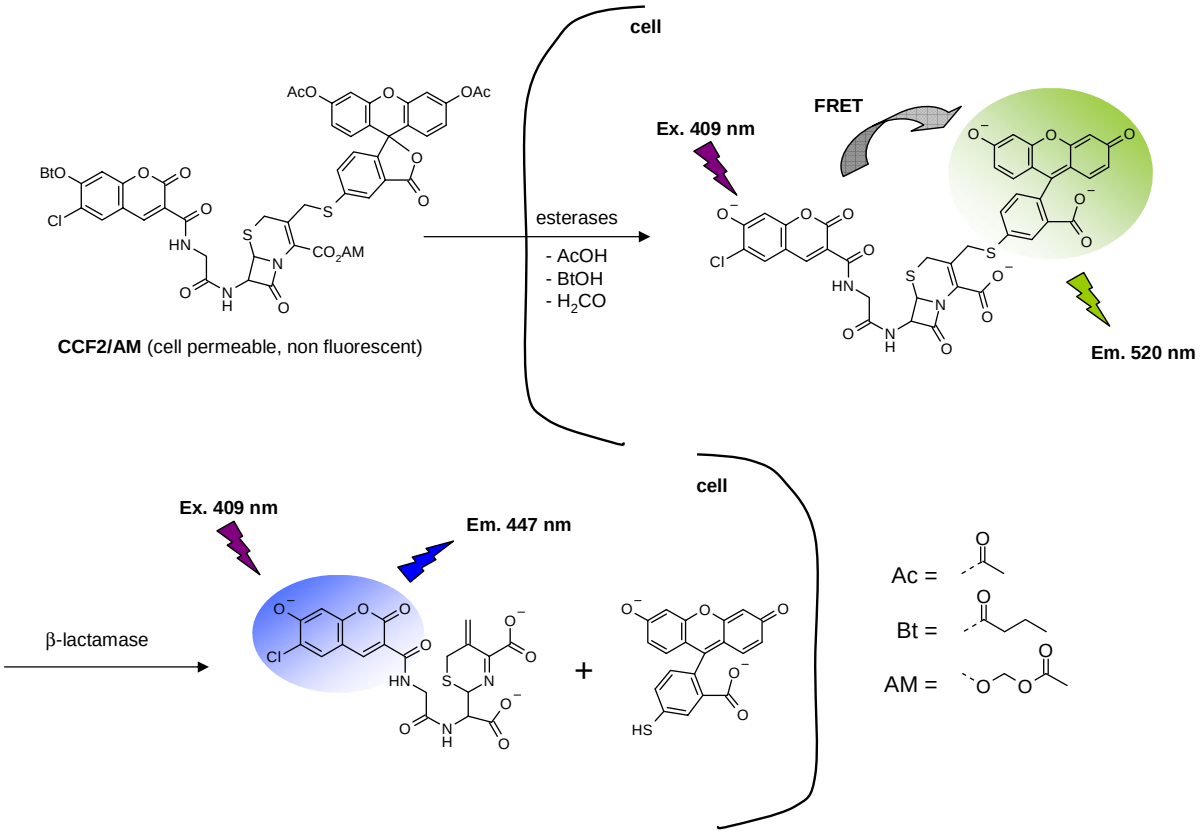

Fig. 1.1.3. The CCF/2AM probe for the β-lactamase assay of gene expression in living cells. The fluorogenic reporter, modified with acetyl, butyryl and acetoxymethyl esters, enters passively into cells and exhibits FRET after the removal of the masking groups by cellular esterases. Expression of a β-lactamase gene in transfected cells produces hydrolysis of the β-lactam ring, β-elimination of the fluorescein moiety and disruption of the FRET pair. As a consequence, only fluorescence from 6-chloro-7-hydroxycoumarine is detected under excitation at 409 nm. The assay reveals useful in the fluorescence automated cell sorting (FACS) of cellular clones co-expressing the β-lactamase gene in tandem with a protein of interest under the same transcriptional promoter (modified from [18]).

The chemical modification of charged functional groups by means of bioactivatable moieties, such as the acetoxymethyl esters, has been instrumental for the facile use of several

small molecule-based fluorescent sensors, which are nowadays commonly available to the cell biologist. The calcium indicators of the Fura or Indo family, or the so-called "viability dyes" of the Calcein family are just an example (Fig. 1.1.4). Such kind of modifications proved useful when applied also to different classes of molecules, e.g. phosphoinositols (IPs) or phosphatidylinositol phosphates (PIPs), enabling their use as permeable probes for cell signalling or cell physiology studies [19-21]. In drug design, moreover, they often form the basis for *prodrugs*, compounds in which an active molecule with little bioavailability is altered to enhance its pharmacokinetic properties, such as absorption and distribution [22, 23].

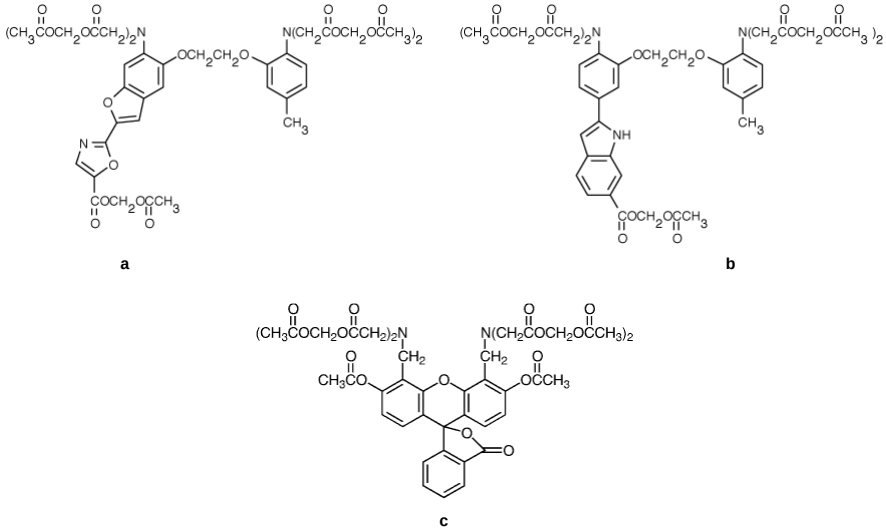

Fig. 1.1.4. Cell-permeable fluorescent indicators. The Ca^{++} indicators Fura-2 AM (**a**) and Indo-2 AM (**b**) are just two examples of the numerous cell-permeable ion indicators now commercially available (e.g. Invitrogen-Molecular Probes). (**c**) The Calcein AM fluorogenic molecule: upon hydrolysis of its protecting groups by cellular esterases, the molecule fluoresces (ex. 495 nm, em. 515 nm). The protection of the carboxylic groups in these molecules with acetyl or acetoxymethyl (AM) esters enables them to freely permeate cell membranes. On the contrary, the product of their hydrolysis is retained within the cell.

Although studies on peptide prodrugs constituting a significant chapter in the drug design literature [24-27], reports on the chemical modification of peptide-based fluorescent probes to permit cell entry are hard to find. To achieve cytoplasmic delivery of membrane-impermeant compounds, microinjection has been routinely used. This technique is normally invasive, time consuming, requires good skills and, more importantly, permits to investigate only a limited number of cells at a time. Despite these disadvantages, this methodology has allowed, for instance, the dynamic study of several kinases, such as protein kinase A (PKA), protein kinase C (PKC), cyclin-dependent kinase 2 (CDK2) in *Xenopus laevis* oocytes [28]. Alternative methods which would make the study of a large specimen feasible are actively pursued, especially in the view of Systems Biology approaches. A class of molecules named

cell-penetrating peptides or *protein transduction domains*, discovered about fifteen years ago, appears to have potential to overcome the limitations inherent in the delivery of hydrophilic compounds into cells. An overview of these peptides is given in the next paragraph.

1.2 Breaking barriers: the Cell-Penetrating Peptides

In 1988, the investigators Frankel and Pabo, while developing an assay to measure the activity of the trans activator protein TAT from the human immunodeficiency virus 1 (HIV-1), an essential component for the transcription and replication of the viral genome, reported "[...] the surprising observation that purified Tat protein can be taken up by cells and transactivate [*a chloramphenicol acetyltransferase reporter gene under*] the HIV-1 promoter" [29]. A similar observation was made independently by Green and Loewenstein [30]. Three years later Joliot and Prochiantz reported how the Antennapedia homeodomain protein from *D. Melanogaster*, exogenously added to cultured neurons, penetrated diffusely into the cells in a receptor-independent manner and increased their morphological differentiation [31]. The two discoveries fuelled deeper investigations aimed at finding the determinants of such surprising behaviour. In the studies that followed, the TAT arginine-rich domain (TAT_{49-57}, [32, 33]) and a 16-residues long peptide from the third helix of the Antennapedia homeodomain ($Antp_{43-58}$, [34]), also characterized by the presence of a short polycationic cluster, were found to mimic the features of their parental proteins. TAT_{49-57} and $Antp_{43-58}$ (the latter commonly known nowadays as Penetratin) were hence the lead sequences in the new research field of cell-penetrating peptides (CPPs, [35]).[1] Also referred to as protein transduction domains (PTDs), one can count nowadays not less than thirty different peptides, natural or artificial, with sequences ranging from 9 to more than 30 amino acids, which share the ability to access the interior of a cell (Tab. 1.2 *a*. For a review, see [36, 37]). The striking feature of these peptides is their capacity to transport across the cell membrane a multitude of different cargoes, regardless of their molecular composition or weight. Intracellular delivery of peptides [33, 38-46], oligonucleotides including peptide-nucleic acids (PNAs) and short-interfering RNAs (siRNAs) [47-55], DNA [56-58], antibody fragments or full-length proteins

[1] It is worth to mention the observation, made already in 1965, that homopolymers of cationic amino acids were able to enhance the internalization of radiolabelled albumin into cells [36], while in 1978 it was shown that the covalent conjugation of poly-L-lysine to proteins and small molecules increased their cellular uptake and, in the case of methotrexate, the biological activity of the drug [37,38].

[59-69], liposomes, phages and nanoparticles [70-73] have been documented.[2] Internalization of CPPs occurs in a large number of different cultured cell types [37], while injection of various CPP-cargo conjugates in whole animals enables access also to tissues notoriously resistant to conventional drug targeting, such as the central nervous system (Fig. 1.2.1) [47, 57, 63, 74].

name	sequence (one-letter code)	comments
TAT_{49-57}	RKKRRQRRR	from HIV-1 TAT protein
penetratin	RQIKIWFQNRRMKWKK	from Antennapedia homeodomain
pVEC	IAARIKLRSRQHIKLRH	from the murine vascular endothelial cadherin
Vpr	DTWPGVEALIRILQQLLFIHFRIGCQH	from the HIV-1 VPR protein
CPP from prion protein	MANLGYWLLALFVTMWTDVGLCKKRPKP	
buforin	TRSSRAGLQWPVGRVHRLLRK	antimicrobial peptide
magainin	GIGKFLHSAKKWGKAFVGQIMNS	antimicrobial peptide
LL-37	LLGDFFRKSKEKIGKEFKRIVQRIKDFLRNLVPRTES	antimicrobial peptide
transportan	GWTLNSAGYLLGKINLKALAALAKKIL	designed (chimeric)
MAP	KLALKLALKALKAALKLA	designed (model amphipathic peptide)
MPG	GALFLGFLGAAGSTMGAWSQPKSKRKVC	designed
Pep-1	KETWWETWWTEWSQPKKKRKV	designed

Tab 1.2 a. A partial list of natural and synthetic CPPs (adapted from [36]).

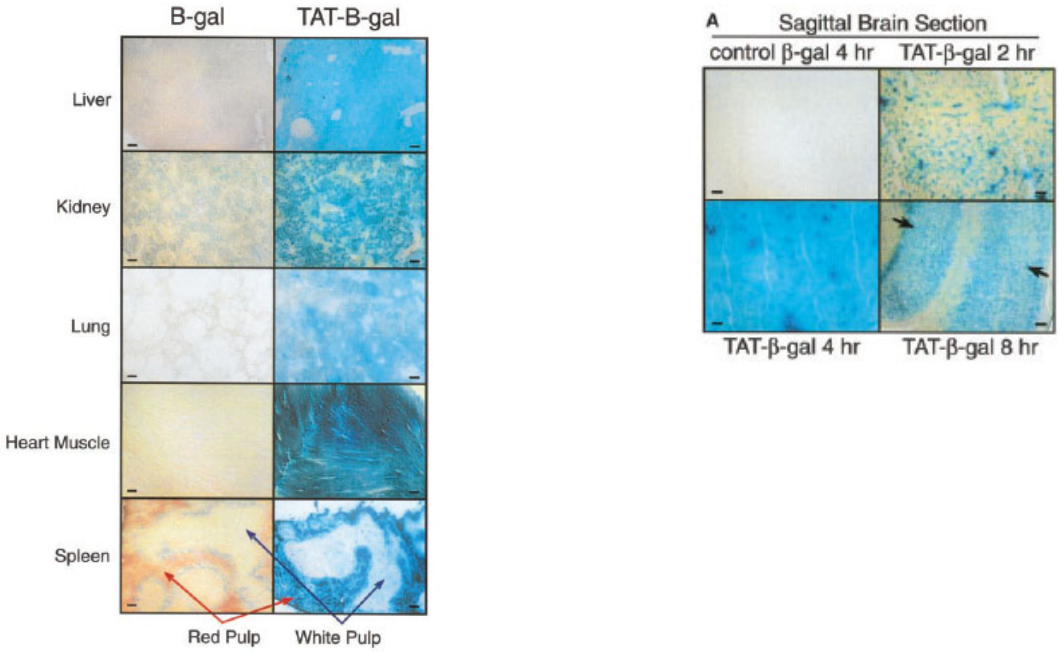

Fig. 1.2.1 TAT-mediated *in vivo* delivery of β-galactosidase (120 kD) in several mouse tissues. The presence in the brain indicated the successful crossing of the blood-brain barrier (From [63]. Reprinted with permission from AAAS).

[2] A more comprehensive list of scientific papers reporting the vectorization properties of TAT, Penetratin and other CPPs can be found in [35].

Such impressive vectorization properties soon raised interest on the mechanism of entry: one or many? Cell specific or non-specific? Energy-dependent or not? Influenced by the cargo? Each reply to any of the questions above would have a high probability to be correct: in fact, few topics in cell biology have been so debated in the last ten years as the so-called *transduction* mechanism of the CPPs. The large number of experiments, conditions and models used surprisingly did not depict a unified view, but a highly diversified scenario, with findings often contrasting one to each other. Much of what is currently known has been gathered (mainly via fluorescence microscopy and, more recently, flow cytometry) from observations using TAT, Penetratin or poly-arginine analogues, which have been – and remain – the most studied peptides of the entire family [75-77].

The first observations performed on cultured cells pointed toward an energy-independent mechanism, since cellular accumulation was not impaired when incubations were made at low temperature (+4°C) [32, 34] or, for poly-arginine analogues, in the presence of sodium azide (an inhibitor of ATP-H^+ synthase) [78]. Mutant analyses revealed the importance of the overall positive charge for TAT [33] and for Penetratin, along with the role, in the latter, of the tryptophan residues [79]. Moreover, no receptor protein appeared involved, because *retro*- (reversed amino acid sequence) or *inverso*- (all *D*-amino acids) peptides were internalized with the same efficiency [80, 81]. The use of biotinylated versions of the peptides probed intracellular localization by means of fluorescently labelled streptavidin after cell fixation. The strong nuclear accumulation, with nucleolar staining, appeared justified by the presence of a putative nuclear localization sequence (NLS) [32, 82].

Many of these early observations were recently disputed because of improper experimental protocols. For instance, the high overall positive charge of the polycationic CPPs promotes a strong adhesion to the negatively charged plasma membrane, which cannot be reversed simply by a washing step after incubation. As a result, the quantification of cellular fluorescence by flow cytometry is inherently overestimated, as this technique cannot discriminate between truly internalized or surface-adherent fluorescent molecules. Indeed, it has been shown that more reliable results could be obtained when a trypsinization step or chemical quenching of the outer-bound molecules were performed prior to cell counting. Notably, it was also demonstrated that intracellular distribution of fluorescent CPPs was a

direct artifact of cell fixation procedures [83].[3] The abandonment of cell fixation, highly encouraged by some investigators [84], in favour of a more rational observation of live specimens clearly demonstrated vesicular accumulation of fluorescently labelled CPPs under a variety of experimental conditions [83, 85-87]. It is now accepted that endocytosis takes part in the uptake of these peptides [36, 83, 88-90]. The term "endocytosis" nevertheless denotes a collection of distinctive processes through which exogenous or membrane-bound macromolecules can be internalized in the cell and redirected to specific locations [91-95]. In accordance with this definition, the examination of endocytic routes conveying CPPs in the intracellular environment revealed a multi-faceted scenario. A lipid raft-dependent macropinocytosis has been described for the internalization of a TAT_{49-57}-Cre recombinase fusion protein in live mouse cells. The rapid uptake, already detectable after 5 min, was strongly impaired by the use of the macropinocytosis inhibitors nystatin and β-cyclodextrin [96]. A similar observation was made in HeLa cells using an octa-arginine peptide (Arg_8) and Penetratin, but in the reported study the use of the macropinocytosis inhibitor ethylisopropylamiloride (EIPA) and the F-actin polymerization inhibitor cytochalasin D particularly suppressed Arg_8 entry with little effect on Penetratin, suggesting two distinct paths to ingression and the general role of actin filaments in the process [88]. Involvement of endocytosis has been shown in several other studies with Penetratin peptides, reporting sometimes contrasting conclusions [85, 87, 97]. The uptake of fluorescently-labelled TAT peptides has been reported to occur via macropinocytosis [90], while appeared to follow mainly a clathrin-dependent pathway in human umbilical vein endothelial cells (HUVEC) [98]. On the contrary, the caveolae-dependent endocytosis was shown to be responsible for the internalization of TAT-EGFP fusions in several cell lines [65]. Clearly, the panorama of the endocytosis-mediated uptake of polycationic CPPs appeares variant, with convincing evidences for several types of intervening mechanisms. An apparent free diffusion has been detected in some cases also in living cells, under particular conditions [99-102]. There is a general agreement now on the fact that a multitude of parameters play their role in the internalization process, such as the nature and size of the cargo, the concentration, the cell type, its density at the time of the experiment and even the cell cycle stage [36]. It is also recognized that CPPs of other classes may have other mechanisms of ingression [35].

[3] Artifactual redistribution of positively charged proteins, like histone H1 or VP22, as a consequence of cell fixation had already been described earlier [87].

Other experimental data have suggested the role of membrane-surface, negatively-charged glucosaminoglycans (GAGs), such as heparan sulfate, as putative "receptors" for the polycationic CPPs through the strong affinity to the arginine residues [103, 104]. The TAT transduction domain showed binding to heparin with high affinity (an analog of heparan sulfate) *in vitro* [105, 106], while heparin itself modulated the angiogenic and transcriptional activity of extracellular TAT [107, 108]. Consisting with these reports, the role of heparan sulfate has been demonstrated in living cells. Uptake of a TAT-GFP fusion protein was impaired in cells genetically defective in heparan sulfate biosynthesis, or it was competitively inhibited by soluble heparin and by treatment with glycosaminoglycan lyases [109]. Similar findings were reported for Penetratin conjugates and Penetratin-derivatized liposomes [110], and polyarginine peptides [111]. The interaction with heparan sulfate or related GAGs would trigger actin organization under the activation of the GTP-binding protein Rac-1 prior to the internalization event [111, 112].

If polycationic CPPs enter mainly via an endocytic process, then one must assume the existence of an endosomal escape mechanism in support of the wealth of published data concerning the biological activity of various and diverse CPPs conjugates [54, 113-119]. Endosomal escape of HIV-1 TAT alone was indeed demonstrated [120], while the nuclear delivery of a functional Tat-Cre recombinase fusion protein required the use of lysosomotropic agents [121]. More elegantly, endosomal escape has been artificially induced by incorporation of a fusogenic peptide from the agglutinin protein of influenza virus to a CPP-protein conjugate [96, 122], demonstrating that the approach could be eventually extended to other kind of constructs.

Despite the persistence of several "dark sides", the research on CPPs is actively pursued world-wide, since many are eager to put into practice the huge pharmacological potential inherent in the targeted delivery into cells and tissues of "information-rich" molecules (proteins and nucleic acids) for the treatment of human diseases [123-126]. As an example, one may cite the numerous applications involving CPPs in disease models such as cancer, ischemic stroke or Parkinsonism [127-135], or the advancement offered in diagnosis and imaging technology [136]. A much awaited step will be the reliable delivery of siRNAs, which is foreseen by many as the "holy grail" of the macromolecular therapeutics of the new millennium [137, 138].

2. Scope of the thesis

This thesis describes in detail the synthesis and the evaluation of fluorescent peptides designed with the aim of creating cell-permeant sensors for enzyme activity in living cells. In particular, our goal was to find the best methodology that could allow the delivery of such peptides directly into the cytoplasm of cells and without the aid of invasive techniques, such as microinjection or electroporation. Moreover, the methodology had to be of general applicability, compatible with a broad range of peptidic substrates, especially those featuring a significant number of charged residues. Finally, the delivery had to be effective in different cell types.

We focused our attention on a short sequence reproducing residues 988-993 of one of the six autophosphorylation domain of the epithelial grow factor receptor (EGFR), namely DADEY^{992}L, and explored the possibility of creating a fluorescent probe for the tyrosine kinase activity of the receptor. This peptide contains two aspartate and one glutamate residue in its sequence, thus presents a net negative charge at physiological pH. Synthetic peptides comprising this and other motifs of the EGFR have already shown to undergo phosphorylation at the tyrosine residue *in vitro* [139, 140]. The EGFR [141] and its role in cancer biology [142-147] has been the object of intensive studies, including several based on fluorescence microscopy [148-152]. In these, nevertheless, the use of fluorescent, cell-permeable peptidic probes has hardly been reported.

To address the problem of cell-permeability of this probe, two strategies were tested: a) the conjugation with a vector belonging to the CPPs family (sect. 1.2); b) the chemical modification of the negatively charged aspartate and glutamate residues with bioactivatable acetoxymethyl (AM) esters to enhance hydrophobicity, thus allowing free diffusion into cells.

The assay we envisioned is based on FRET occurring within the enzyme-substrate complex, between our probe and a genetically-encoded Green Fluorescent Protein-labelled EGFR (GFP-EGFR) or Yellow Fluorescent Protein-labelled EGFR (YFP-EGFR), stably or transiently expressed in cells. The concept of this assay is depicted in Fig. 2.1. This approach has already been validated for the study of phosphatase activity [153].

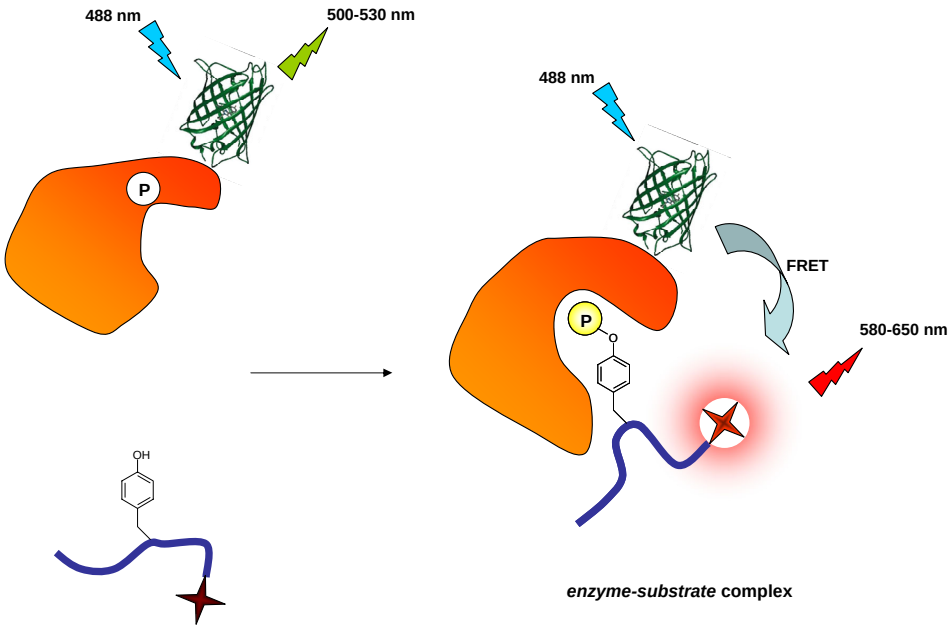

Fig. 2.1. Formation of the enzyme-substrate complex between a generic tyrosine kinase and its substrate can be monitored by FRET. The kinase is expressed as a chimera with GFP or YFP, while the peptide probe is equipped with a red-emitting fluorophore (rhodamine).

To enable the formation of a FRET pair between GFP-EGFR (or YFP-EGFR) and the peptide, we equipped the latter with a red-emitting rhodamine dye, since the emission spectra of either GFP or YFP favourably overlap with the excitation spectrum of rhodamine, as can be seen from Fig. 2.2. In the FRET pair GFP(YFP)/rhodamine the fluorescent protein serves as a donor while the chemical dye as an acceptor.

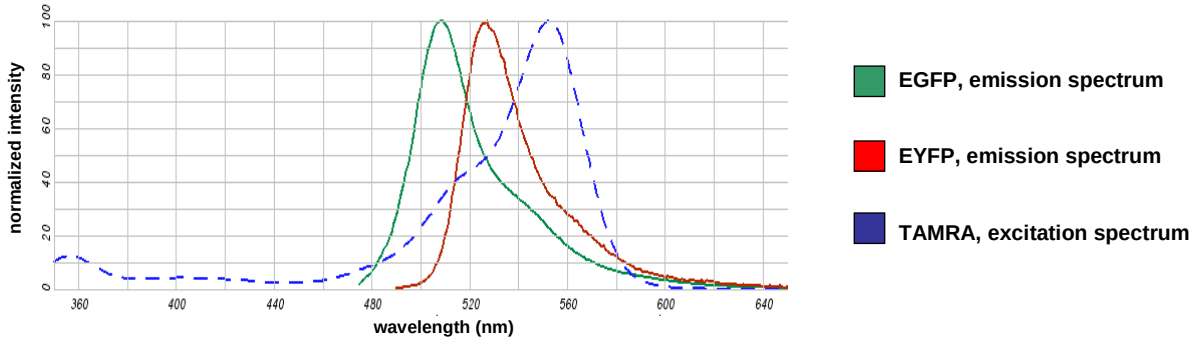

Fig. 2.2. Favourable overlap between emission spectra of Enhanced Green Fluorescent Protein (EGFP, solid green line) or Enhanced Yellow Fluorescent Protein (EYFP, solid red line) and excitation spectrum of rhodamine (dashed blue line) permit the use of the EGFP/rhodamine or EYFP/rhodamine pairs in FRET-based studies (TAMRA = tetramethylrhodamine. Source: Invitrogen-Molecular Probes[4]).

The synthesis and purification of these peptides, as well as their performance in living cells are reported in the following sections.

[4] http:\\probes.invitrogen.com.

3. Material and methods

3.1 Solid-phase peptide synthesis (SPPS)

All peptides were synthesized on polystyrene based resins (cross-linked with 1% DVB,[5] 100 – 200 mesh) using *(L)*N-α-Fmoc protected amino acids[6] and conventional Fmoc chemistry protocols (Chan, 2000). Side chain protecting groups for the amino acids were: *t*Bu for Asp, Glu, Ser, Thr and Tyr; Boc for Lys; Trt for Gln and Cys; Pbf for Arg. When particular orthogonal conditions were required (for side-chain modification on resin) acid-sensitive Mtt and Cl-Trt groups were used for Lys and Tyr residues, respectively. For the synthesis of peptide acids (-COOH terminus) a Wang resin (polymer bound *p*-alkoxybenzyl alcohol) pre-loaded with the required amino acid was used. For the synthesis of peptide amides (-$CONH_2$ terminal group) the Rink amide MHBA resin (polymer bound 4-(2',4'-dimethoxyphenyl-Fmoc-aminomethyl)-phenoxyacetamido-norleucyl-4-methylbenzyl hydramine) was employed [154]. A schematic representation of the two solid supports is given in Fig. 3.1.1.

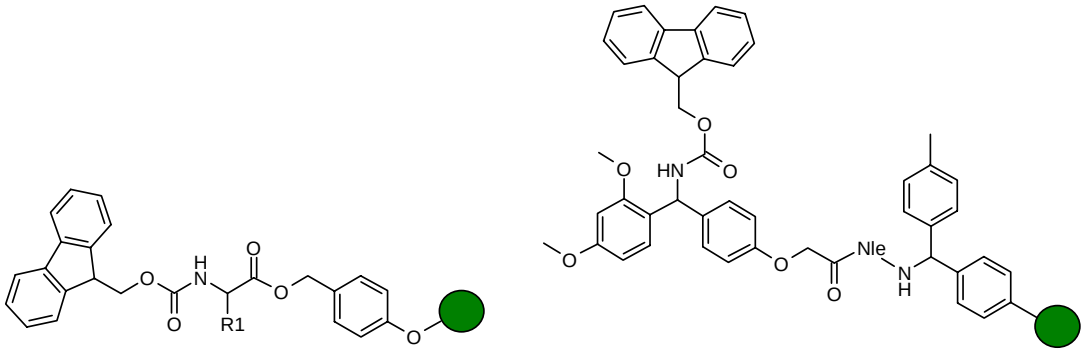

Fig. 3.1.1. (**a**) A generic Fmoc-protected amino acid linked to the Wang resin. (**b**) The Rink amide MHBA support (Nle = norleucine).

Bromomethyl acetate, DIC, DIPEA, DCI, DMF, HBTU, HOBt, NMP, tBuOMe, tBuOOH (5 M sol. in nonane), TFA, TIS, TNBS (1% sol. in DMF) were obtained from Aldrich-Fluka (Steinheim, Germany), and used without further purification. O-*t*-butyl-O'-(4,5-dimethoxy-2-nitrobenzyl)-N,N-diisopropylphosphoramidite was a kind gift from Dr. Sirus Zarbakhsh (Schultz group alumnus, EMBL-Heidelberg, Germany). Pre-loaded Wang resins and N-α-Fmoc protected amino acids were obtained from Fluka and ORPEGEN Pharma GmbH (Heidelberg, Germany). Fmoc-Lys(Mtt)-OH and Fmoc-Tyr(Cl-Trt)-OH were

[5] Please refer to the table of abbreviations for the full name of chemicals and other reagents.

[6] Residues in a sequence are always numerated from the carboxy terminus to the amino terminus, following the order of addition during the synthesis. R1 is the generic amino acid which is directly attached to the solid support (see Fig. 3.1.1 *a*).

purchased from Novabiochem (Merck Biosciences GmbH, Schwalbach/Ts, Germany). Fmoc-AEEAc-OH linker was obtained from IRIS Biotech GmbH (Marktredwitz, Germany). Activated Penetratin (ActPEN) was obtained from MP-QBiogene (Irvine, CA, USA), dissolved into 0.5 mL of degassed water, divided into 50 µL single-use aliquots and stored at – 80°C. DCM, HPLC-grade water and ACN were obtained from Fisher Scientific Ltd (Loughborough, UK). Lissamine™-rhodamine sulfonylchloride (LRh-SO_2Cl) was obtained from Fluka or Acros Organics (Geel, Belgium). 5(6)-carboxytetramethylrhodamine succinimidyl ester (5(6)-TAMRA SE, mixed isomers), Oregon Green® 488 iodoacetamide (mixed isomers) and Rhodamine Red™ C_2-maleimide (mixed isomers) were purchased from Invitrogen-Molecular Probes (Leiden, The Netherlands). The structures of these fluorescent dyes are shown in Fig. 3.1.2.

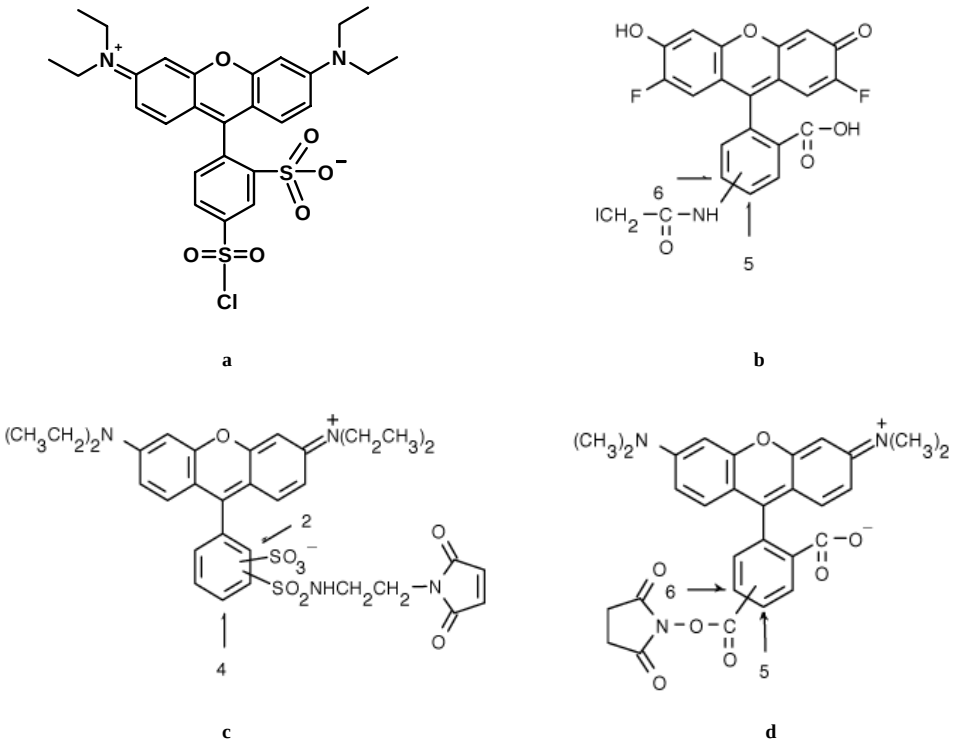

Fig. 3.1.2. The fluorophore reagents used for conjugation to peptides. (**a**) Lissamine™-rhodamine B sulfonylchloride (LRh-SO_2Cl, MW 577.1). (**b**) Oregon Green® 488 iodoacetamide (MW 551.2). (**c**) Rhodamine Red™ C_2-maleimide (MW 680.8). (**d**) 5(6)-carboxytetramethylrhodamine succinimidyl ester (5(6)-TAMRA SE, MW 527.5). Commercial preparations containing mixtures of regioisomers were used for fluorophores ***b***, ***c*** and ***d.*** See also Tab. 3.1 *b* for the spectral properties of these dyes.

Synthesis of peptides was performed manually in fritted polypropylene syringes (MultiSynTech GmbH, Witten, Germany) of variable volumes (2.5 – 10 mL) which were used for resin quantities of up to 300 mg. For larger amounts, a reactor was used made from a 50 mL round glass vessel equipped with a sintered glass filter and a 250 mL round-bottom

flask connected to the filter outlet for waste solvent collection. While addition of reagents was made manually from the top of the vessel through a glass neck (stoppered during the synthesis), the removal of solutions was achieved with positive pressure (latex balloon filled with argon and connected to the top of the vessel via a glass joint equipped with a teflon stopcock). Syringes and the reactor vessel were secured to a flat-bed orbital shaker which provided the necessary agitation.

A typical reaction scheme for peptide synthesis was composed of five steps performed at room temperature:

a. Resin preparation. The resin was poured into a syringe or reaction vessel, washed with DCM and allowed to swell in this solvent for 30 min – 1 h.

b. Fmoc deprotection. The resin was exposed twice to piperidine (20% v/v in DMF), for 3 min and 15 min, respectively; after deprotection the resin was washed with DMF (5 x) and NMP (1 x).

c. Coupling. Fmoc-protected amino acids (4 eq) were combined with HBTU (3.95 eq), HOBt (4 eq) and dissolved in a minimal volume of NMP. DIPEA (8 eq) was added and the solution was stirred for 1 – 2 min before it was transferred to the deprotected resin-bound peptide by aspiration (syringes) or via a pipette (reaction vessel). For large scale synthesis starting from 500 mg of resin, the excess was reduced to 3 eq for each amino acid, HOBt and DIC, 2.95 for HBTU, 6 for DIPEA. The coupling reaction was typically conducted for 40 – 60 min on a orbital shaker at medium speed of agitation and the efficiency of coupling was routinely monitored by the colorimetric TNBS test (see below). When coupling was performed overnight, the use of HOBt (4 eq) and DIC (4 eq) was preferred to avoid potential Fmoc deprotection due to the prolonged exposure of the resin-bound peptide to DIPEA. After successful coupling, the resin was extensively washed with NMP (3 x), iPrOH (3 x) DCM (3 x) and finally end-capped. Steps *b* and *c* are schematically represented in Fig. 3.1.3.

d. End-capping. Residual unreacted amino groups (even when not revealed by the colorimetric test) were capped by swelling the resin in a solution of Ac_2O/pyridine 1:9 (v/v), 2 x 3 min. Afterwards, the resin was extensively washed with DMF (5 x) and a new deprotection cycle was started.

e. Cleavage. Upon completion of the desired sequence the resin-bound peptide was detached from its support with concomitant removal of all side-chain protecting groups. After extensive washing with NMP (3 x), iPrOH (3 x) DCM (3 x) and drying *in vacuo* for 30 – 60 min, the resin was exposed to a cleavage solution composed of TFA/TIS/water (95:2.5:2.5, v/v/v, 1 ml per 10 mg of resin-bound peptide) and left standing for 3 – 4 h with occasional shaking. The

resin was filtered and the filtrate containing the cleaved peptide was concentrated *in vacuo* (rotary evaporator). The peptide was precipitated with ice-cold tBuOMe and collected via low speed centrifugation in polypropilene (PP) tubes,[7] washed with fresh ice-cold tBuOMe, centrifuged and dried before being redissolved in AcOH/water (20%, v/v) and ACN (up to 20 – 25% v/v). The solution was eventually divided in 50 mL PP tubes and lyophilized.

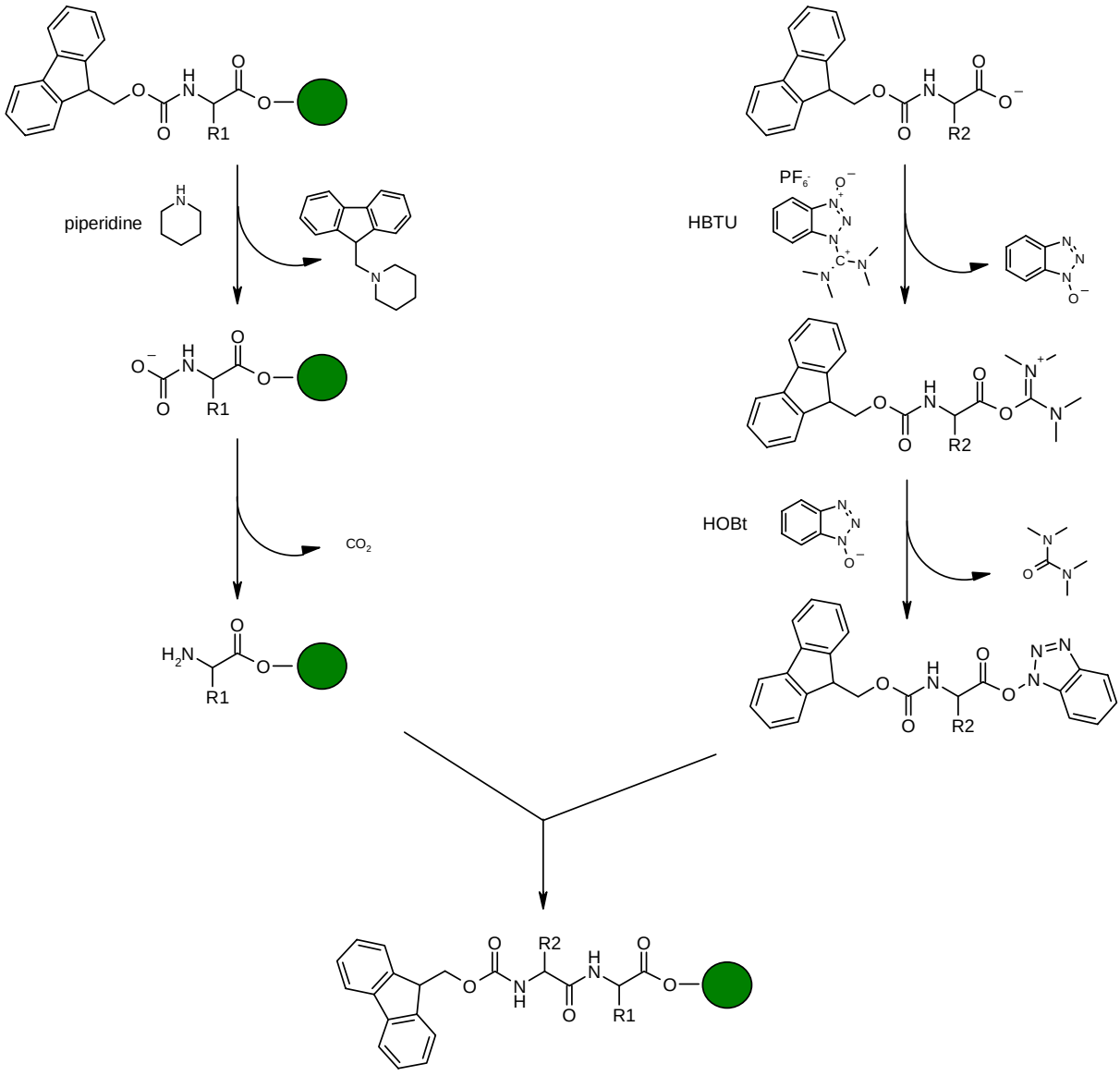

Fig. 3.1.3. Schematic representation of Fmoc deprotection (left panel), activation (right panel), and coupling of two generic amino acids (R1, R2) during SPPS.

[7] PS tubes showed a markedly reduced resistance to TFA under the mechanical stress of centrifugation, thus their utilization is not recommended.

TNBS test [154]

This rapid procedure was routinely performed to check the efficiency of the coupling step as well as to confirm Fmoc deprotection. A few grains of washed resin were withdrawn and placed in a glass test tube. Three drops of DIPEA (10% v/v in DMF) were added, followed by one drop of TNBS/DMF (1%, v/v). The resin was left standing for 5 – 10 minutes and visually inspected. The presence of free amino groups was revealed by the beads changing colour to dark orange-red. This test was normally preferred to the Kaiser test, which requires heat and can in some instances lead to false positives, due to the instability of some amino protecting groups (for example the Mtt group of Lys). When doubts arose a test cleavage was always performed, and the product was checked via ESI-MS. Briefly, a few grains of washed and dried resin were transferred to a glass test tube or an Eppendorf vial and exposed to 100 – 200 µL of the cleavage cocktail for 1 h. The solution was dried under a stream of nitrogen and the cleaved product precipitated by addition of ice-cold tBuOMe. After brief centrifugation the ether was discarded, the precipitate redissolved in 50% ACN in water + 1% formic acid (ca. 300 µL) and the solution directly injected into the mass spectrometer.

On-resin orthogonal deprotection of Lys/Tyr residues

When side-chain modifications on the solid support were necessary, Fmoc-Lys(Mtt)-OH or Fmoc-Tyr(Cl-Trt)-OH were incorporated into the synthesis. These orthogonal side-chain protecting groups could be removed under milder acidic conditions with 1% TFA in DCM (v/v), without cleaving the bond between the peptide and the resin or other protecting groups (such as *t*Bu or Boc). TIS was added as a scavenger at 3% (v/v) concentration. The treatment was performed three to five times (10 – 15 min each) using enough volume of solution to cause the suspension to lose its brilliant yellow colour. Afterwards, the resin was rinsed with fresh DCM and NMP. For successful removal of the Mtt or Cl-Trt groups it was important to first wash the resin with DCM and dry it *in vacuo* for 15 – 20 min, as deprotection failed when performed after the resin was washed with DMF or NMP. On-resin deprotection of Lys(Mtt) residues could easily be monitored by the TNBS test.

High-Performance Liquid Chromatography (HPLC)

HPLC was routinely used to purify (preparative HPLC) and assess the quality of both crude and purified peptides (analytical HPLC). Analytical HPLC was performed with a Waters chromatographic system (Waters Corp., Milford, MA, U.S.A.) composed of a binary pump (mod. 1525) capable of a maximal flow of 10 mL/min and a dual lambda absorbance

UV-VIS detector (mod. 2487). Reverse-phase C18 (RP-18) columns were used: a Merck Lichrosorb RP-18 250 x 4 mm x 10 μm (Merck KGoA, Darmstadt, Germany) run with a flow rate of 1 mL/min or a Waters Symmetry RP-18 75 x 4.6 mm x 3.5 μm run with a flow rate of 0.5 – 0.8 mL/min. The mobile phase was composed of water (+ 0.1% TFA) and ACN (+ 0.1% TFA). Analytical chromatography was normally performed using a linear gradient of ACN: a typical program for the elution of a fluorescently labelled peptide is shown in Tab. 3.1 *a*. The sample was normally dissolved in 30 – 50 μL of 25% ACN immediately prior to injection.

Merck Lichrosorb RP-18 (250 x 4 mm x 10 μm)	**Waters Symmetry RP-18 (75 x 4.6 mm x 3.5 μm)**
solvent A: 10% ACN (+ 0.1% TFA)	solvent A: 10% ACN (+ 0.1% TFA)
solvent B: 90% ACN (+ 0.1% TFA)	solvent B: 90% ACN (+ 0.1% TFA)
flow rate: 1 mL/min	flow rate: 0.5 – 0.8 mL/min
injection loop: 20 μL	injection loop: 20 μL
injection volume: 10 μL	injection volume: 10 μL
detection: double lambda 215 + 254(560) nm	detection: double lambda 215 + 254(560) nm
gradient: linear in 20 min (1.5% per min) T (min) = 0 % ACN (+ 0.1% TFA) = 25 T (min) = 20 % ACN (+ 0.1% TFA) = 55 T (min) = 23 % ACN (+ 0.1% TFA) = 55 T (min) = 25 % ACN (+ 0.1% TFA) = 25 T (min) = 30 % ACN (+ 0.1% TFA) = 25	gradient: linear in 10 min (3% per min) T (min) = 0 % ACN (+ 0.1% TFA) = 25 T (min) = 1 % ACN (+ 0.1% TFA) = 25 T (min) = 11 % ACN (+ 0.1% TFA) = 55 T (min) = 12 % ACN (+ 0.1% TFA) = 55 T (min) = 12.5 % ACN (+ 0.1% TFA) = 25 T (min) = 16 % ACN (+ 0.1% TFA) = 25

Tab. 3.1 a. Standard conditions for analytical HPLC of peptides.

The control of all hardware parameters and the analysis of chromatograms were performed with the proprietary Waters software "Empower 2" run on a Intel Pentium® based PC (Santa Clara, CA, USA) under the Microsoft Windows 2000® operating system (Mountain View, CA, USA).

This equipment and set-up was also used for semi-preparative purifications. Quantities of material up to 0.1 mg (per injection) were purified over the Merck Lichrosorb RP-18 column mentioned above, with an elution rate of 1 mL/min. Quantities of material up to 0.4 mg (per injection) were purified over a Supelco Discovery Bio Wide Pore RP-18 column 250 x 10 mm x 10 μm (Bellefonte, PA, USA) with an elution rate of 5 mL/min. Linear gradients of ACN were commonly used, often requiring optimization for a given peptide.

Preparative HPLC was performed using a Knauer chromatographic system (Knauer GmbH, Berlin, Germany) composed of a binary pump (mod. K-1800) capable of a maximal flow of 100 mL/min, 10 mL injection loop and a single lambda absorbance UV-VIS detector (mod. K-2501). Purifications were routinely performed using a Supelco Discovery Bio Wide Pore RP-18 column 250 x 21.2 mm x 10 μm charged with 2 – 40 mg of material (per

injection). The mobile phase was composed of water (+ 0.1% TFA) and ACN (+ 0.1% TFA). A typical run used a linear gradient of ACN from 25 to 55 % over 30 min with a flow rate of 25 mL/min (1 %/min) and detection at 215, 254 or 560 nm. To improve resolution it was sometimes necessary to reduce the gradient rate from 1 to 0.5 %/min. Chromatograms were recorded on paper over a Juergens chart recorder (mod. SE 120) coupled to the UV-VIS detector, with the gain set to 100 – 200 mV and a chart speed of 30 cm/h.

Stock solutions of fluorescently labelled peptides were prepared in anhydrous DMSO or in dioxane/water 1:1 (v/v) and stored at – 20°C. The concentrations were adjusted according to the absorbance values obtained from a diluted solution (1:150 – 1:300) in MeOH or buffered water (Tab. 3.1 b). Samples were measured in a 100 µL quartz cuvette (Hellma GmbH, Jena, Germany) with an UltroSpec 2100 Pro UV-VIS spectrophotometer (Amersham Biosciences, GE Healthcare). Concentration values were calculated on the basis of spectral parameters (Abs_{max}, ε) obtained from Invitrogen-Molecular Probes technical resource website (Tab. 3.1 b).

LRh-SO_2Cl	Lissamine™-rhodamine B sulfonylchlorhyde	Abs_{max} 568 nm, ε = 88000 (MeOH)
5(6)-TAMRA SE (mixed isomers)	5(6)-carboxytetramethylrhodamine, succinimidyl ester	Abs_{max} 546 nm, ε = 95000 (MeOH)
Rhodamine Red™-C_2 maleimide (mixed isomers)		Abs_{max} 560 nm, ε = 119000 (MeOH)
Oregon Green® 488 iodacetamide (mixed isomers)		Abs_{max} 491 nm, ε = 68000 (H_2O, pH 9)

Tab. 3.1 b. Spectral properties (Abs_{max}, ε) of the fluorophores used (Invitrogen-Molecular Probes data, http://probes.invitrogen.com).

Mass spectrometry

Molecular masses were measured using a bench-top ZQ2000 Waters-Micromass ESI (Electrospray Ionization) mass spectrometer equipped with a single quadrupole ion trap analyzer. Samples were introduced as diluted aqueous solutions, normally 50% ACN and 1% formic acid (ca. 100 µL), via an automated capillary syringe (flow rate 10 µL/min). Typical values of the hardware parameters of the instrument are summarized in Tab. 3.1 *c*.

desolvation temp.: 150°C	gas flow: 380 L/h
capillary voltage: 3.30 kV	cone flow: 80 L/h
cone voltage: 30 V	detection: positive scan mode (ES^+) 200 – 2000 a.m.u., scan time 0.5 sec, inter-scan delay 0.3 sec, total scan time 1 min.

Tab. 3.1 c. Hardware parameters for a typical ESI-MS analysis of peptides.

The mass spectrometer was also connected directly to the HPLC apparatus for LC/MS analysis by joining the capillary probe to the outlet of the UV-VIS detector. A split valve was commonly used to halve the flow of mobile phase reaching the capillary probe. The main hardware parameters were left unchanged. The instrument, in both the MS and LC/MS configurations, was controlled by the "Empower2" software.

MALDI (Matrix Assisted Laser Desorption Ionization) and ESI-ToF (Electrospray Time-of-Flight) mass spectra were performed at the EMBL Proteomic Core Facility by Dr. Thomas Franz and co-workers.

3.2 Synthesis of LRh-TAT peptide (LRh-Ahx-Arg-Lys-Lys-Arg-Arg-Gln-Arg-Arg-Arg-$CONH_2$)

Rink amide MHBA resin (30 mg, 0.74 μmol/mg, Fig. 3.1.1) was poured into a 2.5 mL PP fritted syringe, washed three times with DCM and allowed to swell for 30 min. Synthesis was initiated by Fmoc deprotection, followed by washing and then coupling of Fmoc-Arg(Pbf)-OH (89 μmol, 4 eq) with HOBt/DIC (4 eq each) in NMP for 6 h. The solution was discarded, the resin was washed (3 x NMP, 3 x iPrOH, 3 x DCM, 3 x NMP) and the coupling was checked via the TNBS test. End-capping of resin was performed next with 1 mL of Ac_2O/pyridine (1:9, v/v), twice for 3 min. After rinsing with DMF (5 x) and Fmoc deprotection, the following amino acid (Fmoc-Arg(Pbf)-OH, 4 eq) was coupled in NMP for 40 – 60 minutes using HBTU/HOBt/DIPEA (3.95:4:8 eq). This protocol was used for all the remaining amino acids and exchanged for the HOBt/DIC protocol (4 eq each) for overnight couplings. After addition of the Fmoc-Ahx-OH residue and the Fmoc deprotection cycle, the coupling of the dye was performed thus: LRh-$SOCl_2$ (28.2 mg, 46.7 μmol, 2.1 eq) was dissolved in 500 μL NMP, DIPEA (11 μL, 66.6 μmol, 3 eq) was added and the dark purple solution was drawn into the syringe. The reaction was allowed to proceed overnight in the dark. Extensive washing with neat NMP and pyridine/NMP (20% v/v) was required to remove excess dye. A final washings was done with iPrOH (3 x), DCM (3 x), then the resin was dried *in vacuo* for 1 h. The peptide was cleaved from the solid support by exposing the resin for 3 h to a 5 mL solution of TFA/TIS/water (95:2.5:2.5, v/v/v) in a 10 mL round-bottom flask, with occasional shaking. The resin was then filtered, washed with neat TFA (2 x 2 mL) and the filtrate containing the cleaved peptide was concentrated *in vacuo*. The crude peptide was precipitated with ice-cold tBuOMe, collected via centrifugation, washed with fresh tBuOMe and redissolved in AcOH/water (20% v/v) plus 0.5 mL portions of ACN (up to 2 – 3 mL) to get a clear solution. The entire volume (about 20 mL) was divided into two 50 mL PP tubes and lyophilized. 1.4 mg of the crude lyophilisate were purified by semi-preparative HPLC using a Supelco Discovery Bio Wide Pore RP-18 column (250 x 10 mm x 10 μm) with a linear gradient of ACN (+ 0.1% TFA) from 25 to 40% over 20 min (0.75 %/min), a flow rate of 5 mL/min and detection at 560 nm. Fractions were pooled, lyophilized and the resulting material was dissolved in dioxane/water (50% v/v) to give 44 μL of solution (2 mM, 0.18 mg, 90 nmol. Yield = 0.4%). Further HPLC analysis was performed using a Merck Lichrosorb RP-18 column (250 x 4 mm x 10 μm) with a linear gradient of ACN (+ 0.1% TFA) from 25 to 40% over 20 min (0.75 %/min), a flow rate of 1 mL/min and detection

at 215 and 560 nm. The product eluted as a pair of partially resolved isomers after 9.3 and 9.9 min (98% overall purity) and its identity was confirmed by ESI-MS (calculated mass for $C_{86}H_{147}N_{34}O_{17}S_2$ 1992.11, found 665.13 [M+3H$^+$/3], 499.01 [M+4H$^+$/4], 399.46 [M+5H$^+$/5], 333.06 [M+6H$^+$/6]). The material was kept frozen at – 20°C until use.

3.3 Synthesis of TAT(K-LRh) peptide (CH_3O-Arg-Lys-Lys-Arg-Arg-Lys(Ahx-LRh)-Arg-Arg-Arg-$CONH_2$)

The synthesis of this TAT variant was started from 30 mg of Rink amide MHBA resin (0.74 μmol/mg, Fig. 3.1.1) using the general protocol described above (sect. 3.2). Following Fmoc deprotection of Arg-3, a Fmoc-Lys(Mtt)-OH residue replaced the wild-type Gln-4 and the synthesis proceeded until completion of the sequence. After removal of the terminal Fmoc group from Arg-9, the amino terminus was end-capped by swelling the resin in 0.5 mL of Ac_2O/pyridine (1:9, v/v), twice for 3 min. The resin was washed with NMP (3 x), iPrOH (3 x), DCM (3 x) and dried *in vacuo* for 20 min. The removal of the Mtt group was performed next, using a solution of TFA/TIS/DCM (1:3:96, v/v/v) as described previously (sect. 3.1) and followed by the addition of the Fmoc-Ahx-OH residue. Condensation of LRh dye (28.2 mg, 46.6 μmol, 2.1 eq), subsequent washings and cleavage from the support were all performed as described (sect. 3.2). After lyophilization, 1.9 mg of the crude peptide were purified by semi-preparative HPLC using a Supelco Discovery Bio Wide Pore RP-18 column (250 x 10 mm x 10 μm), with a linear gradient of ACN (+ 0.1% TFA) from 25 to 40% over 20 min (0.75 %/min), a flow rate of 5 mL/min and detection at 560 nm. The pure material was dissolved in dioxane/water (50% v/v) to give 53 μL of a 1 mM solution (0.11 mg, 53 nmol. Yield = 0.2%). Further HPLC analysis was performed using a Merck Lichrosorb RP-18 column (250 x 4 mm x 10 μm) with a linear gradient of ACN (+ 0.1% TFA) from 10 to 50 % over 20 min (2 %/min), a flow rate of 1 mL/min and detection at 215 and 560 nm. The product eluted as a single peak after 13.6 min (97% pure) and its identity was confirmed by ESI-MS (calculated mass for $C_{89}H_{155}N_{34}O_{16}S_2$ 2020.18, found 679.45 [M+3H$^+$/3], 509.78 [M+4H$^+$/4], 408.04 [M+5H$^+$/5], 340.23 [M+6H$^+$/6]). The peptide was kept frozen at – 20°C until use.

3.4 Synthesis of LRh-DADEYL peptide (LRh-Cys-AEEAc-Asp-Ala-Asp-Glu-Tyr-Leu-$CONH_2$)

Rink amide MHBA resin (50 mg, 0.74 μmol/mg, Fig. 3.1.1) was poured into a 2.5 mL PP fritted syringe, washed three times with DCM and allowed to swell for 30 min. Synthesis was initiated by Fmoc deprotection followed by washing and the coupling of Fmoc-Leu-OH (4 eq, 148 μmol) with HOBt/DIC (4 eq each) in NMP overnight. The solution was discarded, the resin was washed (3 x NMP, 3 x iPrOH, 3 x DCM, 3 x NMP) and the coupling was checked via the TNBS test. Residual unreacted amino groups on the resin (which were nevertheless not detected by the TNBS test) were end-capped by treatment with 1 mL of Ac_2O:pyridine (1:9, v/v) twice for 3 min. The resin was then rinsed with DMF (5 x), deprotected and the succeeding amino acid (Fmoc-Tyr(tBu)-OH, 4 eq) was coupled in NMP for 40 – 60 minutes using HBTU/HOBt/DIPEA (3.95:4:8 eq). This protocol was used for all the remaining amino acids and exchanged for the HOBt/DIC protocol (4 eq each) for overnight couplings. A TNBS test and a capping step were always performed after each coupling. Finally, LRh-SO_2Cl (64 mg, 0.11 mmol, 3 eq) was dissolved in 800 μL NMP followed by addition of TEA (31 μL, 0.22 mmol, 6 eq). The dark purple solution was drawn into the syringe and the resin was allowed to swell for 4 hours in the dark. The whole procedure was repeated with fresh materials overnight. Following extensive washings with NMP, the resin was rinsed with iPrOH (3 x), DCM (3 x) and dried *in vacuo* for 1 h. The peptide was cleaved from the solid support by exposing the resin for 3 h to a 5 mL solution of TFA/TIS/water (95:2.5:2.5, v/v/v) in a 10 mL round-bottom flask, with occasional shaking. The resin was then filtered, washed with neat TFA (2 x 2 mL) and the solution containing the cleaved peptide was concentrated *in vacuo*. The dried residue was carefully washed with ice-cold tBuOMe (3 x) and the crude peptide redissolved in AcOH/water (20% v/v) + ACN (in 0.5 mL portions up to 2 – 3 mL until the solution was clear). The volume (about 20 mL) was divided into two 50 mL PP tubes and lyophilized.

The crude peptide was redissolved in a small volume of 25% ACN (+ 0.1% TFA) and chromatographed in 100 – 200 μL portions using a Supelco Bio Wide Pore RP-18 column (250 x 10 mm x 10 μm) with a step gradient of ACN (+ 0.1% TFA): linear 25 to 40% over 10 minutes; isocratic 40%, 6 minutes; linear 40 to 55% over 4 minutes, flow rate 5 mL/min, detection 215 and 560 nm. The desired product eluted after 13.5 minutes. Fractions were pooled and lyophilized. The peptide was obtained in high purity, as shown by analytical HPLC (Merck Lichrosorb RP-18 column, 250 x 4 mm x 10 μm) and eluted as a single peak

with a retention time of ca. 15 minutes. The identity was confirmed by ESI-MS (calculated mass for $C_{67}H_{89}N_{11}O_{23}S_3$ 1511.53, found 1513.36 [M+H$^+$], 757.32 [M+2H$^+$/2]). The purified peptide was dissolved in 30 µL of anhydrous DMSO (3.5 mM, Tab. 3.1 b; 0.16 mg, 105 nmol. Yield = 0.3%), aliquoted into 0.5 mL vials, sealed under argon and stored at – 20°C.

3.5 Synthesis of LRh-DADEYL-PEN conjugate (LRh-Cys(S-PEN)-AEEAc-Asp-Ala-Asp-Glu-Tyr-Leu-CONH$_2$)

50 µL (18.4 nmol) of ActPEN peptide in degassed water were mixed with 5.25 µL of a 3.5 mM solution in DMSO of the LRh-DADEYL peptide (18.4 nmol) in a 0.5 mL Eppendorf vial, followed by the addition of 20 µL of degassed ACN to achieve complete solubilization. The vial was sealed under argon and the solution was shaken at room temperature overnight. Using a modification to this protocol, the ActPEN solution (50 µL) was first lyophilized, resuspended in 50 µL of anhydrous ACN saturated with argon, mixed with the LRh-DADEYL peptide solution in DMSO (5.25 µL) and treated as described above. The conjugate was purified over a Merck Lichrosorb RP-18 column (250 x 4 mm x 10 um) as described (Tab. 3.1 a). The desired product eluted after 12 minutes and its identity was confirmed by ESI-MS (calculated mass: 4072,[8] found 1358.51 [M+3H$^+$/3], 1019.10 [M+4H$^+$/4]). Collected fractions were pooled and lyophilized. The product from the two conjugation reactions was redissolved in anhydrous DMSO to afford 7.5 µL of solution (0.6 mM, Tab. 3.1 b; 17 µg, 4.42 nmol. Yield = 12%). The material was stored at – 20°C.

3.6 Synthesis of Fmoc-PEN1 Penetratin (Fmoc-*Cys*-Arg-Gln-Ile-Lys-Ile-Trp-Phe-Gln-Arg-Arg-Met-Lys-Trp-Lys-Lys-COOH)

Fmoc-Lys(Boc)-Wang resin (300 mg, 0.4 – 0.6 µmol/mg) were loaded into a 10 mL PP fritted syringe, washed three times with DCM and allowed to swell in this solvent for 60 min. Fmoc deprotection, coupling, end-capping and washing steps were performed as previously described. Each amino acid was used in an excess of 4 eq. The HBTU/HOBt/DIPEA coupling protocol (3.95:4:8 eq) was used (40 – 60 min coupling time) and exchanged with the HOBt/DIC protocol (4 eq each) for overnight condensations. A TNBS test was always performed to assess efficiency of coupling, followed by an end-capping step. Following the attachment of the last residue in the sequence, namely Fmoc-Cys(Trt)-OH-17, the resin was

[8] The exact sequence and composition of the commercial activated Penetratin are not known. Molecular weight of the conjugate could only be estimated by the sum of the single molecular weights.

extensively washed and dried *in vacuo* for 1 h. Cleavage was performed at this stage without prior removal of the terminal Fmoc group. The dried resin was placed in a round-bottom flask and treated with 30 mL of a solution of TFA/TIS/water (95:2.5:2.5, v/v/v) at room temperature for 4 h with occasional shaking. The cleavage mixture was filtered and the filtrate concentrated *in vacuo*. The crude peptide was precipitated with the addition of ice-cold tBuOMe, triturated and the suspension transferred into 50 mL PP tubes. The crude product was collected via low-speed centrifugation (1000 rpm, 4 min), resuspended in fresh ice-cold tBuOMe, again centrifuged and dried. Finally, it was redissolved in AcOH/water (20% v/v) and lyophilized. The crude material was redissolved in 15 mL of 25% ACN in water (+ 0.1% TFA) and purified in three 5 mL injections over a Supelco Discovery Bio Wide Pore RP-18 column (250 x 21.2 mm x 10 μm) using a linear gradient of ACN (+ 0.1% TFA) as described in sect. 3.1. Under these conditions the product eluted after ca. 13 min. Fractions were pooled and concentrated *in vacuo* to eliminate ACN. The remaining solution was divided into 50 mL PP tubes and lyophilized to obtain 173.6 mg of product (67.5 μmol. Yield = 45%). The purified peptide was assayed by analytical HPLC (Waters Symmetry RP-18 column, 75 x 4.6 mm x 3.5 μm) using a flow rate of 0.8 mL/min (Tab. 3.1 a): the product eluted as a single peak after ca. 7 min. The identity was confirmed by ESI-MS (calculated mass for $C_{122}H_{186}N_{35}O_{23}S_2$ 2573.38, found 858.66 [M+3H$^+$/3], 644.30 [M+4H$^+$/4], 515.60 [M+5H$^+$/5]).

3.7 Synthesis of Oregon Green® and Rhodamine Red™ Penetratin derivatives OG-PEN1 and RR-PEN1

Two solutions of Oregon Green® 488 iodoacetamide (mixed isomers) and Rhodamine Red™ C_2-maleimide (mixed isomers) were prepared by dissolving a small aliquot of each in a few microlitres of anhydrous DMF and DMSO, respectively. The concentration of the two solutions was measured spectrophotometrically by making a 1:300 dilution in aqueous bicarbonate (pH 9) for Oregon Green® 488 iodoacetamide or MeOH for Rhodamine Red™ C_2-maleimide and adjusted to 10 mM (final volume 23.4 μL) and 5 mM (final volume 23.0 μL), respectively. Two 0.5 mg aliquots of lyophilized Fmoc-PEN1 peptide (0.2 μmol) were redissolved into 25 μL of degassed 25% (v/v) ACN in water and the entire volume was mixed with the solutions of the two dyes. Vials were sealed under argon and shaken overnight at room temperature in the dark to allow condensation between the free sulfhydryl group of the terminal Cys residue in Fmoc-PEN1 peptide and the iodoalkyl moiety of Oregon Green® or the maleimide group of Rhodamine Red™. The fluorescent conjugates were purified by semi-

preparative RP-HPLC using a Merck Lichrosorb RP-18 column (250 x 4 mm x 10 µm), detection 215 and 254 nm for OG-PEN1 or 215 and 560 nm for RR-PEN1 peptide (Tab. 3.1 a). Further analytical HPLC was performed using a Waters Symmetry RP-18 column (75 x 4.6 mm x 3.5 µm) and a flow rate of 0.8 mL/min (Tab. 3.1 a). Retention times were between 6.4 – 7.2 min for OG-PEN1 peptide and 7.6 – 8.4 min for RR-PEN1 peptide. The identity of products was confirmed by ESI-MS (OG-PEN1: calculated mass for $C_{144}H_{197}F_2N_{36}O_{29}S_2$ 2996.45, found 999.31 [M+3H$^+$/3], 749.70 [M+4H$^+$/4]. RR-PEN1: calculated mass for $C_{155}H_{222}N_{39}O_{31}S_4$ 3253.59, found 1085.33 [M+3H$^+$/3], 814.21 [M+4H$^+$/4]). The two fluorescent Penetratin derivatives were stored at – 20°C as 5 mM (OG-PEN1, 13 µL, 65 nmol. Yield = 33%) and 1 mM (RR-PEN1, 35 µL, 35 nmol. Yield = 18%) solutions in anhydrous DMSO.

3.8 Bulk synthesis of resin-bound Fmoc-DADEYL peptide (Fmoc-AEEAc-Asp(tBu)-Ala-Asp(tBu)-Glu(tBu)-Tyr(Cl-Trt)-Leu-Rink amide resin)

Rink amide MHBA resin (500 mg, 0.72 µmol/mg) was placed in the 50 mL reaction vessel, washed three times with DCM and allowed to swell in this solvent for 1 h. Synthetic steps, including colorimetric TNBS test, end-capping and washings were made as specified earlier (sect. 3.1). Amino acids, coupling reagents and protocols were used as reported in the following table (Tab. 3.8 a):

1) Fmoc-Leu-OH	3 eq a.a., HOBt/DIC (3:3 eq), overnight
2) Fmoc-Tyr(Cl-Trt)-OH	1 eq a.a., HOBt/DIC (1:1 eq), 1 h + 1x overnight + 0.5 eq a.a., HBTU/HOBt/DIPEA (0.5:0.5:1 eq), 2 h
3) Fmoc-Glu(tBu)-OH	3 eq a.a., HBTU/HOBt/DIPEA (2.95:3:6 eq), 1 h + 1 eq a.a., HBTU/HOBt/DIPEA (0.95:1:2 eq) 1h
4) Fmoc-Asp(tBu)-OH	3 eq a.a., HBTU/HOBt/DIPEA (2.95:3:6 eq), 1 h
5) Fmoc-Ala-OH	*see entry 4*
6) Fmoc-Asp(tBu)-OH	*see entry 4*
7) Fmoc-AEEAc-OH	1 eq a.a., HBTU/HOBt/DIPEA (0.5:0.5:1 eq), 1h + 1 eq a.a., HOBt/DIC (1:1 eq), overnight

Tab. 3.8 a. Preparation of the Fmoc-DADEYL peptide (bulk synthesis on Rink amide MHBA resin).

Following the addition of the Fmoc-AEEAc-OH residue, the resin-bound peptide was extensively washed and dried *in vacuo*. A cleavage test was performed on a small quantity of resin, without prior removal of the terminal Fmoc group, followed by analytical HPLC using a Waters Symmetry RP-18 column (75 x 4.6 mm x 3.5 µm) and a flow rate of 0.8 mL/min (Tab. 3.1 a). The product eluted after 8.7 min and its identity was confirmed by ESI-MS (calculated mass for $C_{52}H_{66}N_8O_{18}$ 1090.45, found 1091.76 [M+H$^+$]).

3.9 Synthesis of TAMRA-DADEYL peptide (5(6)-TAMRA-AEEAc-Asp-Ala-Asp-Glu-Tyr-Leu-$CONH_2$)

Resin-bound Fmoc-DADEYL peptide (13.2 mg, corresponding to 6.9 mg of fully protected peptide, 4.5 μmol[9], sect. 3.8) was placed in a 1.5 mL Eppendorf vial, deprotected twice (10 min each) with 500 μL of 20% (v/v) piperidine in DMF, rinsed with DMF (5 x 500 μL) and NMP (1 x 1 mL). After brief centrifugation, the excess of solvent was removed by careful aspiration with a pipette, allowing the resin to swell in a minimal amount of liquid. 5 mg of 5(6)-TAMRA SE (9.5 μmol, 2.1 eq) were dissolved into 150 μL of NMP/DCM 1:1 (v/v) containing 4.8 μL of DIPEA (3 eq) and the solution was transferred to the resin. The coupling of the dye was performed in a mixer (900 rpm) at room temperature in the dark. Over time, the initial brilliant red solution largely decolourized, while the resin beads appeared dark red. After 3 h the solution was discarded and the resin was rinsed with 1 mL portions of NMP until the solvent appeared colourless, then it was transferred into a 2.5 mL PP syringe, rinsed with DCM (5 x 1 mL) and briefly dried *in vacuo*. Cleavage from the solid support was made by exposing the resin to 2 mL of TFA/TIS/water (95:2.5:2.5, v/v/v) for 3 h with gentle shaking. The resin was filtered, washed with neat TFA (2 x 1 mL) and the filtrate was concentrated *in vacuo*. The peptide was triturated in ice-cold tBuOMe, collected by centrifugation, rinsed again with fresh tBuOMe, centrifuged, dried, redissolved in AcOH/water (20%, v/v) with the addition of ACN (ca. 20% v/v) and lyophilized. The total amount of crude labelled peptide was 5.3 mg (4.1 μmol. Yield = 91%). HPLC analysis was performed using a Waters Symmetry RP-18 column (75 x 4.6 mm x 3.5 μm) with a flow rate of 0.8 mL/min (Tab. 3.1 a). The product eluted in the form of two regioisomers after 4.9 and 5.4 min. The identity of both was confirmed by ESI-MS (calculated mass for $C_{62}H_{76}N_{10}O_{20}$ 1280.42, found 1281.83 [$M+H^+$], 641.67 and 641.60 [$M+2H^+/2$]). The lyophilized peptide was stored at – 20°C and used directly in the next synthetic step.

3.10 Synthesis of TAMRA-DADEYL-AM_3 peptide (5(6)-TAMRA-AEEAc-Asp(AM)-Ala-Asp(AM)-Glu(AM)-Tyr-Leu-$CONH_2$)

Crude TAMRA-DADEYL peptide (5 mg, 3.9 μmol, 1 eq) was placed in a 2 mL screw-capped PP vial, sonicated in 250 μL of anhydrous dioxane and freeze-dried. The material was

[9] The amount of bound peptide can be calculated from the following formula: mg peptide = (Qty x MW x s.l.) / (1000 + (MW x s.l.)) where Qty = amount of weighed resin, MW = molecular weight of the fully protected peptide, s.l. = substitution level of the resin., The value obtained has nevertheless to be considered indicative, as the substitution level is *per se* approximate and tends to decrease during the course of the synthesis.

then dissolved in 90 µL of anhydrous DMF, followed by the addition of 1 M DIPEA in anhydrous DMF (14 µL, 14 µmol, 3.6 eq) and 3.4 µL of bromomethyl acetate (5.4 mg, 35.1 µmol, 9 eq). The vial was capped under argon and the reaction was carried out for 1 h at room temperature. After this time, the solution was concentrated *in vacuo*. Analytical HPLC was carried out using a Waters Symmetry RP-18 column (75 x 4.6 mm x 3.5 µm) a flow rate of 0.8 mL/min (Tab. 3.1 a). The crude product was redissolved in 20% ACN in water (+ 0.1% TFA) and purified using a Supelco Bio Wide Pore RP-18 column (250 x 21.2 mm x 10 µm) with a linear gradient of ACN (+ 0.1% TFA) from 25 to 48% over 30 min (0.75 %/min), a flow rate of 25 mL/min and detection at 560 nm. The desired product was isolated as a mixture of isomers eluting at 16.5 min. Fractions were pooled, concentrated *in vacuo* and lyophilized. Further HPLC analysis was performed using a Waters Symmetry RP-18 column (75 x 4.6 mm x 3.5 µm) with a linear gradient of ACN (+ 0.1% TFA) from 30 to 50% over 15 min (1.3 %/min), a flow rate of 0.8 mL/min and detection at 215 and 560 nm: the peptide was detected as a pair of partially resolved isomers eluting after 6.8 and 7.1 min (overall purity 91.3%). The identity was confirmed by ESI-MS (calculated mass for $C_{71}H_{88}N_{10}O_{26}$ 1496.59, found 1498.13 [$M+H^+$], 749.85 [$M+2H^+/2$]). Finally, the lyophilized peptide was redissolved in a few microlitres of dioxane/water 1:1 (v/v) and the concentration was adjusted to 1 mM (Tab 3.1 b). The final volume was 165 µL (165 nmol, 0.25 mg. Yield = 4.2%). This solution was divided into screw-capped PP vials in 15 µL aliquots, lyophilized and stored at – 20°C until use. Immediately before experiments, the product of a single vial was reconstituted in 15 µL of dioxane/water 1:1 (v/v).

3.11 Synthesis of TAMRA-EYL-AM_1 peptide (5(6)-TAMRA-AEEAc-Glu(AM)-Tyr-Leu-$CONH_2$)

A bulk preparation of the sequence Fmoc-Glu(tBu)-Tyr(tBu)-Leu on Rink amide MHBA resin (0.72 µmol/mg) was first performed starting from 500 mg of support and using standard protocols (sect. 3.1). 30 mg of this batch (corresponding to 12 µmol of fully protected peptide on resin) were first deprotected, rinsed and the Fmoc-AEEAc-OH linker (18.5 mg, 48 µmol, 4 eq) was coupled overnight with the HOBt/DIC protocol. Following further deprotection and washing cycles, the support was transferred to a 1.5 mL Eppendorf vial. 5(6)-TAMRA SE (6.3 mg, 13.2 µmol, 1.1 eq) was dissolved in 150 µL of NMP/DCM 1:1 (v/v), along with DIPEA (4.4 µL, 24 µmol, 2 eq) and the solution was added to the resin. Mode of coupling and rinsing were the same as described in sect. 3.9. The cleavage was

performed with 5 mL of TFA/TIS/water (95:2.5:2.5, v/v/v) for 3 h, the crude product was precipitated in ice-cold tBuOMe, dried, redissolved in AcOH/water (20%, v/v) and lyophilized. The lyophilisate was redissolved in 20% ACN in water (+ 0.1% TFA) and the two regioisomers were separated using a Supelco Discovery Bio Wide Pore RP-18 column (250 x 21.2 mm x 10 μm) with a linear gradient of ACN (+ 0.1% TFA) from 20 to 33% over 26 min (0.5 %/min), a flow rate of 25 mL/min and detection at 560 nm. The fractions were pooled and lyophilized to get 1.9 and 4.2 mg of each regioisomer, respectively (in total, 6.1 mg of material, 6.2 μmol. Yield = 52%). 1.1 mg (1.12 μmol, 1 eq) of one regioisomer were first resuspended in anhydrous dioxane, lyophilized then dissolved in 30 μL of anhydrous DMF, followed by the addition of DIPEA (0.56 μL, 3.4 μmol, 3 eq) and bromomethyl acetate (0.33 μL, 3.4 μmol, 3 eq). The reaction was carried out in a screw-capped vial for 30 min under argon, then the solution was dried *in vacuo*. The crude peptide was purified by semi-preparative HPLC using a Supelco Discovery Bio Wide Pore RP-18 column (250 x 10 mm x 10 μm) with a linear gradient of ACN (+ 0.1% TFA) from 30 to 42% over 12 min (1 %/min), a flow rate of 5 mL/min and detection at 560 nm. Fractions were pooled and lyophilized to obtain 0.8 mg (0.76 μmol. Yield = 68%) of a single esterified peptide (TAMRA-EYL-AM_1) and traces of a double esterified peptide (TAMRA-EYL-AM_2). The identities of the products were confirmed by ESI-MS (TAMRA-EYL-AM_1, calculated mass for $C_{54}H_{65}N_7O_{15}$ 1051.45, found 1052.69 [$M+H^+$]; TAMRA-EYL-AM_2, calculated mass for $C_{57}H_{69}N_7O_{17}$ 1123.47, found 1124.72 [$M+H^+$]). For cell experiments, 1 – 2 mM stock solutions in anhydrous DMSO (Tab 3.1 b) were prepared just before. The material was stored at – 20°C.

3.12 Synthesis of TAMRA-EAEEYL-AM_3 peptide (5(6)-TAMRA-AEEAc-Glu(AM)-Ala-Glu(AM)-Glu(AM)-Tyr-Leu-$CONH_2$)

Resin-bound Fmoc-Glu(tBu)-Tyr(tBu)-Leu (52 mg, corresponding to 24.2 μmol of fully-protected peptide on resin, sect. 3.11) was deprotected and completion of the sequence was performed similarly to what described previously (sect. 3.8). Following addition of the linker and a new deprotection cycle, 5(6)-TAMRA SE (14 mg, 26.5 μmol, 1.1 eq) dissolved in 250 μL of NMP/DCM 1:1 (v/v) was added to the resin, along with DIPEA (14.7 μL, 79.5 μmol, 3 eq). Coupling was performed for 4 h in the dark. After the cleavage from the solid support, the separation of the two regioisomers was performed over a Supelco Bio Wide Pore RP-18 column (250 x 21.2 mm x 10 μm) using a linear gradient of ACN (+ 0.1% TFA) from

25 to 35% over 20 min (0.5 %/min), a flow rate of 25 mL/min and detection at 560 nm. The two products eluted after 8.2 and 9.4 min, respectively. Fractions were pooled and lyophilized to obtain 7.7 mg of the first isomer and 10.7 mg of the second, for a total of 18.4 mg (14 μmol. Yield = 58%) of labelled peptide. Further HPLC analysis was performed using a Waters Symmetry RP-18 column (75 x 4.6 mm x 3.5 μm) with a flow rate of 0.8 mL/min (Tab. 3.1 a). The two isomers eluted after 4.7 and 5.3 min, respectively. Their identity was confirmed by ESI-MS (calculated mass for $C_{64}H_{80}N_{10}O_{20}$ 1308.56, found 1309.82 [M+H$^+$]). For the AM ester synthesis, 3.8 mg of one isomer (2.9 μmol) were first resuspended in anhydrous dioxane, lyophilized, then dissolved in 90 μL of anhydrous DMF in a screw-capped vial. DIPEA (4.5 μL, 26.1 μmol, 9 eq) and bromomethyl acetate (2.6 μL, 26.1 μmol, 9 eq) were added to the solution and the reaction was carried out for 30 min at room temperature under argon. The solution was divided in three vials and dried *in vacuo*. The crude material from one vial was purified by semi-preparative HPLC over a Supelco Discovery Bio Wide Pore RP-18 column (250 x 10 mm x 10 μm) using a linear gradient of ACN (+ 0.1% TFA) from 30 to 42% over 12 min (1 %/min), a flow rate of 5 mL/min and detection at 560 nm. Fractions were pooled and lyophilized to get 0.9 mg of the desired product (0.57 μmol. Yield = 59%). A peptide carrying four AM esters was isolated in traces. Further HPLC analysis was performed using a Merck Lichrosorb RP-18 column (250 x 4 mm x 10 μm) with a flow rate of 1 mL/min (Tab. 3.1 a). The product eluted after 14.8 min and its identity was confirmed by ESI-MS (calculated mass for $C_{73}H_{92}N_{10}O_{26}$ 1524.62, found 1525.91 [M+H$^+$]). For cell experiments, 1 – 2 mM stock solutions in anhydrous DMSO (Tab. 3.1 b) were prepared just before use. The material was stored at – 20°C.

3.13 Synthesis of TAMRA-DADEY(cgdP)L-AM$_4$ (5(6)-TAMRA-AEEAc-Asp(AM)-Ala-Asp(AM)-Glu(AM)-Tyr(O$_2$P-O'-AM-O''-(4,5-dimethoxy-2-nitrobenzyl))-Leu-CONH$_2$)

Resin-bound Fmoc-DADEYL peptide (50 mg, corresponding to 28.7 mg of fully protected peptide, 18.7 μmol, sect. 3.8) was rinsed with anhydrous DCM and briefly dried *in vacuo*. Removal of the orthogonal Cl-Trt protecting group was performed with a mixture of TFA/TIS/DCM (1:3:96, v/v/v), as described (sect. 3.1). Afterwards, the resin was rinsed with DCM (5 x), transferred into a 1.5 mL eppendorf vial and carefully dried *in vacuo* (the vial was closed with a spare cap which was previously punctured by a needle). DCI (22 mg, 0.18 mmol, 10 eq) was mixed with O-*t*-butyl-O'-(4,5-dimethoxy-2-nitrobenzyl)-N,N-diisopropylphosphoramidite (78 mg, 0.18 mmol, 10 eq) and both were dissolved in 300 μL

anhydrous DCM. The solution was transferred onto the resin and the vial was shaken overnight in the dark. The solution was then discarded and the resin was rinsed with NMP (5 x 1 mL). Oxidation was performed by swelling the resin in 500 µL of a 0.5 M solution of tBuOOH in NMP (9 volumes NMP + 1 volume 5 M tBuOOH in nonane), twice for 1 h. The phosphorylation was confirmed at this stage by performing a test cleavage on a few grains of resin after N-terminal Fmoc deprotection. The peptide was assayed by analytical HPLC (Waters Symmetry RP-18 column, 75 x 4.6 mm x 3.5 µm) using a linear gradient of ACN (+ 0.1% TFA) from 10 to 50% over 10 min (4 %/min), a flow rate of 0.8 mL/min and detection at 215 and 280 nm. The product eluted after 7.6 min and its identity was confirmed by ESI-MS (calculated mass for $C_{47}H_{66}N_9O_{23}P$ 1143.40, found 1144.83 [$M+H^+$]). Following N-terminal Fmoc deprotection with 20% (v/v) piperidine in DMF and washing cycles, coupling of the dye was performed by swelling the resin 4 h in the dark in 250 µL of a NMP/DCM 1:1 (v/v) solution containing 5(6)-TAMRA SE (11.8 mg, 37.4 µmol, 1.2 eq) and DIPEA (10.4 µL, 56.1 µmol, 3 eq) for 4 h in the dark. After extensive washing with NMP, the cleavage was performed with 5 mL of TFA/TIS/water (95:2.5:2.5, v/v/v) for 3 h. The crude product was precipitated from ice-cold tBuOMe, dried, redissolved in AcOH/water (20% v/v) and lyophilized. The lyophilisate was redissolved in 15% ACN in water (+ 0.1% TFA) and purified using a Supelco Discovery Bio Wide Pore RP-18 column (250 x 21.2 mm x 10 µm) with a linear gradient of ACN (+ 0.1% TFA) from 15 to 45% over 30 min (1 %/min), a flow rate of 25 mL/min and detection at 560 nm. The fractions were pooled and lyophilized to obtain 13.2 mg of the mixture of the two regioisomers (8.5 µmol. Yield = 45 %). Further HPLC analysis was performed using a Waters Symmetry RP-18 column (75 x 4.6 mm x 3.5 µm), using a linear gradient of ACN (+ 0.1% TFA) from 10 to 50% over 10 min (4 %/min), a flow rate of 0.8 mL/min and detection at 215 and 560 nm: the two partially resolved regioisomers eluted after 8.5 and 8.7 min. Their identity was confirmed by ESI-MS (calculated mass for $C_{71}H_{86}N_{11}O_{27}P$ 1555.54, found 1557.65 [$M+H^+$], 779.58 [$M+2H^+/2$]). For the AM ester synthesis, 3.5 mg of product (2.2 µmol) were first resuspended in anhydrous dioxane, lyophilized, then dissolved in 90 µL of anhydrous DMF in a screw-capped vial. DIPEA (4.6 µL, 26.4 µmol, 12 eq) and bromomethyl acetate (2.6 µL, 26.4 µmol, 12 eq) were added to the solution and the reaction was carried out for 30 min at room temperature under argon. The crude mixture was concentrated *in vacuo*. ESI-MS analysis revealed the $–AM_4$ product (m/z 1845.15) along with the presence of a $–AM_5$ species (m/z 1917.22). Despite various attempts at purification, isolation of a clean product failed.

Mammalian cell culture, media, transfection protocols

In vivo experiments were performed using HeLa Kyoto, human adeno-carcinoma (MCF-7) and mouse embryonic fibroblast (MEF) cell lines. In some instances, HeLa Kyoto stably transfected with YFP-EGFR[10] were also used. HeLa Kyoto and HeLa Kyoto/YFP-EGFR were kind gifts from Dr. Vibor Laketa (Pepperkok/Schultz, EMBL, Heidelberg, Germany). MCF-7 were provided by Prof. Philippe Bastiaens (MPI Molecular Physiology, Dortmund, Germany). MEF and plasmids encoding for GFP-PTP1B or GFP-EGFR proteins were kind gifts from Prof. Fawaz Haj (UC Davis, CA, USA). Frozen stocks of cells were prepared according to the guidelines of the German Collection of Microorganisms and Cell Cultures Centre (DSMZ[11] - Deutsche Sammlung von Mikroorganismen und Zellkulturen GmbH, Braunschweig, Germany).

Cells were routinely cultured in a humidified atmosphere (37°C, 5% CO_2) and grown in monolayers in 250 mL flasks (Greiner Bio-One GmbH, Frickenhausen, Germany) with phenol red-containing DMEM (Invitrogen-Gibco, Paisley, U.K.) at 1.0 g/L (HeLa Kyoto) or 4.5 g/L (MEF, MCF-7) glucose and supplemented with 10% FBS (PAN Biotech, Aidenbach, Germany), 2 mM L-glutamine (Invitrogen-Gibco, Paisley, U.K.), 100 U/mL penicillin (Sigma, Steinheim, Germany) and 100 µg/mL streptamycin (Sigma, Steinheim, Germany). Cells were regularly passaged twice a week at a sub-confluent state and detached from flasks by treatment with 1 mL of a solution of trypsin/EDTA (Sigma, Steinheim, Germany). Upon detachment, the cells were resuspended in 9 mL of complete medium and seeded in new flasks containing 12 – 14 mL of fresh culture medium. Below is a summary of the dilution factors commonly used during cell passages (Tab. 3.14 *a*).

cell type	dilution factor (1^{st} passage, 1^{st} day of week)	dilution factor (2^{nd} passage, 4^{th} day of week)
HeLa Kyoto	1:5	1:10
MCF-7	1:4	1:8
MEF	1:10	1:20

Tab. 3.14 a. Dilution factors used for standard cell culture.

The imaging medium used for cell microscopy was based on a HEPES buffer (without phenol red, pH 7.4) and its composition is reported in Tab 3.14 *b*. Peptide solutions were also

[10] The EGFR used in this study represent the isoform Erb1.
[11] www.dsmz.de.

prepared in this medium; it was additionally supplemented with 1% FBS only for MCF-7 cells.

ingredient	final concentration
NaCl	115 mM
$CaCl_2$	1.2 mM
$MgCl_2$	1.2 mM
K_2HPO_4	2.4 mM
glucose	10 mM
HEPES	20 mM
$NaHCO_3$	2.2 g/L

Tab. 3.14 b. Composition of the imaging medium.

For microscopic observations, 35 mm-MatTek dishes (MatTek Corp. Ashland, MA, USA) or Ibidi µ-VI slides (Integrated Biodiagnostics GmbH, Munich, Germany) were routinely used. Each Ibidi µ-VI slide is composed of a high quality plastic material on which six parallel chambers are reproduced. Each chamber has a volume of 30 µL and has two small reservoirs at either end, through which cells can be seeded and solutions can be dispensed. This new product features several advantages: a) the small chamber volume limits the waste of test substances; b) the plastic surface allows easy attachment of cells; c) each individual chamber guarantees an homogeneous cell growth and the closed space avoids drying of the cell monolayer during the experiment; d) up to six experiments can be run simultaneously. The small dimensions and the restricted access to the cells may, nevertheless, create some discomfort in cases where the experiment requires a frequent exchange of solutions with the support fitted onto the microscope stage. The Ibidi µ-VI slide is illustrated in Fig. 3.14.1.

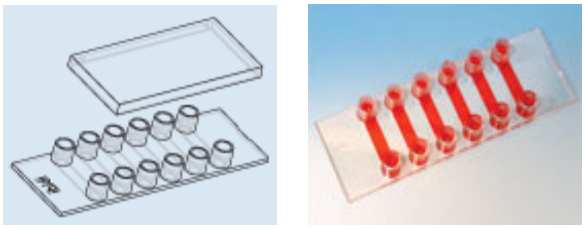

Fig 3.14.1. The Ibidi µ-6 slide (Integrated Biodiagnostics GmbH, Munich, Germany).

Cells were normally seeded following trypsin/EDTA treatment on a sub-confluent monolayer (see above), with a specific protocol according to the support used and the necessity of transfection:

MatTek without transfection: 1.8 – 2.2x10^5 cells were seeded in 2.0 mL complete medium and allowed to adhere overnight. The experiment was normally performed the day after, with the cell monolayer at 60 – 80% confluency.

MatTek with transfection: 48 h before the experiment 0.9 – 1.1x10^5 cells were seeded in 2.0 mL of complete medium and allowed to adhere overnight. Transfection was performed the following day with the reagent Fugene-6 (Roche, Mannheim, Germany) following manufacturer's recommendations and mixing 2 μg of plasmid DNA with 3 μL of reagent in 150 μL of Optimem (Invitrogen-Gibco, Paisley, U.K.). The solution was left standing 30 min at room temperature before being transferred to the cells, which were previously washed and incubated in 1.5 mL Optimem. For MCF-7 cells, the standard culture medium was used for incubation, while the DNA/transfection reagent complex was prepared in Optimem. Experiments and observations were normally performed 16 – 20 h *post*-transfection, with the cell monolayer at 60 – 80% confluency.

Ibidi μ-VI slide without transfection: 1.0 – 1.2x10^4 cells (total volume 40 – 50 μL) were seeded in each chamber and allowed to adhere overnight. The following day, the cells (60 – 80% confluent) were washed and incubated with 70 μL of fresh culture medium until the experiment began.

Ibidi μ -VI slide with transfection: 48 h before the experiment 6.8 – 7.2x10^3 cells (total volume 40 – 50 μL) were seeded in each chamber and allowed to adhere overnight. Transfection was performed the following day with the reagent Fugene-6, mixing in an Eppendorf vial 0.2 μg of plasmid DNA with 0.3 μL of transfection reagent in 10 μL Optimem per chamber. The mixture was left standing for 30 min, 60 μL of Optimem per chamber (or complete medium for MCF-7 cells) were added and the solution was transferred to the cells (about 70 μL per chamber) previously rinsed with Optimem (or complete medium for MCF-7 cells). Before the addition, the excess of medium was removed, leaving 30 μL on the cells, so that the final volume was about 100 μL per chamber. Experiments and observations were normally performed 16 – 20 h *post*-transfection with cells 60 – 80% confluent.

3.15 Cell microscopy

Live cell fluorescent microscopy was performed using a Leica SP2 AOBS laser scanning confocal microscope (Leica Microsystem, Heidelberg, Germany) equipped with a 63X / 1.4 NA apochromatic oil objective. Excitation of fluorophores was achieved using the 488 nm line of an Argon laser (for GFP, YFP and green fluorescent dyes) or the 561 nm line of a DPSS (diode pumped solid state) laser (for rhodamine dyes). Fluorescence was detected in the spectral window 500 – 530 nm (detector PMT 2) for GFP, YFP, green fluorescent dyes and 580 – 650 nm (detector PMT 3) for the rhodamine dyes. Laser scanning was normally unidirectional at 400 Mhz speed and the confocal pinhole was set to 1 Airy unit (ca. 114 μm), except where indicated. Multi-color images were acquired in sequential mode using the "between lines" option (detectors were switched on sequentially after each single line), and the signal was averaged every four lines.

Experiments were performed on cells seeded in MatTek dishes or Ibidi μ-VI slides, as described (sect. 3.14). Peptide solutions were typically prepared in 100 μL of serum-free imaging medium if MatTek dishes were used, while the volume was reduced to 70 μL in case of the Ibidi μ-VI slides, taking into account the residual 30 μL present in each chamber (Fig. 3.14.1). Only for MCF-7 cells, the level of serum was kept to 1% (v/v) throughout the experiment.

When fluorescent Penetratins or their conjugates were used, the cells were incubated in serum-free culture medium (or at 1% FBS v/v for MCF-7 cells) containing 3% BSA (w/v) and 30 μg/mL DNAse I, for one hour prior the experiment (37°C). Afterwards, the cells were rinsed and incubated at room temperature or 37°C with solutions of the fluorescent peptides in concentrations and for the time periods indicated. Cells were then washed at least five times with imaging medium containing 3% BSA and imaged. To assess co-localization of dyes in endosomal compartments, some hardware parameters of the microscope were changed: the scanning speed was increased to 800 – 1000 Mhz, while the average of the signal was reduced to two lines. These changes resulted in a faster microscopic acquisition which was necessary to cope with the rapid movements of the endosomes. The drop of the intensity of the signal due to the faster scanning velocity had to be compensated with an increase of the pinhole aperture which, in turn, increased the thickness of the confocal plane.

Acquired images were analyzed with the open-source software ImageJ (NIH, USA).

3.16 Time lapse recording of TAMRA-DADEYL-AM$_3$ uptake in living HeLa Kyoto and MCF-7 cells

HeLa Kyoto and MCF-7 cells were seeded in MatTek dishes or Ibidi µ-VI slides as described (sect. 3.14) and cultured overnight to allow adhesion. Before the experiment was started, cells were washed three times with imaging medium and incubated in this for 15 min at room temperature. Having secured the support to the microscope stage, the medium was carefully removed and a 10 µM solution of the peptide in imaging medium was dispensed in the centre of the MatTek dish (or in one reservoir of a single chamber in the Ibidi µ-VI slide). The microscope turret was placed back in position for acquisition, the focal plane and exposition were rapidly checked and time lapse recording was started. All these operations were normally completed within 20 – 30 sec of the addition of the peptide. While laser power and detector gain were previously adjusted using an equally concentrated solution of the peptide, care was taken to verify that the detector gain was set to a low-medium value to avoid pixel saturation at the end of the experiment, due to the strong increase of the fluorescence signal. Images were acquired every 6.5 sec for a total of 15 min (HeLa Kyoto cells) or every 15 sec for a total of 20 min (MCF-7 cells). Finally, the cells were rinsed five times with fresh imaging medium and a new single acquisition was recorded.

For quantification of peptide uptake in a single cell, three regions of interest (ROIs) were selected: one in the cytoplasm, one in the nucleus and one in an unoccupied portion of the support which served as a background reference. First, the background intensity was calculated through the entire stack of pictures, averaged and normalized. Subsequently, the ratio between the average fluorescence values within the cellular ROIs and the normalized background was calculated for each time point. The resulting values were plotted using the analysis software “Origin” (OriginLab Corp., Northampton, MA, USA).

3.17 FLIM of YFP-EGFR in HeLa Kyoto cells incubated with the TAMRA-DADEYL-AM$_3$ peptide

HeLa Kyoto stably transfected with YFP-EGFR were seeded in MatTek dishes as described (sect. 3.14) and cultured overnight to allow adhesion. Cells were rinsed, incubated with a 10 μM solution of the peptide in imaging medium for 20 minutes at room temperature, rinsed again and incubated with freshly prepared EGF in imaging medium at a final concentration of 100 ng/mL. Microscopic observation was performed with an Olympus Fluoview 1000 laser scanning microscope equipped with a 60X / 1.35 NA apochromatic oil objective. Excitation of YFP was achieved using the 488 nm line of an Argon laser and its fluorescence emission was detected in the spectral window 500 – 550 nm. Excitation of TAMRA was achieved using the 561 nm line of a DPSS (diode pumped solid state) laser and its fluorescence emission was detected in the spectral window 580 – 650 nm. For FLIM measurements, the YFP was excited with a 25 ns pulsed diode laser radiation at 470 nm. Emitted light was collected in a photon counter through a 525/50 nm passband filter. Normally, the signal was collected with a continuous exposure to the pulsed laser for 1 – 2 minutes, according to the level of expression of the protein. Analysis of the YFP lifetime was done via the software "SymphoTime" vers. 4.3 (PicoQuant GmbH, Berlin, Germany).

3.18 Acceptor photobleaching experiment in HeLa Kyoto cells incubated with the TAMRA-DADEYL-AM$_3$ peptide

HeLa Kyoto cells were seeded in MatTek dishes or Ibidi μ-VI slides and transfected with GFP-EGFR plasmid as described (sect. 3.14). 24 h *post*-transfection, the cells were washed and incubated with a 5 μM solution of TAMRA-DADEYL-AM$_3$ peptide in imaging medium, for 45 min at room temperature. After rinsing, the cells were incubated with freshly prepared EGF in imaging medium (100 ng/mL) for 15 min at room temperature. The cells were then rinsed and fixed with a 3.7 % (v/v) PFA solution in imaging medium for 20 min at room temperature. After rinsing, excess of PFA was quenched with a 50 mM glycine solution in imaging medium for 20 min at room temperature. Finally, cells were rinsed and imaged under the Leica SP2 AOBS microscope (sect. 3.15). For the photobleaching procedure, selected cells were exposed to 30 cycles of irradiation with the 561 nm laser set at the highest power. FRET efficiencies were calculated using the Leica software routines, according to the formula $FRET_{eff} = (D_{post} - D_{pre})/ D_{post}$, where D_{post} is the fluorescence intensity of the donor after bleaching, D_{pre} is the fluorescence intensity of the donor before the bleaching. During the

experiment, care was taken to keep a constant value for the area of any ROIs, so to have an equal value of the irradiation intensity : area ratio during the photobleaching.

3.19 Preparation of cell lysates

HeLa Kyoto, MCF-7 and MEF cells were each cultivated in monolayers in five 600 mL flasks (Nunc A/S, Kamstrupvej, Denmark). The cells were harvested at 95% confluency by treatment with trypsin/EDTA, resuspended in 50 mL of complete medium, centrifuged (800*g*, 3 min) washed twice with 50 mL of HEPES 20 mM (pH 7.4) containing 10% FBS and twice with the same buffer without FBS, and centrifuging at 800*g* for 4 min after each wash. Finally, the cells were resuspended in 10 mL of ice-cold HEPES 20 mM (pH 7.4) and lysed on ice by sonication. The lysates were divided into 1.5 mL tubes and the cell debris was pelleted by centrifugation (15000*g*, 20 min, + 4°C). The supernatants were pooled and mixed with glycerol up to a final concentration of 20% (v/v). The solutions were clarified through 0.45 μm filters (Millex-HV Durapore membrane, Millipore, Carrigtwohill, Co. Cork, Ireland). 3 mL of these preparations were further concentrated by centrifugation (14000*g*, 3 h, + 4°C over Amicon Microcon concentrators, cut-off 3000 daltons, Millipore). The protein content was quantified with the Bradford assay in a 96-well plate reader (λ = 595 nm) using BSA as a standard and adjusted to 2 μg/μL for each cell lysate. The preparations were kept frozen (– 20°C) in 50 μL aliquotes.

3.20 Esterase assay of cell lysates, PLE, mouse and fetal bovine sera using α-naphthyl acetate

95 μL of HEPES (20 mM, pH 7.4) was added to a 96-well plate, followed by 3 μL of HeLa Kyoto, MEF or MCF-7 cell lysates, or 3 μL of mouse or fetal bovine serum,[12] or 3 μL (3 mU) of a diluted solution of PLE (Sigma, Steinheim, Germany) in HEPES (20 mM, pH 7.4). 2 μL of a 10 mM stock solution in ethanol of α-naphthyl acetate was subsequently added (0.2 mM final concentration). The reactions were stopped after 30 min (for cell lysates) or 10 min (for PLE, mouse serum, fetal bovine serum) by adding 25 μL of a solution of Fast Blue B salt (tetra-azotized *o*-dianisidine/$ZnCl_2$ 0.3% w/v) in aqueous 3.5% (w/v) SDS, freshly prepared and kept in the dark. After 15 min of incubation (at room temperature and at dark), the plate was inserted in a Tecan 96-well plate spectrophotometer and the absorbance reading

[12] Heparin-containing mouse serum was provided by the EMBL Mouse facility and kept at – 20°C until use.

was performed at 620 nm. Each sample was assayed in triplicate. Blank solutions were prepared as described but without addition of α-naphthyl acetate, while a 0.2 mM solution of α-naphthol (from a 10 mM ethanolic stock solution) in HEPES (20 mM, pH 7.4) served as a positive control. To assess esterase activity after heat treatment, small aliquotes of cell lysates, mouse and fetal bovine sera were incubated at 56°C for 45 min and then used as described above. The protease inhibitor cocktail (EDTA-free, in tablets, Roche, Mannheim, Germany) was prepared as a 7x stock solution by dissolving one tablet in 1.5 mL of water and it was used at 1x final concentration as recommended by the manufacturer.

3.21 Mass analysis of products of esterase activity over AM-esterified peptides

To a 5 μM solution of TAMRA-DADEYL-AM_3, TAMRA-EYL-AM_1, TAMRA-EAEEYL-AM_3 peptides in HEPES 20 mM (pH 7.4) were added cell lysates or mouse serum up to a final concentration of 3% (v/v) (100 μL total volume), or 3 mU of PLE. The samples were incubated at room temperature for 30 min (cell lysates, mouse serum) or at 37°C overnight (PLE). Proteins were precipitated by adding 400 μL of ice-cold ethanol and solutions were kept on ice for 30 min. Afterwards, the samples were centrifuged at + 4°C (15000*g*, 30 min) and the supernatants were concentrated *in vacuo*. The concentrated material was resuspended in 1 mL of a 10% (v/v) ACN solution in water containing 0.1% TFA (v/v). The solution was desalted through a SPE-RP C-18 cartridge (50 mg resin/1 mL capacity, Supelco, Bellefonte, PA, USA), previously rinsed with 1 mL MeOH and equilibrated with 1 ml of a 10% (v/v) ACN solution in water (+ 0.1% TFA, v/v), by washing with 1 mL of the equilibration solution and eluting the products with 1 mL of a 50% (v/v) ACN solution in water (+ 0.1% TFA, v/v). The eluate was concentrated *in vacuo* up to ca. 150 μL and directly used for MALDI or ESI-MS analysis.

4. Results

4.1 The rhodamine-labelled LRh-TAT$_{49-57}$ and TAT(K-LRh) peptides and their uptake in living cells

The arginine-rich TAT$_{49-57}$ domain (Arg-Lys-Lys-Arg-Arg-Gln-Arg-Arg-Arg) is among the most studied cell-penetrating peptides, as documented by the extensive literature available [76, 125, 137]. While green fluorescent derivatives have been described in several investigations [32, 83, 101, 156, 157], the use of a red fluorescent conjugate has been reported less often [157]. Moreover, a previous study indicated that the substitution Gln54Ala in the wild-type sequence was not detrimental to the translocation of the peptide in living cells, while any single Arg/Ala or Lys/Ala substitution had a remarkable negative influence [81].

Following these indications, two peptides were synthesized and equipped with the red fluorophore Lissamine™-rhodamine (LRh). The peptides, named LRh-TAT$_{49-57}$ and TAT(K-LRh), differed for the site of conjugation: while in LRh-TAT$_{49-57}$ the fluorophore was linked to the N-terminus via an aminohexanoic acid spacer, in the branched derivative TAT(K-LRh) the fluorophore occupied a lateral position. In order to obtain this novel TAT conjugate, a Lys residue was incorporated (as Fmoc-Lys(Mtt)-OH) in the sequence in place of the wild-type Gln (Gln54Lys). Upon completion of the linear sequence and acylation of the free N-terminus, the orthogonal Mtt protecting group was removed, allowing the sequential coupling of the aminohexanoic acid linker and the LRh dye on the resin. The structures of the two peptides are represented in Fig. 4.1.1.

It is important to underline the fact that, at the time the TAT peptides were synthesized, our research group lacked pieces of equipment (mass spectrometer, double-pump preparative HPLC, semi-preparative RP columns) which later allowed accurate purification and characterization of these and the peptides synthesized thereafter. Thus, silica-gel plates were initially used for purification of the TAT peptides, with eluent mixtures composed of ammonia, alcohols (methanol, isopropanol or *n*-butanol) and chloroform in different ratios. This procedure was overall unsatisfying. In particular, desorption of the compounds from the chromatographic plate was always troublesome, with significant loss of material and contamination with silica particles. Despite the removal of the bulk of by-products (visible as discrete fluorescent bands on the silica plate) and the identification of the fractions containing the desired peptides via MALDI mass spectrometry, the quality of these purifications remained poor and could not be improved until HPLC and LC/MS analyses became a regular routine in our laboratory, and the necessary instrumental skills were acquired.

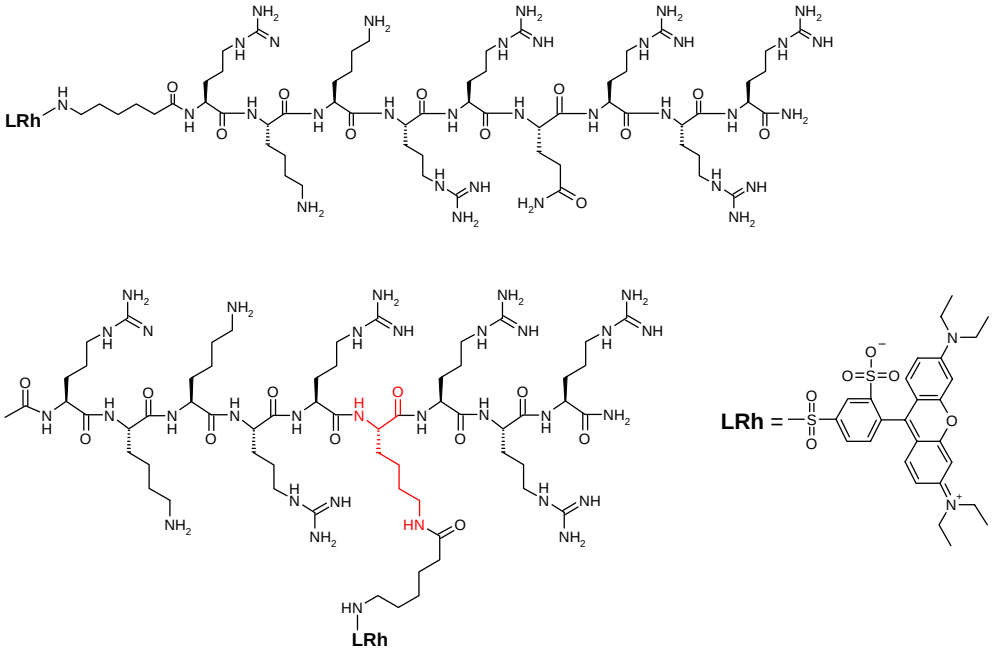

Fig. 4.1.1. Lissamine™-rhodamine derivatives of the TAT$_{49-57}$ peptide. (**top**) LRh-TAT$_{49-57}$. (**bottom**) TAT(K-LRh), with the Lys residue substituting the wild-type Gln coloured in red (Materials and methods, sect. 3.2, 3.3).

In preliminary experiments, HeLa Kyoto cells were incubated with a solution of partially-purified TAT peptides. As a result, both peptides showed uptake into vesicles, which were scattered throughout the cytoplasm and the perinuclear area (Fig. 4.1.2 *a*, *b*). No staining of the cell nuclei was detected, despite a putative nuclear localization sequence (NLS) being previously argued in this region of the TAT peptide [32, 82]. Moreover, the distribution was in contrast from that documented in fixed cells [32, 157]. Interestingly, the TAT(K-LRh) peptide was internalized with the same efficiency, indicating that the location of the dye in the molecule did not impair the uptake (Fig. 4.1.2 *b*).

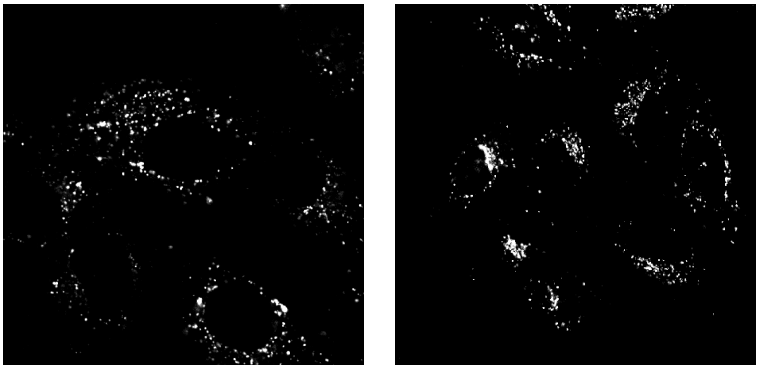

a b

Fig. 4.1.2. Partially-purified LRh-TAT and TAT(K-LRh) peptides showed uptake in vesicles in living HeLa Kyoto cells. Cells were incubated with a 10 μM solution of either LRh-TAT (**a**) or TAT(K-LRh) (**b**) peptides in imaging medium for 15 min at room temperature. After rinsing, cells were imaged unfixed. Both peptides, which had a low grade of purity, were internalized in vesicles distributed throughout the cytoplasm and the perinuclear area. No nuclear fluorescence was visible (Material and methods, sect. 3.15).

Nevertheless, more recent literature data warned about an artifactual redistribution of TAT (and other polycationic peptides) as a result of fixation procedures [83]. Indeed, those observations could be verified when HeLa Kyoto cells were fixed after exposure to the LRh-TAT_{49-57} and TAT(K-LRh) peptides: the fluorescent signal redistributed evenly in the cytoplasm of the cells, with additional staining of the nucleoli (Fig. 4.1.3).

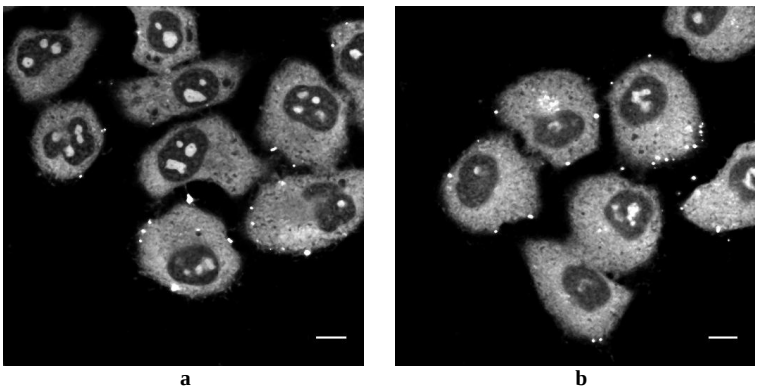

a b

Fig. 4.1.3. LRh-TAT and TAT(K-LRh) peptides redistributed evenly into cytoplasm and nucleoli of HeLa Kyoto cells following fixation. Cells were incubated with a 10 μM solution of either LRh-TAT (**a**) or TAT(K-LRh) (**b**) peptides in imaging medium for 15 min at room temperature, washed, fixed with a solution of MeOH:acetone (1:1, v/v) at room temperature for 3 min, washed and imaged. As a result of fixation, both peptides redistributed evenly in the cytoplasm, showing at the same time a high affinity for nucleolar structures. Scale bar = 10 μm (Material and methods, sect. 3.15).

More recently (during the completion of this experimental work), a careful purification and characterization of the LRh-TAT_{49-57} and TAT(K-LRh) peptides could be achieved. Surprisingly, analytical HPLC showed the LRh-TAT_{49-57} peptide as a mixture of regioisomers, obtained in 98% overall purity after semi-preparative purification (Fig. 4.1.4).

On the contrary, the TAT(K-LRh) peptide was obtained as a single product of 97% purity (Fig. 4.1.5). This finding may reflect the fact that, routinely, different batches of the rhodamine dye were used. Nevertheless, none of these preparations clearly stated the presence of isomers in the composition of the product. Final purification afforded these peptides in low yield (0.4 and 0.2%, respectively), nevertheless enough material was obtained to perform new experiments in HeLa Kyoto cells.

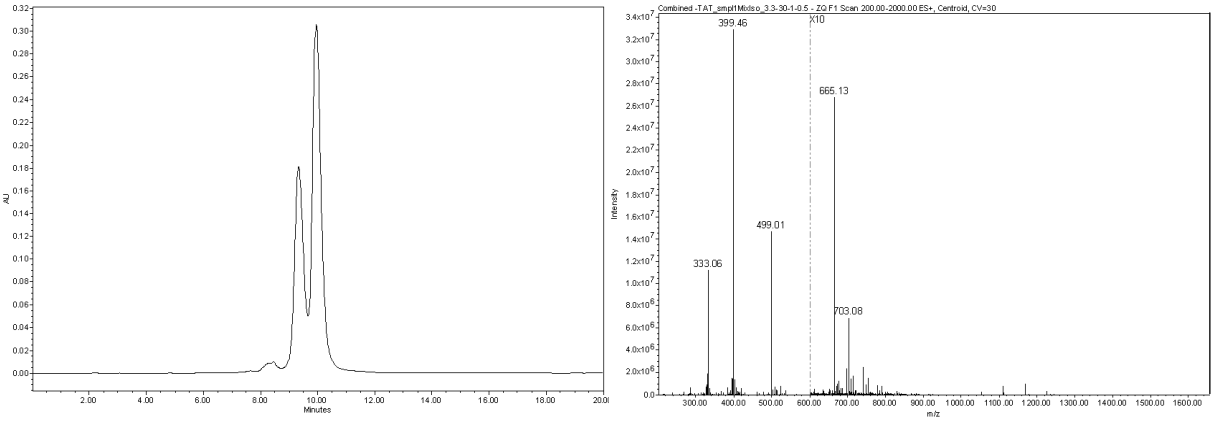

a **b**

Fig. 4.1.4. The LRh-TAT$_{49-57}$ peptide. (a) Analytical HPLC performed after semi-preparative purification showed two regioisomers eluting after 9.3 and 9.9 min, with a 98% overall purity. (**b**) ESI-MS confirmed both regioisomers as [M+3H$^+$/3] (m/z 665.13), [M+4H$^+$/] (m/z 499.01), [M+5H$^+$/5] (m/z 399.46) and [M+6H$^+$/6] (m/z 333.06) species (Material and methods, sect 3.2).

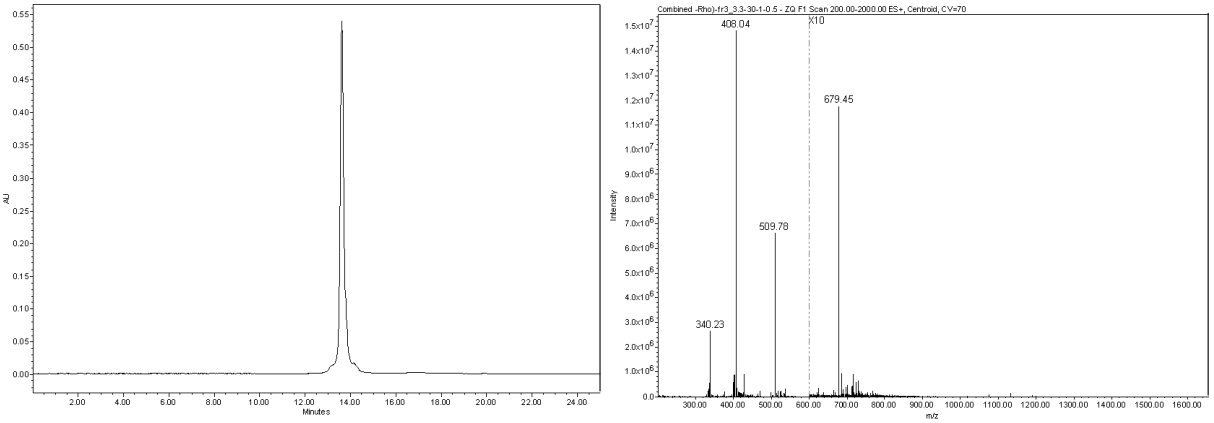

a **b**

Fig. 4.1.5. The TAT(K-LRh) peptide. Analytical HPLC performed after semi-preparative purification showed a single product eluting after 13.6 min (purity = 97%). (**b**) ESI-MS confirmed the identity of the peptide as [M+3H$^+$/3] (m/z 679.45), [M+4H$^+$/4] (m/z 509.78), [M+5H$^+$/5] (m/z 408.04) and [M+6H$^+$/6] (m/z 340.23) species (Material and methods, sect 3.3).

Surprisingly, after incubation with a 5 μM solution of either LRh-TAT$_{49-57}$ or TAT(K-LRh), the fluorescence localized differently from what observed earlier (Fig. 4.1.2): the peptides appeared to concentrate in compartments resembling the endoplasmic reticulum or

mitochondria (Fig. 4.1.6). Vesicles were virtually absent, while some bright spots were noticed in the periphery of the plasma membrane, indicating possible sites of peptide aggregation [101].

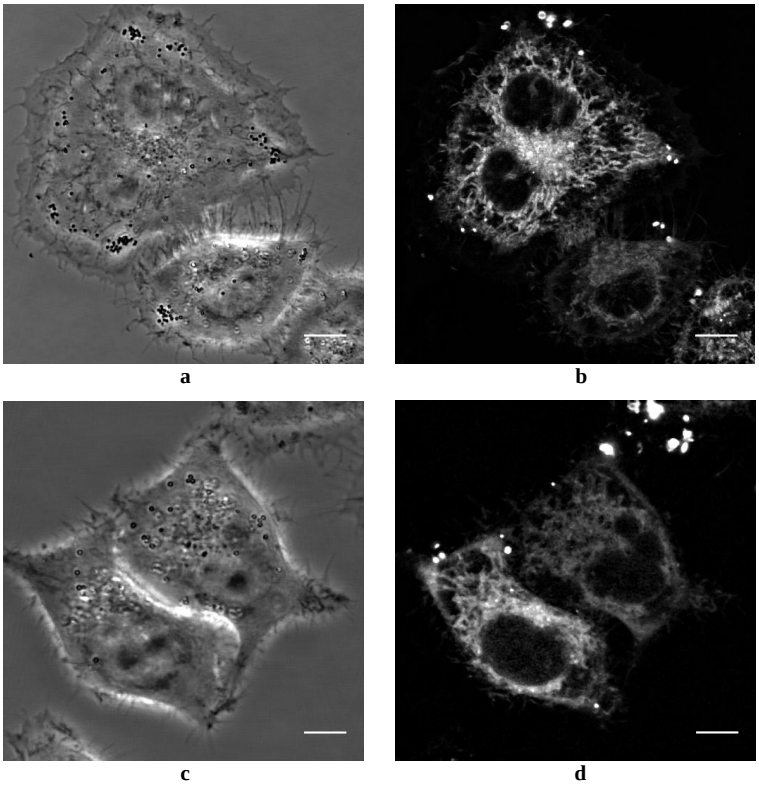

Fig. 4.1.6. Distribution of purified LRh-TAT$_{49-57}$ and TAT(K-LRh) peptides in living HeLa Kyoto cells. Cells were incubated with a 5 μM solution of either LRh-TAT$_{49-57}$ (**a, b**) or TAT(K-LRh) (**c, d**) peptides in imaging medium for 10 min at room temperature. Fluorescence distribution suggested localization of peptides in compartments such as endoplasmic reticulum or mitochondria. Bright fluorescent spots were also detected on the plasma membrane. Pictures ***a*** and ***c*** represent transmitted light (phase contrast) images. Scale bar = 10 μm (Material and methods, sect. 3.15).

Notably, LRh-TAT$_{49-57}$ appeared to exert toxic effects when HeLa Kyoto cells were incubated with a 10 μM solution for 5 min, a circumstance which induced abnormal changes in the cell shape and cytoplasmic vacuolization (Fig. 4.1.7). TAT(K-LRh) was not tested under these conditions, nevertheless both peptides appeared to be well tolerated by this cell type when used at 5 μM concentration and up to 10 min of incubation time (room temperature).

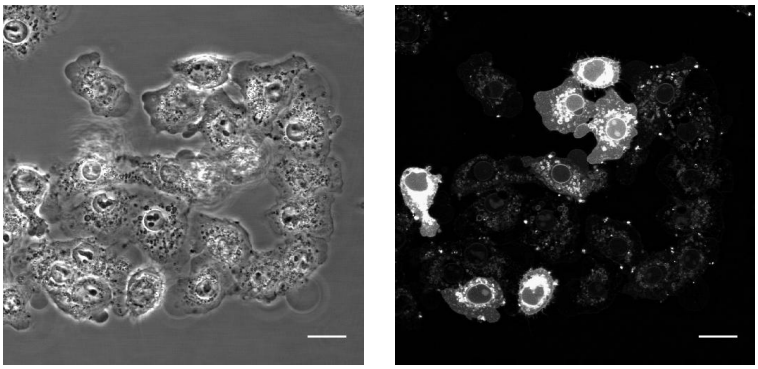

a b

Fig. 4.1.7. LRh-TAT$_{49-57}$ exerted toxic effects on HeLa Kyoto cells at a higher concentration. Cells were incubated with a 10 μM solution of LRh-TAT peptide in imaging medium (**a, b**) for 5 min at room temperature. Abnormal changes in cell shape were evident, with a concomitant cytoplasmic vacuolization. Picture ***a*** represent a transmitted light (phase contrast) image. Scale bar = 20 μm (Material and methods, sect. 3.15).

The behaviour of the LRh-TAT$_{49-57}$ peptide was also tested in other cell types. In MEF cells, uptake was evident after an incubation of 10 min and a peptide concentration of 5 μM (results not shown), but a higher number of cells appeared stained after 30 min with a peptide concentration of 10 μM. No clear sign of toxicity was visible under these conditions (Fig. 4.1.8). MCF-7 cells were stained after exposure to a 2.5 μM solution for 30 min (Fig. 4.1.9), while the peptide was toxic when cells were incubated 10 min with a concentration of 10 μM (results not shown).

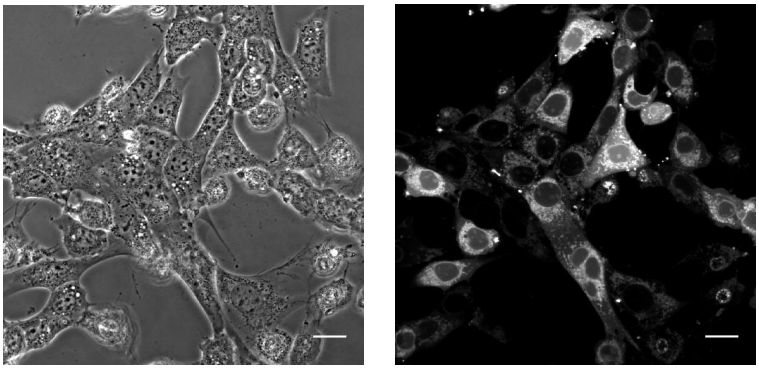

a b

Fig. 4.1.8. Uptake of the LRh-TAT$_{49-57}$ peptide by MEF cells. Cells were incubated with a 10 μM solution of LRh-TAT$_{49-57}$ peptide in imaging medium for 30 min at room temperature (**a, b**). Uptake was visible in a large number of cells. Picture ***a*** represent a transmitted light (phase contrast) image. Scale bar = 20 μm (Material and methods, sect. 3.15).

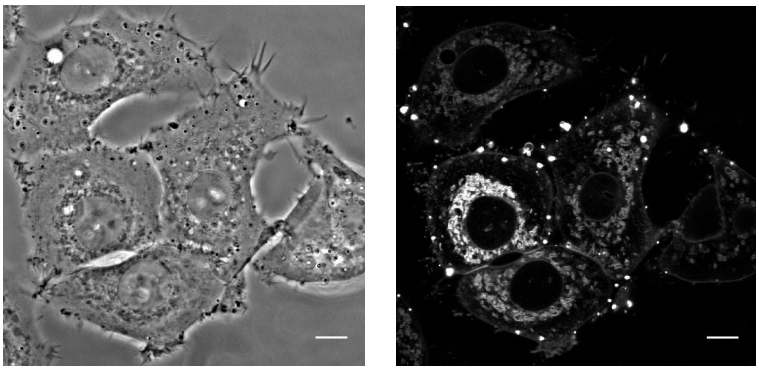

a **b**

Fig. 4.1.9. Uptake of the LRh-TAT$_{49-57}$ peptide by MCF-7 cells. Cells were incubated with a 2.5 μM solution of LRh-TAT peptide in imaging medium for 30 min at room temperature (**a, b**). Uptake was visible in membrane-bound compartments in the perinuclear area. Picture ***a*** represent a transmitted light (phase contrast) image. Scale bar = 20 μm (Material and methods, sect. 3.15).

The uptake of the TAT(K-LRh) peptide in MEF and MCF-7 cell types is currently under investigation. The use of known fluorescent markers will be instrumental in order to possibly clarify the nature of the compartments where these rhodamine-labelled TAT peptides appear to accumulate. In particular, it will be of interest to verify whether the two peptides distribute in the same organelles in living cells and to test the possible effect on the distribution due to the use of different fluorophores.

4.2 The rhodamine labelled LRh-DADEYL probe and its Penetratin conjugate LRh-DADEYL-PEN peptide

The condensation of the Lissamine™-rhodamine dye (Fig. 3.1.2) was the most troublesome step toward the synthesis of the LRh-DADEYL probe (Fig. 4.2.1). While it is common practice in the synthesis of fluorescently labelled peptides to insert a spacer between a bulky fluorophore and the peptide sequence, previous studies in our laboratory had shown the benefits afforded by the insertion of a polar, hydrophilic linker to enhance water solubility of this probe [158]. Thus, the linker AEEAc was inserted following the residue Asp-6. Moreover, earlier observations revealed how the conjugation of the dye itself to this linker was enhanced by the presence of a cysteine residue as a "junction node". With the additional aim of linking the probe to the Penetratin sequence via a disulfide bond, this residue could indeed accomplish two functions simultaneously.

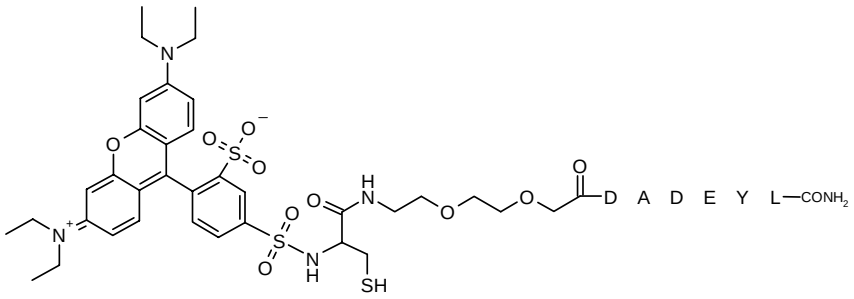

Fig. 4.2.1. The LRh-DADEYL probe. Upon completion of the amino acid sequence the hydrophilic linker AEEAc was introduced, while a Cys residue served as "junction node" to facilitate conjugation of the Lissamine™-rhodamine dye as a sulfonamide. The free sulfhydryl group served for the subsequent fusion to the ActPEN peptide. The carboxy terminal group was in the form of amide ($CONH_2$) due to the use of the Rink amide resin (Materials and methods, sect. 3.4).

Notably, differences were observed in the coupling of the dye according to its commercial source and the protocol used for conjugation: LRh-SO_2Cl obtained from Acros (certified "pure" by the manufacturer) failed to couple in the presence of DIPEA; on the other hand, LRh-SO_2Cl from Fluka successfully coupled only in the presence of TEA. Repeating the protocol twice did not guarantee saturation of all free amino groups on resin, as revealed by HPLC of the crude reaction mixture (Fig. 4.2.2, *a*). Furthermore, the utilization of the dye from this commercial source – for which no specification of purity was given – was always characterized by the appearance of several by-products, the most prominent being a [M + 34] a.m.u. species eluting 1.5 min later than the desired product (Fig. 4.2.2, *a*). Despite the

presence of various contaminants the desired product was successfully purified by semi-prep HPLC (Fig. 4.2.2, *b*), although the final yield was low (0.3%, sect. 3.4)

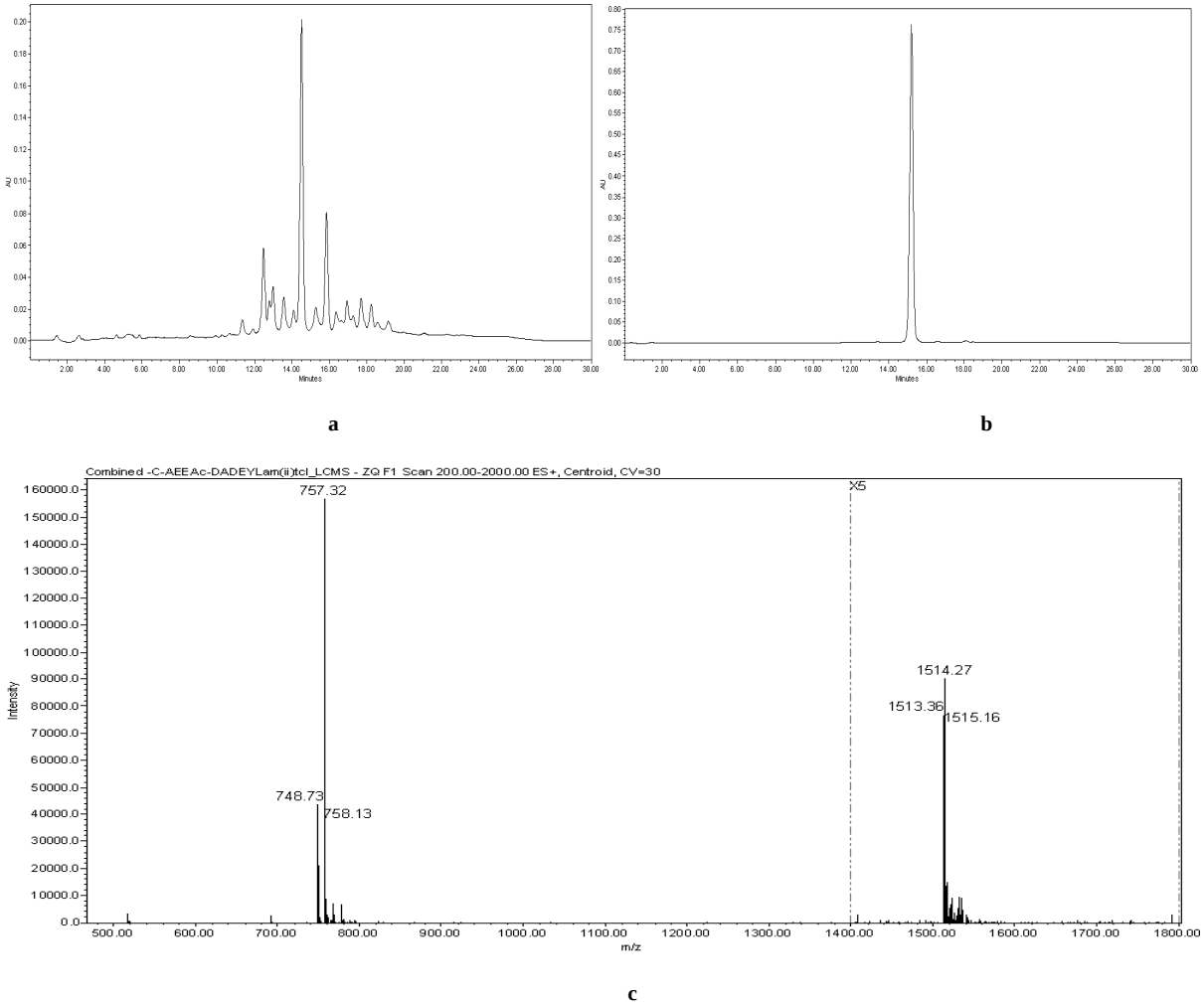

Fig. 4.2.2. Analytical HPLC and MS over LRh-DADEYL peptide (Merck Lichrosorb RP-18 250 x 4 mm x 10 um). (a) Chromatogram of the crude product after LRh conjugation to the resin-bound peptide: the peak eluting at 12.5 min represented unlabelled peptide, the peak eluting at 14.6 min corresponded to the desired product and the peak eluting at 16 min was an uncharacterized by-product with a mass difference of + 34 a.m.u. **(b)** LRh-DADEYL peptide after semi-preparative purification. (**c**) ESI-MS of the product identified as a [M + H^+] (m/z 1513.36) and [M + $2H^+$/2] (m/z 757.32) species (Material and methods, sect. 3.4).

The conjugation of the LRh-DADEYL probe to the commercially available vector "activated Penetratin" (ActPEN) was possible due to the presence of a N-terminal pyridyl disulfide function.[13] Such a group enables the fusion via a disulfide bond to a free thiol group. Thus, the branched peptide LRh-DADEYL-PEN was synthesized by mixing equimolar amounts of the two species in a water/ACN solution (Fig.4.2.3, *a*).

[13] The exact sequence and composition of the commercial "activated Penetratin" are not known. The activating function is likely to be the 3-nitro-2-pyridylthio group of a N-terminal cysteine. Indeed, this kind of amino acid is available as a building block for SPPS (see Fig. 4.2.3 b).

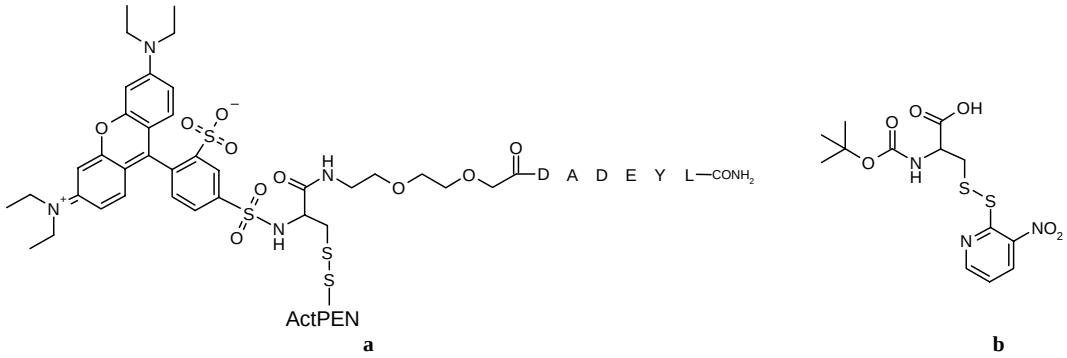

Fig. 4.2.3. LRh-DADEYL-PEN conjugate. (a) Conjugation to the sulfhydryl group of the cysteine residue in LRh-DADEYL peptide via the N-terminal pyridyl disulfide function in the "activated Penetratin" (Materials and methods, sect. 3.5). **(b)** Boc-Cys(Npys)-OH, a commercially available, activated cysteine residue for SPPS, suitable for the formation of disulfides (see also footnote 1).

In practice, the conjugation proceeded poorly (Fig. 4.2.4, *a*). Notably, most of the probe simply did not fuse to ActPEN. In addition to that, and despite the utilization of degassed solvents in an argon atmosphere, a significant portion of LRh-DADEYL homodimerized (Fig. 4.2.4 *a*; 4.2.5 bottom panel) indicating that the steric hindrance due to the adjacent rhodamine may not be the explanation for the low conjugation levels to ActPEN. A similar protocol using neat ACN reduced significantly the formation of the dimer without any increase of the desired product (Fig. 4.2.4, *b*). Poor solubility of the ActPEN peptide in these conditions could be reasoned. Nevertheless, an organic co-solvent appeared necessary in the reaction mixture in order to keep the LRh-DADEYL peptide freely soluble. Despite the low efficiency of the conjugation, all the species eluted with distinct retention times, making purification straightforward. The desired product could be isolated in 12% yield (sect. 3.5). The homodimer $[LRh\text{-}DADEYL]_2$ could also be isolated and treated with the disulfide reducing agent TCEP, although this step was not routinely performed. However, this product was employed as a negative control in the uptake experiments in living cells (sect. 4.3).

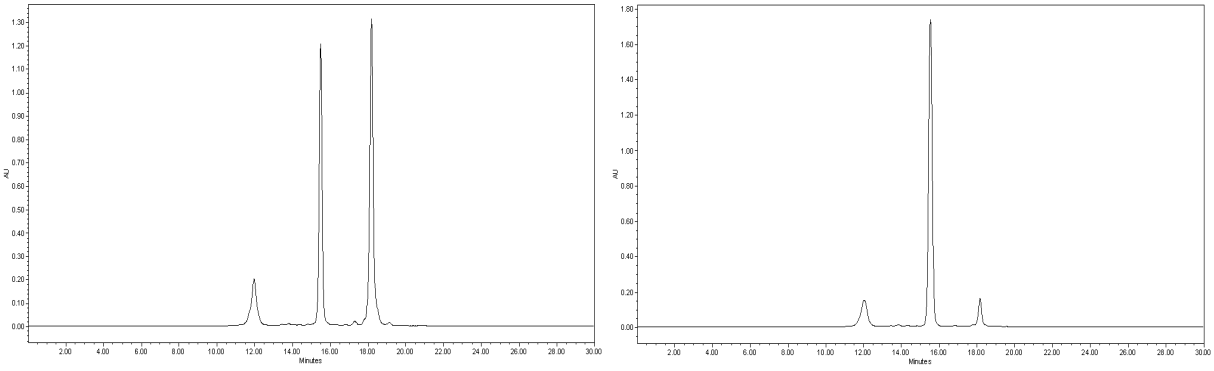

a **b**

Fig 4.2.4. HPLC analysis of the conjugation products between ActPEN and LRh-DADEYL peptides (Merck Lichrosorb RP-18 250 x 4 mm x 10 µm). (a) Reaction performed in water/ACN between equimolar amounts of LRh-DADEYL and ActPEN peptides: the product eluting at ca. 12 min corresponded to the conjugate, the product eluting at ca. 15.5 min was unreacted LRh-DADEYL and the product eluting at ca. 18 min appeared to be the $[LRh\text{-}DADEYL]_2$ homodimer **(b)** The same reaction performed in ACN. (Materials and methods, sect. 3.5).

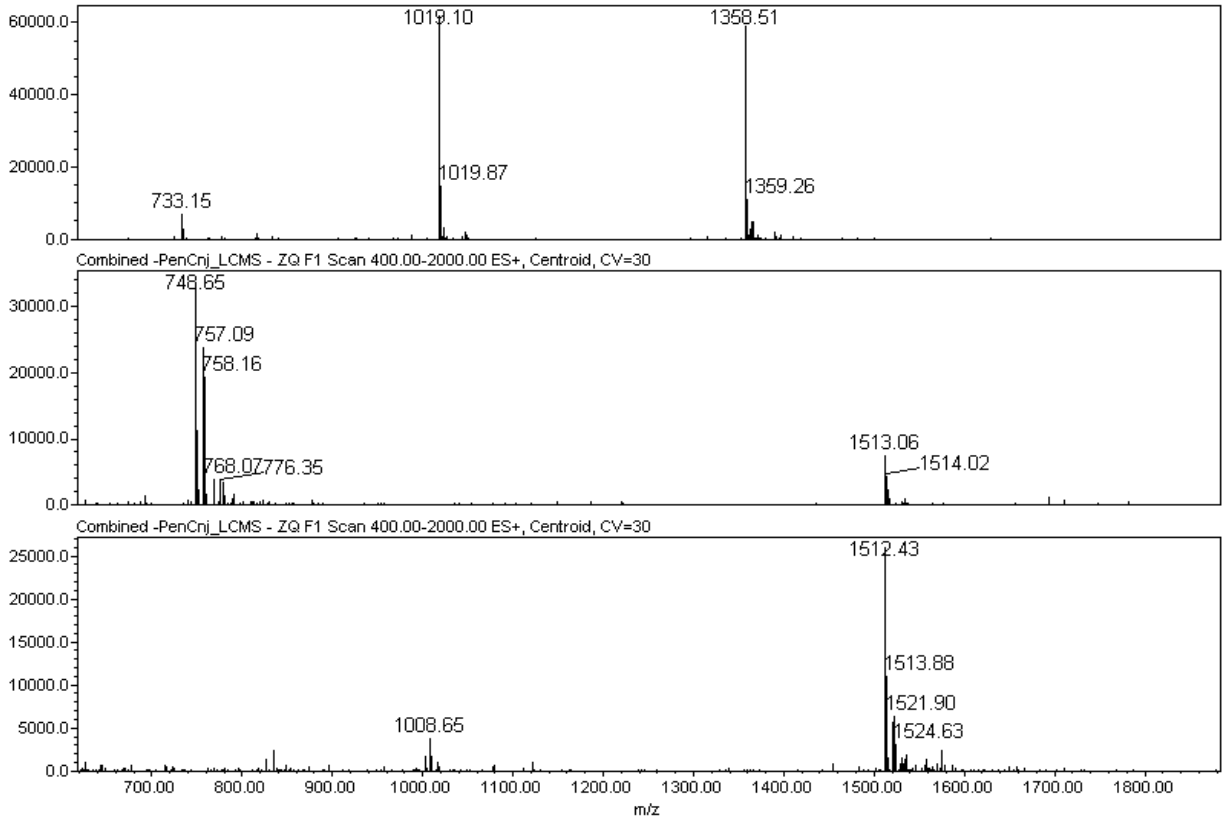

Fig 4.2.5. ESI-MS analysis of the conjugation products between ActPEN and LRh-DADEYL peptides. Top panel: conjugated product LRh-DADEYL-PEN peptide as $[M+3H^+/3]$ (m/z 1358.51) and $[M+4H^+/4]$ (m/z 1019.10) species. Centre panel: monomer LRh-DADEYL as $[M+H^+]$ (m/z 1513.06) and $[M+2H^+/2]$ (m/z 757.09) species. Bottom panel: dimer $[LRh\text{-}DADEYL]_2$ as $[M+2H^+/2]$ (m/z 1512.43) and $[M+3H^+/3]$ (m/z 1008.65) species (Materials and methods, sect. 3.5).

4.3 Uptake of LRh-DADEYL-PEN conjugate by living MEF and MCF-7 cells

The conjugate product LRh-DADEYL-PEN was designed with the rationale of creating a system where the vector Penetratin could, once inside the cells, release its cargo moiety thanks to the susceptibility of disulfide bridges toward reduction in the cytoplasmic environment. Differently from the "tandem" constructs where vector and cargo are permanently fused [116, 117], here the cargo molecule would not suffer from an unpredictable behaviour of the vector inside the cell. Moreover, the use of a purified conjugated product enables us to perform observations and draw conclusions free from artefacts that fluorescent contaminant species (i.e. unconjugated peptide, dye, by-products, etc.) may create.

When living MEF cells were incubated with purified LRh-DADEYL-PEN conjugate (1 μM) at room temperature, the cells specifically accumulated the construct, as shown by the lack of staining by the fluorescent unconjugated monomer LRh-DADEYL or the faint staining by the homodimer $[LRh\text{-}DADEYL]_2$ under the same experimental conditions (Fig. 4.3.1 *b*, *e*, *g*). A magnified inspection of the cells' interior revealed however a distinct focal distribution in cytoplasm and the perinuclear area, suggesting an endosomal accumulation of the probe (Fig. 4.3.1 *c*). These findings would support recent literature data on uptake of the Penetratin vector in living cells [85].

Surprisingly, there was no internalization by MCF-7 cells (Fig. 4.3.2). The microscopic observations revealed how the conjugate remained excluded from the cell cytoplasm, or strongly adhered in patches along the plasma membrane even after repeated washing. This led to the speculation that MEF and MCF-7 cells may have a different behaviour toward the internalization of the Penetratin vector, or its conjugates.

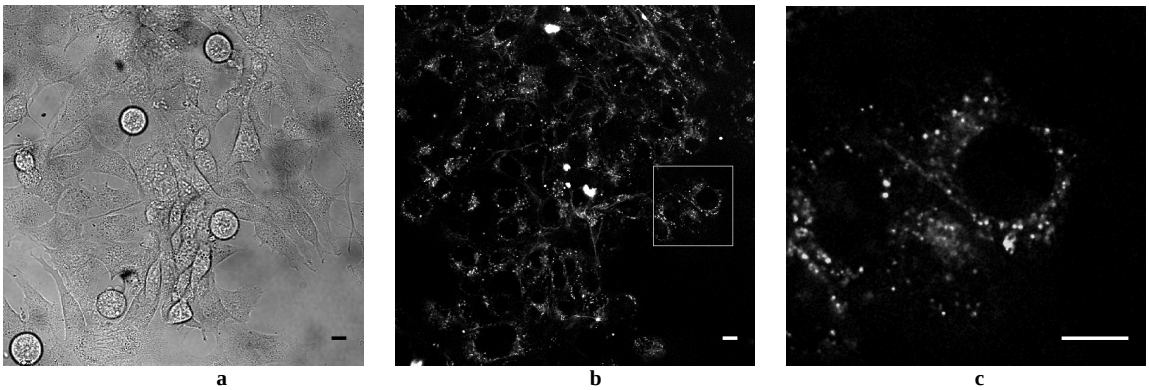

a **b** **c**

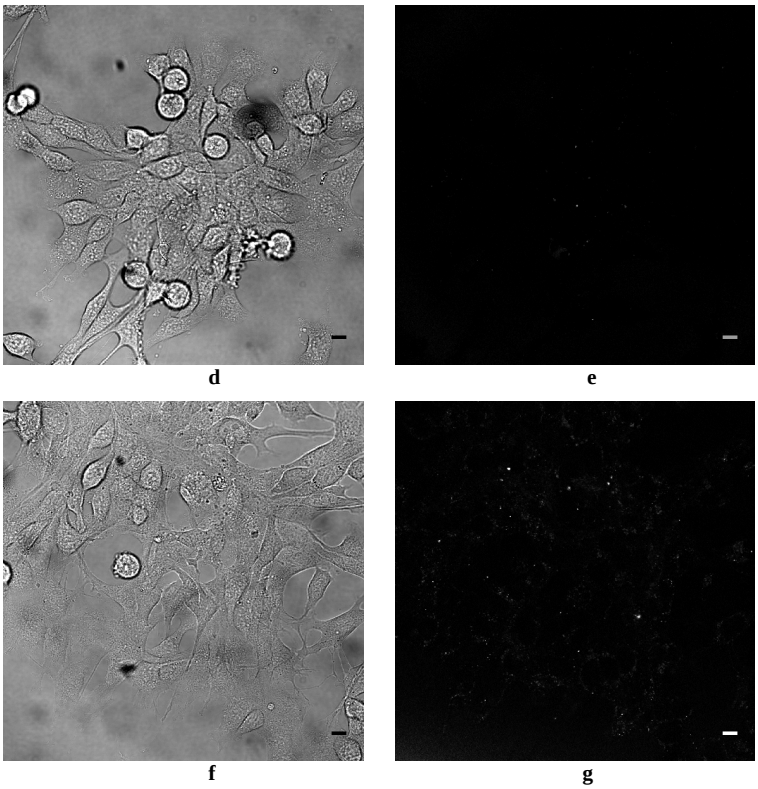

Fig. 4.3.1. LRh-DADEYL-PEN conjugate showed focal cytoplasmic distribution in MEF cells. Cells were incubated for 45 min at room temperature with a 1 μM solution of the probe conjugate in imaging medium. The Penetratin conjugate was taken up by the cells in endosomal compartments (**b**, **c**. **Note**: the diffused level of fluorescence visible is due to out-of-focus fluorescence and not to a real diffused distribution of the probe). The monomer LRh-DADEYL (**d-e**) or the dimer $[LRh\text{-}DADEYL]_2$ (**f-g**) showed no or neglegible uptake in the same experimental conditions. Pictures ***a***, ***d***, ***f*** represent transmitted light images. Fluorescent images ***b***, ***c***, ***e***, ***g*** were acquired using constant microscope settings (laser power and detector gain). Picture ***c*** represent an enlarged view of the area marked in picture ***b***. Scale bar = 10 μm.

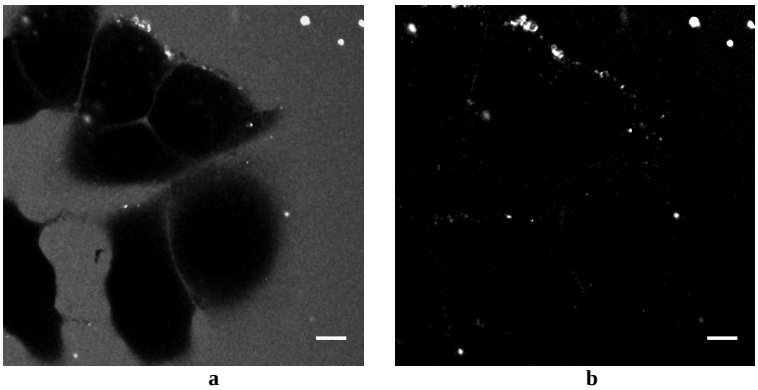

Fig. 4.3.2. LRh-DADEYL-PEN conjugate did not penetrate into MCF-7 cells. (**a**) Cells were incubated with a 1 μM solution of the probe conjugate in imaging medium (+ 1% FBS) for 45 min at room temperature. No significant uptake was visible in the cytoplasm while aggregates appeared on the plasma membrane. (**b**) The same area imaged after extensive rinsing of the dish. Scale bar = 20 μm.

4.4 The fluorescent Penetratin derivatives OG-PEN1 and RR-PEN1

In order to understand further the different uptake behaviour of the LRh-DADEYL-PEN conjugate by MEF and MCF-7 cells a synthesis of novel fluorescent derivatives of Penetratin was undertaken. This was necessary, since fluorescent Penetratins are not available commercially at present. The aim here was to elucidate how differences in the cargo (simulated now by two different fluorophores) could affect the internalization in one or more cell type.

These new fluorescent probes were based on the original sequence of Penetratin, termed PEN-1, which has been described in detail in the literature [34, 75]. The fluorophores Oregon Green® 488 iodoacetamide and Rhodamine Red™ C_2-maleimide were chosen (Fig. 3.1.2) and conjugated *post synthesis* to the free thiol group of an N-terminal cysteine residue. Differently to the LRh-DADEYL-PEN conjugate (Fig. 4.2.3 *a*) the covalent bond between the fluorophore and the peptide was in this case not susceptible of reduction in the cell.

The synthesis started with the assembly of the Fmoc-PEN1 peptide (Fig. 4.4.1). The Fmoc group of the N-terminal cysteine residue was deliberately left in place before the final cleavage from the resin, because it was observed that its presence was beneficial in retarding the elution of the peptide, allowing better conditions for purification by HPLC (Fig. 4.4.2).

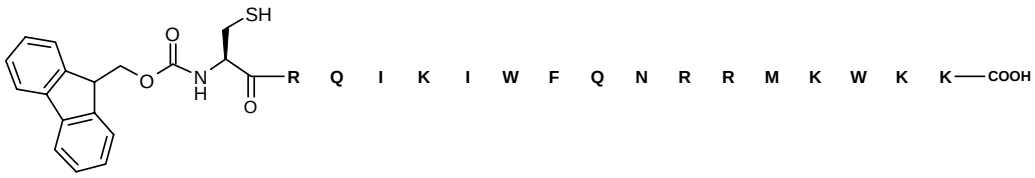

Fig. 4.4.1. The Fmoc-PEN1 peptide. A Cys residue was introduced N-terminally to the Arg-16 to allow conjugation with fluorescent dyes. The Fmoc group was left in place to facilitate the purification of the peptide (Materials and methods, sect. 3.6).

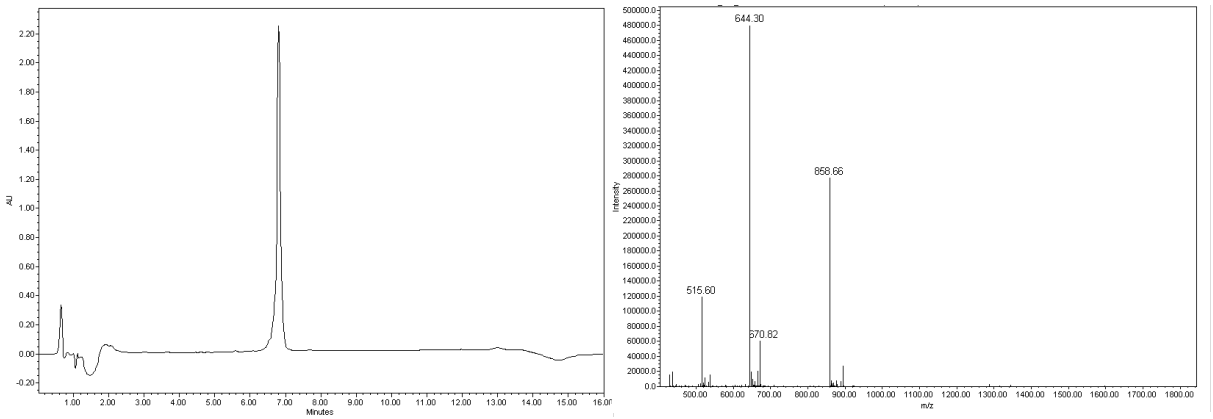

b **c**

Fig. 4.4.2. LC/MS analysis over the Fmoc-PEN1 peptide. Analytical HPLC (**a**) and ESI-MS (**b**) of the pure product, characterized as [M+3H$^+$/3] (m/z 858.66), [M+4H$^+$/4] (m/z 644.40) and [M+5H$^+$/5] (m/z 515.60) species (Materials and methods, sect. 3.6).

The products of the conjugation between Fmoc-PEN1 and the fluorophores, depicted in Fig. 4.4.3, were in both cases composed of two species, due to the use of commercial mixtures of isomers for both Rhodamine Red™ C_2-maleimide and Oregon Green® 488 iodoacetamide (Fig. 3.1.2). These isomers could be resolved – at least partially – by analytical HPLC and characterized by ESI-MS (Fig. 4.4.4).

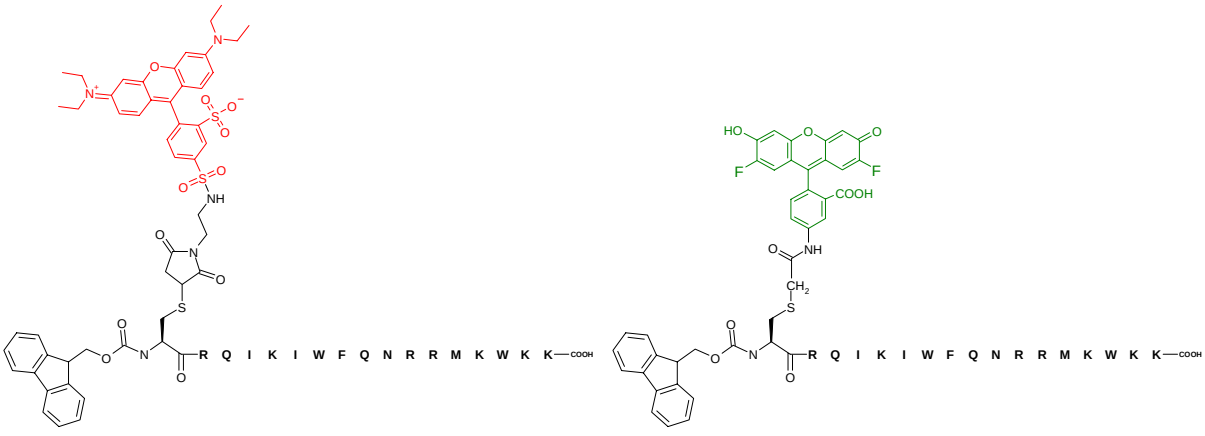

a **b**

Fig. 4.4.4. The RR-PEN1 and OG-PEN1 peptides. The two dyes were linked to the Penetratin sequence via the sulfhydryl group of the terminal Cys residue. (**a**) RR-PEN1. (**b**) OG-PEN1 (Material and methods, sect. 3.7).

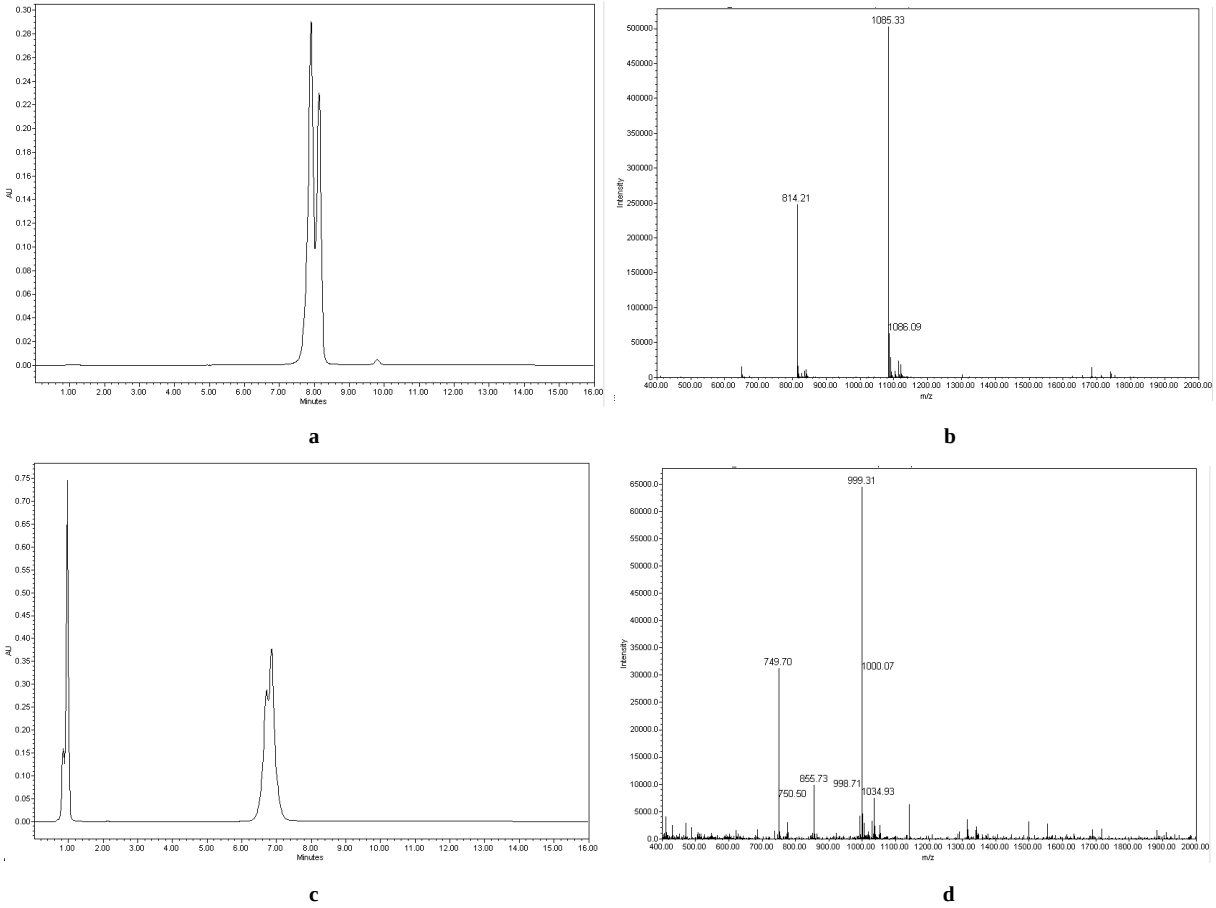

Fig. 4.4.4. LC/MS analysis over the RR-PEN1 and OG-PEN1 peptides. (**a**) HPLC of purified RR-PEN1. (**b**) ESI-MS of RR-PEN1: the peptide was identified as [M+3H$^+$/3] (m/z 1085.33) and [M+4H$^+$/4] (m/z 814.31) species. (**c**) HPLC of purified OG-PEN1. (**d**) ESI-MS of OG-PEN1: the peptide was identified as [M+3H$^+$/3] (m/z 999.31) and [M+4H$^+$/4] (m/z 749.70) species (Materials and methods, sect. 3.7).

4.5 Uptake of OG-PEN1 and RR-PEN1 in living MEF cells

In addition to the previous experiments, a comparative study of the new Penetratin derivatives was made using MEF and MCF-7 cells as model.

An initial observation was made when MEF cells were incubated at room temperature with the two conjugates: while RR-PEN1 appeared to be internalized into the cell body in a focal, perinuclear fashion (Fig. 4.5.1 *a*, *b*), the uptake of OG-PEN1 was not detected (Fig. 4.5.1 *c*, *d*). Notably, the latter conjugate was only internalized when the experiment was performed at 37°C (Fig. 4.5.1 *e*, *f*). These observations suggested how the different cargo may have contributed to the adoption of a different mechanism of internalization by MEF cells, which in the case of OG-PEN1 proved effective only at physiological temperature (37°C).

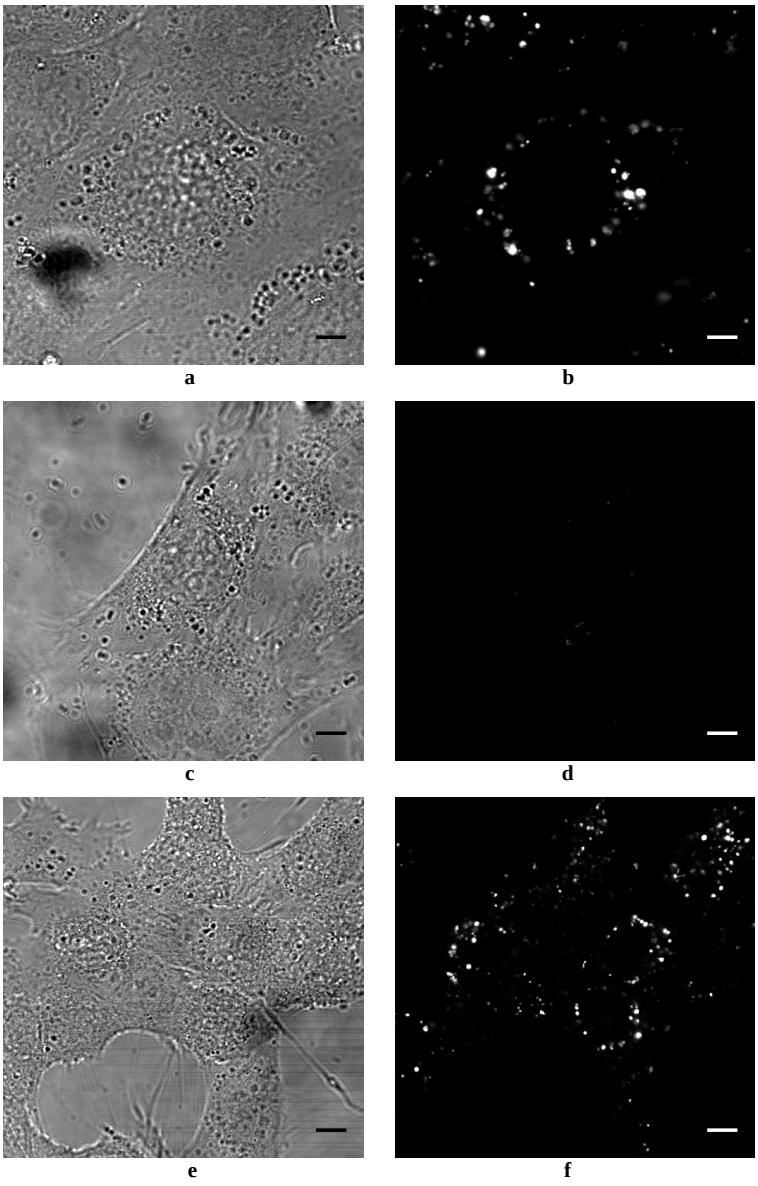

Fig. 4.5.1. RR-PEN1 and OG-PEN1 Penetratin derivatives showed different uptake behaviour in MEF cells. Cells were incubated with 5 μM RR-PEN1 or OG-PEN1 in imaging medium for 3h at room temperature. Only RR-PEN1 showed focal, perinuclear accumulation in cells (**a**, **b**) while OG-PEN1 was not internalized under these conditions (**c**, **d**). Nevertheless, the latter was taken up by cells at 37°C showing a distribution similar to that of RR-PEN1 (**e**, **f**). Pictures ***a***, ***c***, ***e*** represent transmitted light images. Scale bar = 20 μm (Material and methods, sect. 3.15).

Further analyses were performed with the goal of understanding the nature of the endosomal vesicles which appeared to trap the two fluorescent Penetratins. Since the shape and distribution of these structures closely resembled those typical of lysosomes, co-localization experiments with lysosomal markers were attempted.

MEF cells were incubated with a mixture of RR-PEN1 and LysoTracker® Green (LTG). The two dyes visibly co-localized (Fig. 4.5.2), indicating that many of the vesicles which entrapped RR-PEN1 were of lysosomal origin. This conclusion was nevertheless harder to

make when the converse experiment was performed, namely the incubation in the same conditions with a mixture of OG-PEN1 and LysoTracker® Red (LTR). Overall, the uptake was reduced with a concomitant reduction in co-localization (Fig.4.5.3). Although further experiments should be performed to reinforce these findings, one explanation could be that RR-PEN1 and OG-PEN1 distribute in MEF in endosomal compartments of a different nature. This could also explain why OG-PEN1 gained entry to the cell interior only at 37°C (Fig. 4.5.1 *e, f*). Ultimately, co-incubation with a mixture of OG-PEN1 and RR-PEN1 could have solved this riddle: surprisingly, the combination of the two caused (in this cell line) toxic effects which complicated the experiment and made the interpretation of the fluorescence distribution cumbersome (results not shown).

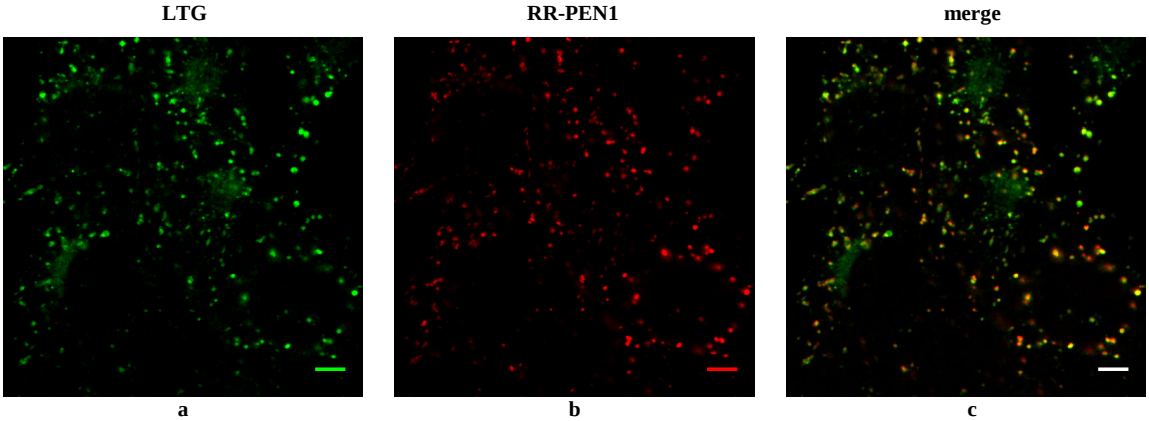

Fig. 4.5.2. RR-PEN1 and the lysosomal marker LysoTracker® Green (LTG) co-localize in living MEF cells. Cells were incubated (1h 45min, 37°C) with a mixture of LTG (**a**) and RR-PEN1 (**b**) in imaging medium at 0.75 µM and 2.5 µM, respectively. The dye and the peptide appeared to co-localize, as shown in the overlay picture (**c**). Scale bar = 20 µm (Material and methods, sect. 3.15).

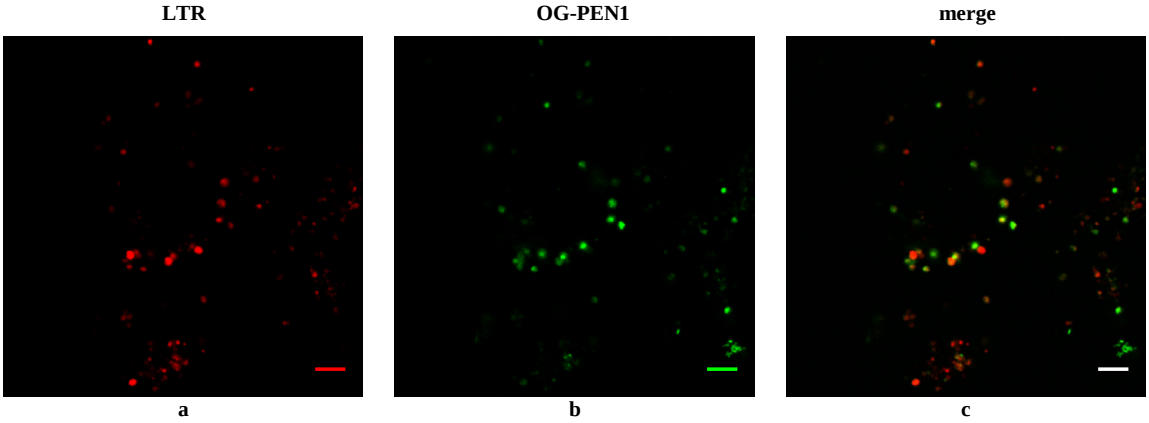

Fig. 4.5.3. OG-PEN1 and the lysosomal marker LysoTracker® Red (LTR) showed reduced uptake and co-localization in living MEF cells. Cells were incubated (3h, 37°C) with a mixture of LTR (**a**) and OG-PEN1 (**b**) in imaging medium at 0.75 µM and 2.5 µM, respectively. Images showed both a reduced number of fluorescent vesicles and a less evident co-localization between the OG-PEN1 peptide and the LTR lysosomal marker (**c**). Scale bar = 20 µm (Material and methods, sect. 3.15).

Literature data on Penetratin indicated that this vector exerted toxic effects from concentration doses of 30 µM, above which permeabilization of cell membranes occurred [85]. Despite these findings, intracellular distribution of Penetratin following incubation at high doses was not specified in the published study. Hence, an experiment was performed in which MEF cells were exposed to a short pulse of a high concentration (100 µM) of OG-PEN1 peptide. Propidium iodide, a nuclear dye which is normally excluded by cells that preserve membrane integrity, was also added. Microscopic observation revealed that, during the pulse, propidium iodide gained access to the nucleus of all cells, indicating a permeabilization effect exerted by the high dose of Penetratin (Fig. 4.5.4 *b, e*). OG-PEN1 distributed richly in vesicles and, in addition, to the plasma membrane, nuclear envelope and some fine cytoplasmic structures. In some cases, portions of the nuclear compartment were also weakly stained (Fig. 4.5.4 *a, d*). Whether membrane permeabilization can be considered a threat for cell viability may be a matter of discussion. Nevertheless, in all subsequent experiments the use of a low concentration of Penetratins (1 – 5 µM) was preferred.

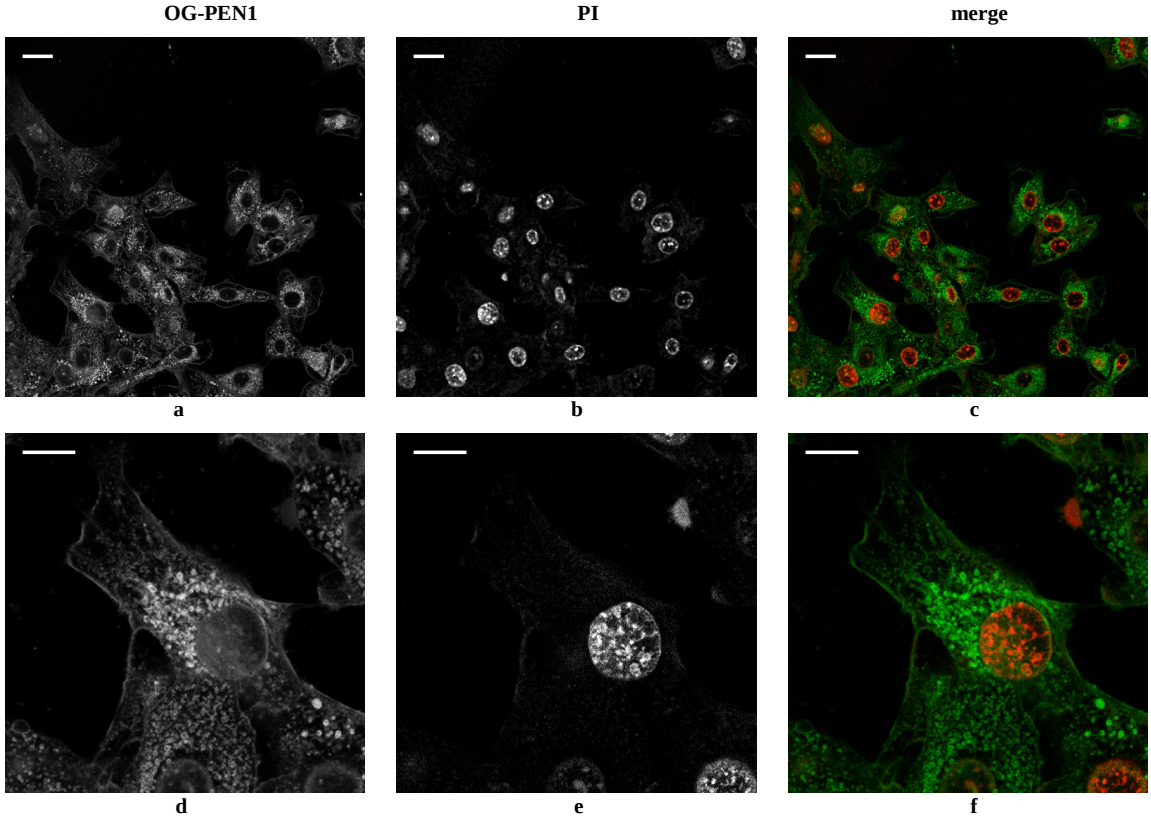

Fig. 4.5.4. Exposure to high dose of Penetratin caused membrane permeabilization in living MEF cells. Cells were pulsed (10 min, room temp.) with 100 µM OG-PEN1 and 1 µg of propidium iodide (PI, from 1 mg/mL stock solution in water) in imaging medium. OG-PEN1 distributed in large vesicles, plasma membrane, nuclear membrane and possibly nucleus and other cytoplasmic structures (**a**, **d**). All cells presented noticeable nuclear staining by PI (**b**, **e**) indicating that the high dose of Penetratin induced membrane permeabilization, hence the access to the nuclear compartment to PI. Scale bar = 20 µm (**a** – **c**), 10 µm (**d** – **e**) (Material and methods, sect. 3.15).

4.6 Uptake of OG-PEN1 and RR-PEN1 by living MCF-7 cells

As illustrated previously (sect. 4.3), human adeno-carcinoma cells showed no evident uptake of the LRh-DADEYL-PEN probe at room temperature. On the contrary, this cell line showed uptake of both RR-PEN1 and OG-PEN1 peptides when the experiment was performed at 37°C. Similarly to MEF cells (sect. 4.5), the distribution appeared mainly in vesicles in the cytoplasm and in the perinuclear area (Fig. 4.6.1).

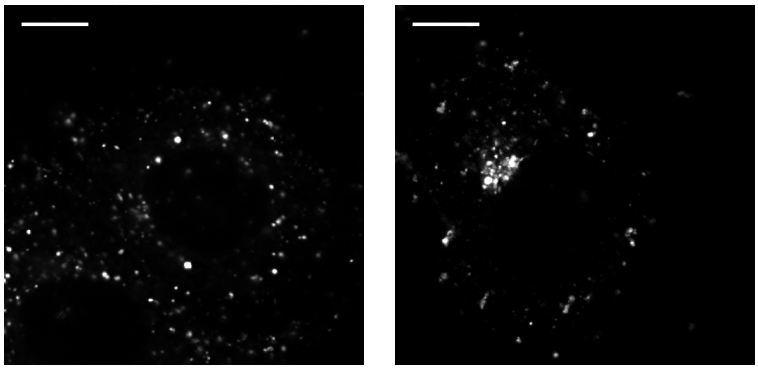

Fig. 4.6.1. RR-PEN1 and OG-PEN1 were internalized by MCF-7 cells at 37°C. Cells were incubated with 5 µM of either RR-PEN1 (**a)** or OG-PEN1 peptide (**b**) in imaging medium (+ 1% FBS) for 3 h at 37°C. Under these conditions the cells internalized both the fluorescent peptides into vesicles. OG-PEN1 could also be observed locally concentrated in the perinuclear space (**b**). Scale bar = 10 µm (Material and methods, sect. 3.15).

Moreover, the two fluorescent peptides appeared to co-localize in the same compartments (Fig. 4.6.2 *a* – *c*). Interestingly, and in contrast to what was observed for MEF cells (sect. 4.5), RR-PEN1 alone showed a less evident co-localization with the lysosomal marker LTG (Fig. 4.6.2 *d* – *i*). This could indicate that in MCF-7 cells the membrane-bound compartments that trapped RR-PEN1 (and for homology, OG-PEN1) may differ from the acidic late endosomes (lysosomes).

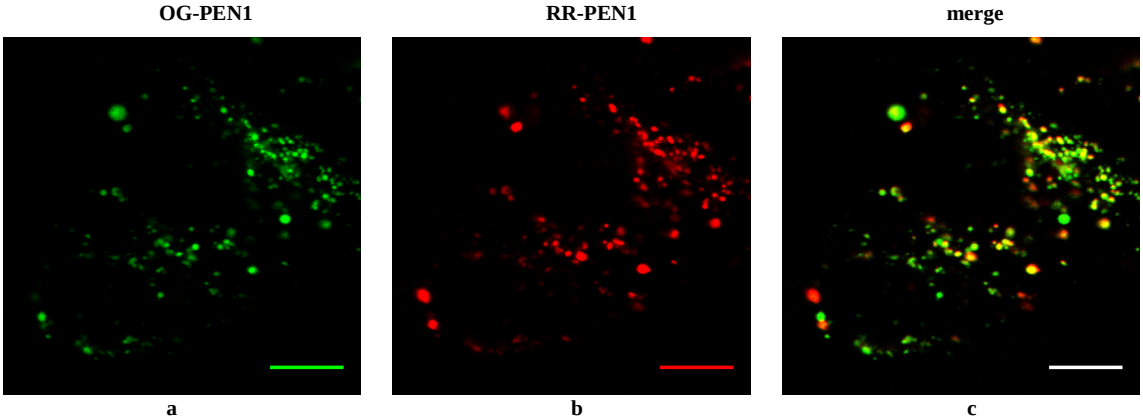

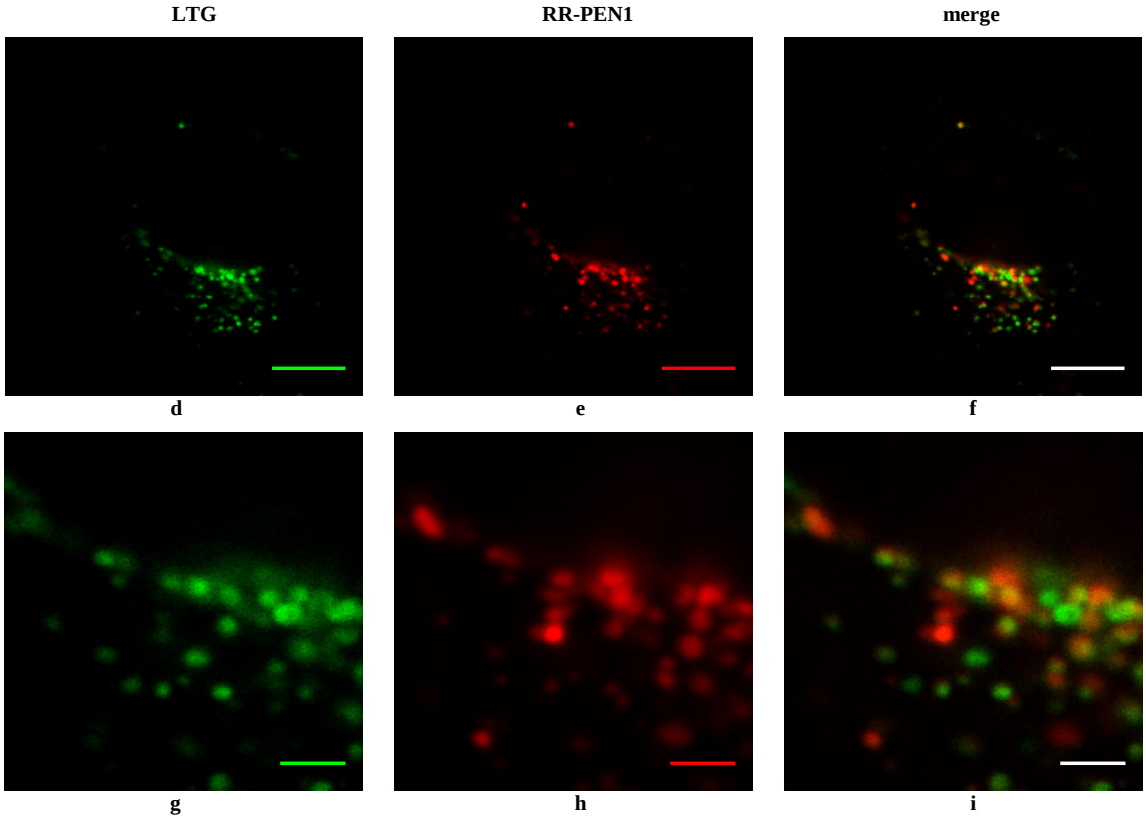

Fig. 4.6.2. RR-PEN1 and OG-PEN1 co-localized, while weak co-localization appared between RR-PEN1 and LysoTracker® Green (LTG) in living MCF-7 cells. Cells were incubated with a mixture of OG-PEN1 and RR-PEN1 (2.5 µM + 2.5 µM, picts. **a, b**) in imaging medium (+ 1% FBS) for 3.5 h at 37°C or with a mixture of LTG and RR-PEN1 peptide (1 µM+2.5 µM, picts. **d, e**) for 3.5 h at 37°C in the same medium. While the two fluorescent Penetratins appeared to share the same compartments (**c**), a less clear co-localization was observed between LTG and RR-PEN1 peptide (**f, i**), indicating that the latter could distribute into endosomal compartments of a different nature from the acidic late endosomes stained by LTG. Pictures **g – i** represent an enlarged area of pictures **d – f**. Scale bar = 10 µm (**a** – **f**); 2 µm (**g** – **i**) (Material and methods, sect. 3.15).

The photo-induced release of fluorescent substances from endosomal compartments has been already documented in the literature as a possible means for the redistribution of probes within the cell body [159]. This phenomenon was also observed when MCF-7 cells incubated with RR-PEN1 were pulse-exposed to the irradiation of the mercury lamp of the microscope. A redistribution of fluorescence was evident, but a more accurate observation revealed that the peptide did not appear homogeneously distributed in the cytoplasm, while it was dispersed in a higher number of membrane-bound compartments from the initial endosomes. Background intensity became also appreciable, suggesting membrane damage and leakage from cells (Fig. 4.6.3 *a* – *c*). Despite some investigator speculating that this procedure may be usefully exploited [159], possible photo-toxicity may be a practical limitation of this approach (Fig. 4.6.3 *d, e*).

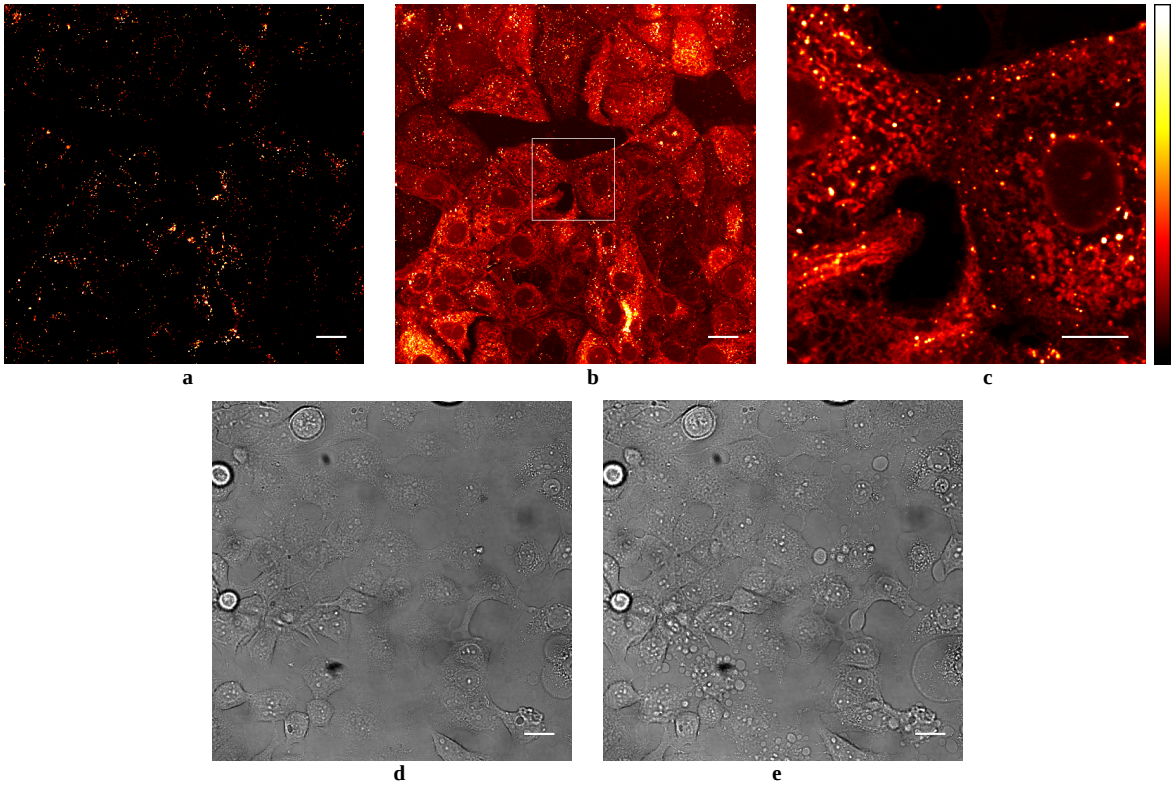

Fig. 4.6.3. Redistribution of RR-PEN1 peptide in MCF-7 cells upon wide-field arc-lamp illumination. Cells were incubated with 5 μM RR-PEN1 in imaging medium (+ 1% FBS) for 3 h at 37°C. After a first image acquisition (**a**), the specimen was illuminated with three pulses (10 sec + 5 sec pause) of white light. A new picture of the same area was then recorded (**b**), showing evident redistribution of the peptide. The localization appeared mainly in globular structures scattered in the cytoplasm, as well as in the nuclear membrane and, to a lesser extent, in the nucleus (**c**). Another area of the specimen (**d**) revealed noticeable induction of "blebbing" and apoptosis in the cells after a similar exposure (**e**). Picture **c** represents an enlarged view of the area marked in picture **b**. Pictures **d, e** are transmitted light images. Scale bar = 20 μm (**a, b, d, e**); 10 μm (**c**) (Material and methods, sect. 3.15).

4.7 The AM ester strategy for cell penetration and cytoplasmic distribution: the TAMRA-DADEYL-AM$_3$ peptide

The focal, endosomal distribution of the Penetratin-conjugated DADEYL peptide (LRh-DADEYL-PEN, sect. 4.2) appeared to be the limiting characteristic of the approach based on a polycationic vector for the cytoplasmic delivery of the designed probe when used in lower, cell-amenable concentrations. To circumvent the problem of sequestration in membrane-bound compartments and to allow an effective cytoplasmic distribution of the probe, a different strategy was investigated, based on the modification of the negatively-charged residues of the peptide (Asp, Glu) as alkyl esters. The intention was to create an uncharged molecule and to assess its capability of diffusing across the plasma membrane. The advantage of this protection would rely upon the activity of non-specific esterases present in cells: the hydrolysis of the ester moieties would allow, in the biological milieu, the restoration of the charge and the entrapment in the cell, facilitating the interaction of the peptidic probe with the target enzyme.

For this reason, it was decided to equip the DADEYL peptide with acetoxymethyl (AM) groups. While this strategy has been applied to various compounds (sect. 1.1), to the best of our knoledge it has not been documented so far on fluorescently-labelled peptides. Upon esterification, the envisioned peptide structure looked as represented in Fig. 4.7.1 *a*.

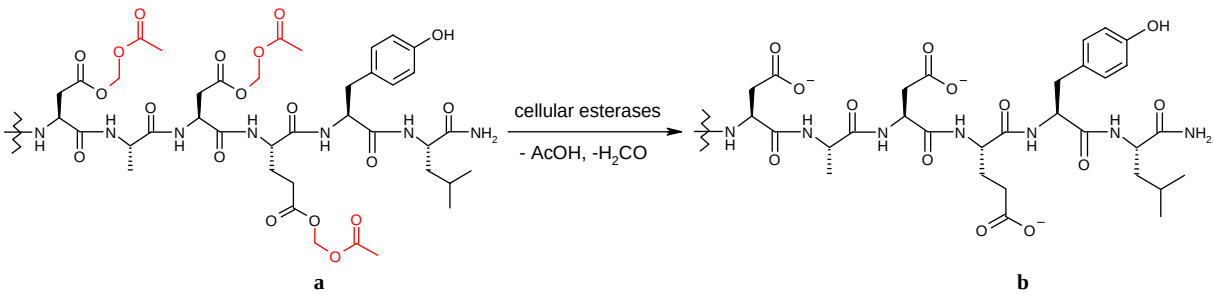

Fig. 4.7.1. The acetoxymethyl ester (AM) modification of Asp and Glu residues of the DADEYL peptide. (**a**) The alkylation product by the action of bromomethyl acetate and DIPEA (note the C-terminal amidation; the linker and the fluorophore molecules are omitted). (**b**) The hydrolysis of the AM esters by non-specific cellular esterases, with concomitant loss of acetic acid and formaldehyde, would restore the peptide in its native condition (Material and methods, sect. 3.10).

To rely upon the ready availability of the probe without the need of costant re-syntheses, a bulk preparation of resin-bound DADEYL peptide was started from 500 mg of Rink amide support. The synthesis proceeded according to the standard Fmoc-SPPS protocols, with some minor modifications (sect. 3.8, Tab. 3.8 a):

– the Fmoc-Tyr(Cl-Trt)-OH residue was incorporated into the sequence instead of the standard Fmoc-Tyr(tBu)-OH. The lability of the Cl-Trt protecting group to mild acidic treatment afforded the possibility to perform side-chain modifications directly on the solid support, namely phosphorylation (see sect. 4.13 below). Nevertheless, this building block failed to couple with the HBTU/HOBt/DIPEA protocol when used in a single step with an excess of 3 eq. The condensation was on the contrary successful when performed in three successive steps, using twice 1 eq of a.a. with the HOBt/DIC protocol, followed by 0.5 eq of fresh reagents using the HBTU/HOBt/DIPEA protocol;
– the Fmoc-Glu(tBu)-OH residue required a total of 4 eq (3 + 1) in order for the TNBS test to appear negative;
– the Fmoc-AEEAc-OH linker was successfully coupled using a total of 2 eq in two successive steps, limiting the waste of this costly building block.

HPLC analysis performed after a test cleavage confirmed that the product was obtained in high purity, although a smaller excess of reagents was used in the synthesis (Fig. 4.7.2).

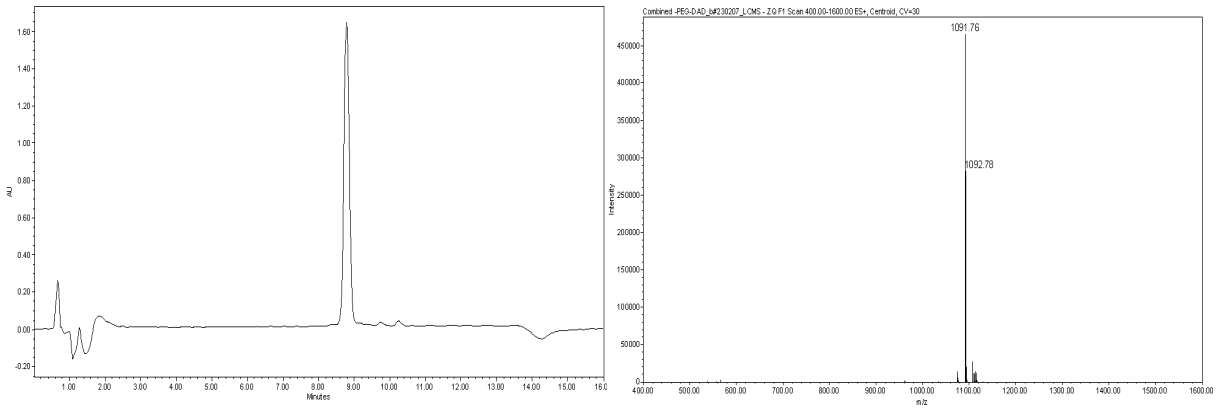

a **b**

Fig. 4.7.2. Bulk synthesis of resin-bound DADEYL peptide. The product was obtained in high purity, as showed by HPLC (**a**) and confirmed by ESI-MS (**b**) as a $[M+H^+]$ (m/z 1091.76) species (Material and methods, sect. 3.8).

The utilization of the Lissamine™-rhodamine presented several drawbacks and limitations, as previously mentioned. While the material obtained from one commercial supplier (Fluka) coupled efficiently, its low grade of purity required a careful purification of the labelled peptide (Fig. 4.2.2 *a*). Moreover, whereas the condensation to the TAT peptides via the aminohexanoic linker was straightforward (sect. 4.1), an additional cysteine residue needed to be added as a "junction node" after the AEEAc linker in the DADEYL peptide. Finally, the dye itself proved to adversely affect the solubility of the latter (sect. 4.2). With the

aim of reducing these limitations, a different fluorophore of the rhodamine family was chosen for labelling, namely carboxytetramethylrhodamine, commercially obtained as a mixture of isomers and pre-activated by means of a succinimidyl ester (5(6)-TAMRA SE, Fig. 3.1.2 *d*).

Conjugation of 5(6)-TAMRA SE to the Fmoc-deprotected peptide was straightforward and complete using an excess of about 2 eq of reagent.[14] The crude product was obtained in high yields (ca. 91%) and good purity (94%). The two regioisomers were also clearly resolved by HPLC (Fig. 4.7.3).

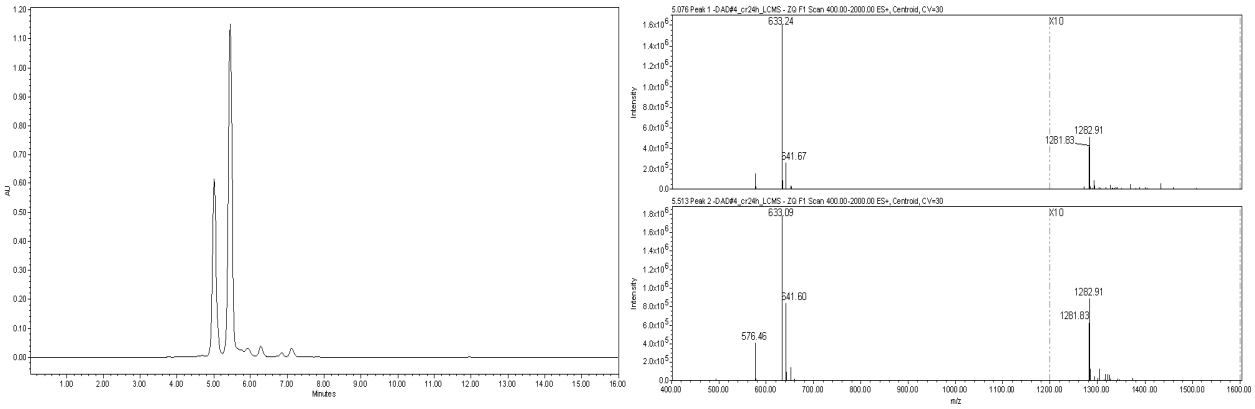

a **b**

Fig. 4.7.3. The TAMRA-DADEYL peptide. (**a**) Regioisomers due to commercial preparation of the dye could be resolved analytically by HPLC (retention times of 4.9 and 5.4 min) and confirmed by ESI-MS analysis (**b**) as $[M+H^+]$ and $[M+2H^+/2]$ species. Due to its purity (94%), the product was used directly in the next synthetic step (Material and methods, sect. 3.9).

AM ester formation was performed on the labelled peptide in anhydrous DMF with an excess of bromomethyl acetate and DIPEA – 9 and 3.6 eq, respectively – and without any prior purification (sect. 3.10). LC/MS analysis on the crude product revealed numerous species, mainly due to the presence of isomer mixtures: in addition to the desired product (m/z 1497.70) and some starting material (m/z 1281.59), peptides carrying one (m/z 1353.65) or two (m/z 1425.75) AM esters were clearly recognized. Other m/z values belonged to a peptide with an intact *t*-butyl group (m/z 1338.69, + 57 a.m.u.) which underwent one (m/z 1410.69), two (m/z 1482.79), three (m/z 1554.85) and finally four (m/z 1627.86) alkylations with bromomethyl acetate (Fig. 4.7.4). These results proved an additional alkylation on the molecule.[15]

[14] It was observed that a slight excess of 1.2 eq was generally sufficient to obtain a complete conjugation reaction.
[15] From a repeated alkylation reaction, the peptide TAMRA-DADEYL-4AM (four AM esters) could indeed be isolated in traces.

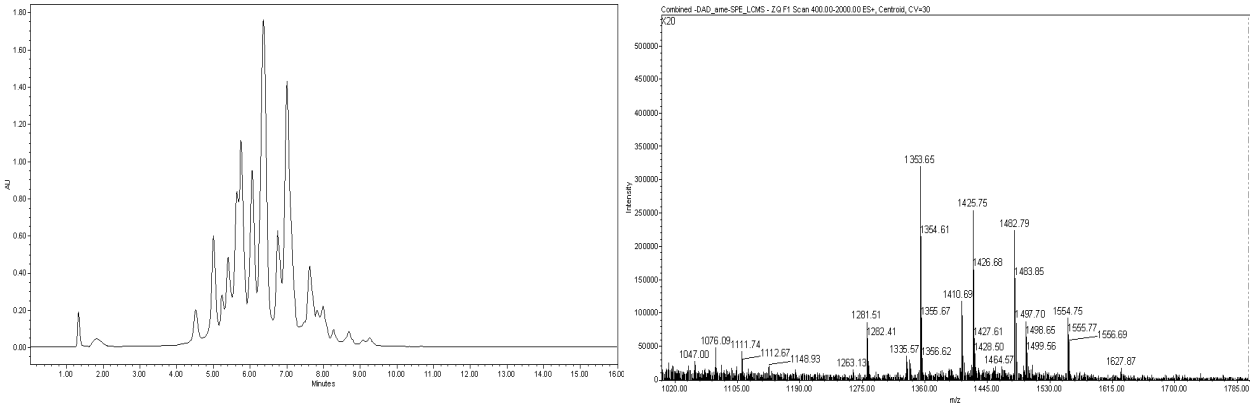

a **b**

Fig. 4.7.4. TAMRA-DADEYL-AM peptides. (**a**) The crude mixture showed a high number of peaks, mainly due to the presence of regioisomers. The various products could be nevertheless recognized by the ESI-MS analysis (**b**) (Material and methods, sect. 3.10).

Careful purification allowed the isolation of the product bearing three AM esters in 4.2% yield (Fig. 4.7.5). With a satisfactory overall purity (> 91%), the little amount obtained was nevertheless sufficient to carry out the *in vitro* and *in vivo* experiments described here. The lyophilized peptide was normally reconstituted in 15 µL of dioxane/water 1:1 (v/v) to get a 1 mM stock solution and was routinely used *in vivo* at a final concentration of 10 µM (1:100 dilution). In total, eleven vials of TAMRA-DADEYL-AM_3 peptide were prepared. The product proved to be stable for several months when stored lyophilized at – 20°C.[16]

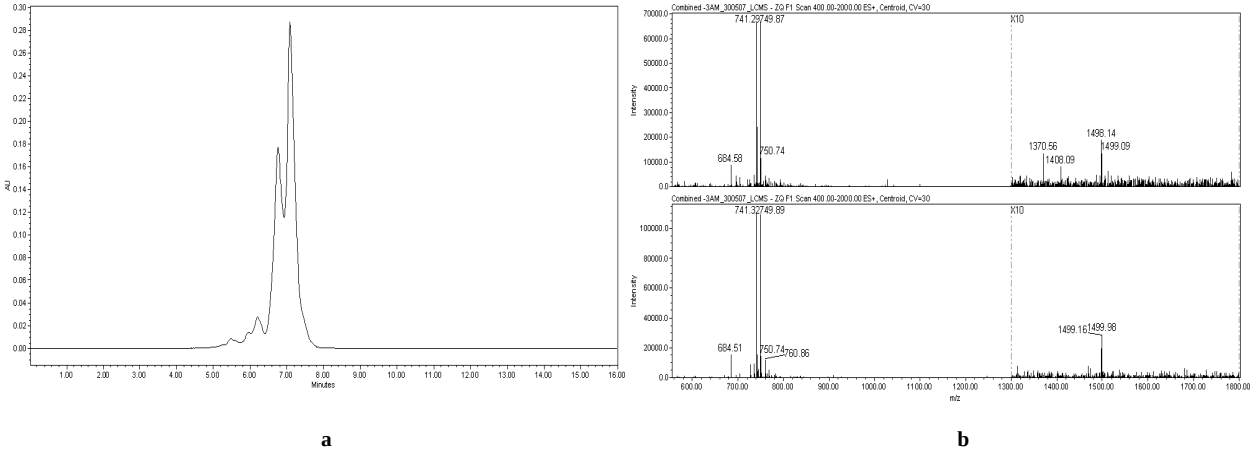

a **b**

Fig. 4.7.5. The TAMRA-DADEYL-AM_3 peptide. The purification afforded the product alkylated with three AM esters as a pair of partially resolved regioisomers (**a**). Despite the low yield (ca. 4%), the product was obtained with more than 90% overall purity. By ESI-MS analysis (**b**), both isomers could be identified as $[M+H^+]$ and $[M+2H^+/2]$ species (Material and methods, sect. 3.10).

[16] Solutions in water/dioxane were also stable up to one month when stored under the same conditions.

4.8 Uptake of TAMRA-DADEYL-AM_3 in living HeLa Kyoto, MCF-7 and MEF cells

The use of the TAMRA-DADEYL-AM_3 peptide in *in vivo* experiments immediately revealed significant differences compared to the LRh-DADEYL-PEN probe (sect. 4.2) in two out of three cell lines tested. HeLa Kyoto and MCF-7 cells revealed a strong intracellular accumulation already detectable after 20 min of incubation at room temperature (Fig. 4.8.1). Remarkably, both the cytoplasm and the nucleus were homogeneously stained; fluorescent vesicles were also detectable at higher magnification (Figs. 4.8.3, 4.8.4). The evident accumulation in the nuclear compartment was probably due to a possible affinity of the TAMRA dye to chromatin. While Kyoto cells showed an equal uptake in virtually all cells (Fig. 4.8.1 *a*), the intracellular concentration of the peptide appeared to vary in different MCF-7 cells (Fig. 4.8.1 *b*). In both cases, however, the goal of cytoplasmic delivery of the TAMRA-DADEYL-AM_3 peptide was successfully achieved, even in MCF-7 cells, which previously showed no uptake of the LRh-DADEYL-PEN peptide (sect. 4.2).

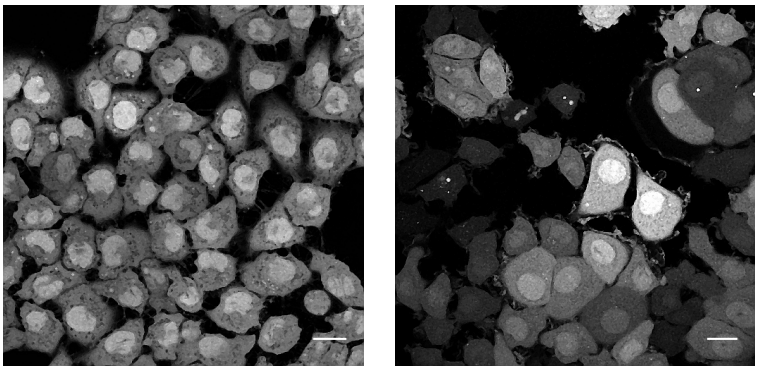

a **b**

Fig. 4.8.1. TAMRA-DADEYL-AM_3 peptide distributed homogeneously in living HeLa Kyoto or MCF-7 cells. HeLa Kyoto (**a**) and MCF-7 cells (**b**) were incubated with a 10 μM solution of TAMRA-DADEYL-AM_3 in imaging medium for 20 min at room temperature. Under these conditions the fluorescent peptide distributed in both cytoplasm and nucleus. Scale bar = 20 μm (Material and methods, sect. 3.15).

While the probe was routinely used on these cells at a final concentration of 10 μM, a good level of staining was also achieved at 5 μM. Serum was normally omitted throughout the incubation time, or kept at 1% for MCF-7 cells. Nevertheless, presence of serum even at 10% concentration did not appreciably disturb the intracellular accumulation of the peptide (Fig. 4.8.2).

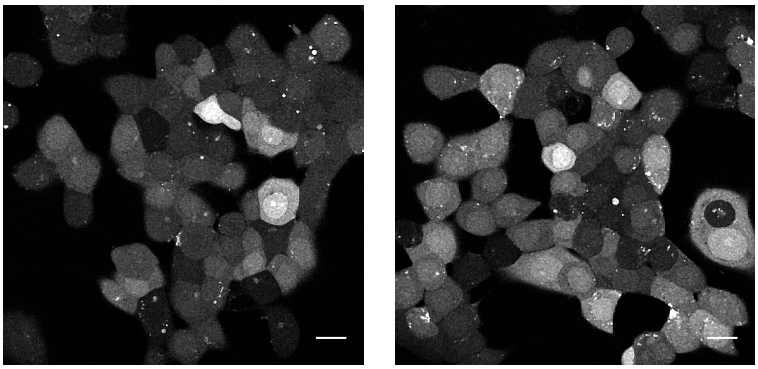

a b

Fig. 4.8.2. Serum did not impair accumulation of TAMRA-DADEYL-AM$_3$ peptide in living MCF-7 cells. Cells were incubated for 20 min at room temperature with a 10 µM solution of TAMRA-DADEYL-AM$_3$ in imaging medium containing either 1% (**a**) or 10% FBS (**b**). The presence of serum at 10% concentration did not adversely affect uptake of the peptide. Scale bar = 20 µm (Material and methods, sect. 3.15).

Over-expression of a given protein did also not interfere with the uptake of the probe. HeLa Kyoto stably transfected with YFP-EGFR (Fig. 4.8.3) or MCF-7 cells transiently transfected with GFP-PTP1B (Fig. 4.8.4) gave equally strong levels of fluorescent signal from the internalized peptide. Moreover, the distribution matched that which was observed in non transfected cells.

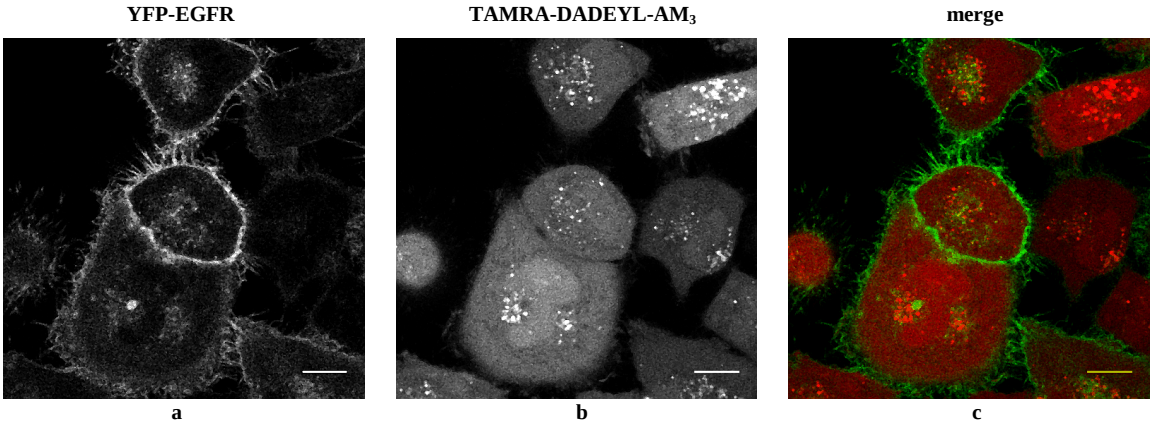

Fig. 4.8.3. Expression of YFP-EGFR did not interfere with TAMRA-DADEYL-AM$_3$ uptake in HeLa Kyoto cells. HeLa Kyoto stably transfected with YFP-EGFR (**a**) were incubated with a 10 µM solution of TAMRA-DADEYL-AM$_3$ in imaging medium for 20 min at room temperature. Over-expression of the membrane protein did not adversely affect uptake of the probe (**b**, **c**). Scale bar = 10 µm (Material and methods, sect. 3.15).

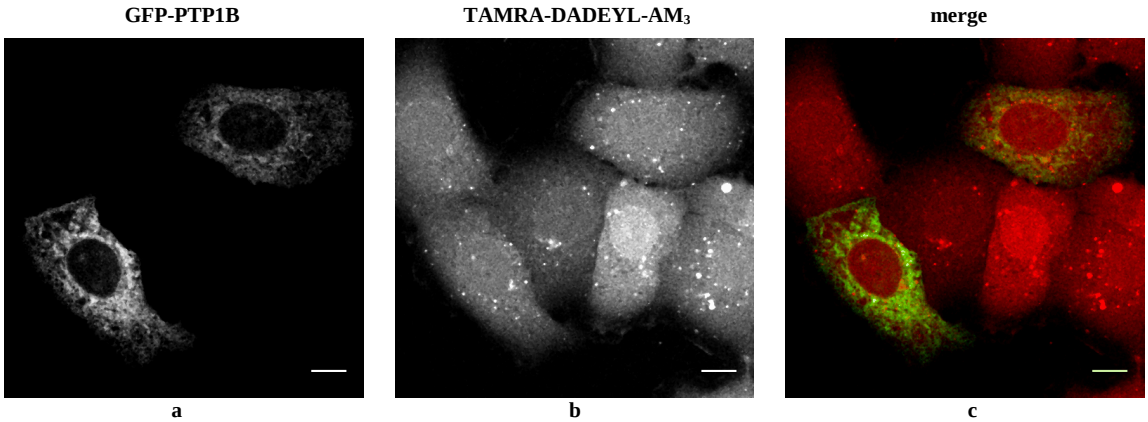

Fig. 4.8.4. Expression of GFP-PTP1B did not interfere with uptake of TAMRA-DADEYL-AM$_3$ in MCF-7 cells. Cells transiently transfected with the ER localized GFP-PTP1B chimera (**a**) were incubated with a 10 µM solution of TAMRA-DADEYL-AM$_3$ in imaging medium (+ 1% FBS) for 20 min at room temperature. Over-expression of the protein did not adversely affect uptake of the probe (**b**, **c**). Scale bar = 10 µm (Material and methods, sect. 3.15).

Surprisingly, the probe behaved differently in MEF cells: a diffuse staining was observed only at high concentration (45 µM), along with accumulation in vesicles (Fig. 4.8.5 *b, c*). Nevertheless, the cells appeared to suffer this condition, featuring a more round shape and a tendency to detach from the surface of the support. At a lower concentration (30 µM), only vesicles were detected (Fig. 4.8.5 *e, f*), reminiscent of the situation experienced with the LRh-DADEYL-PEN probe and the fluorescent Penetratins (sect. 4.2 and sect. 4.5). Moreover, TAMRA-DADEYL-AM$_3$ appeared to co-localized with the lysosomal marker LTG in late endosomes (Fig. 4.8.6 *a – c*). Taking into consideration these findings, along with the notorious resistance of MEF cells to standard protocols for cell transfection, this cell line was not investigated further.

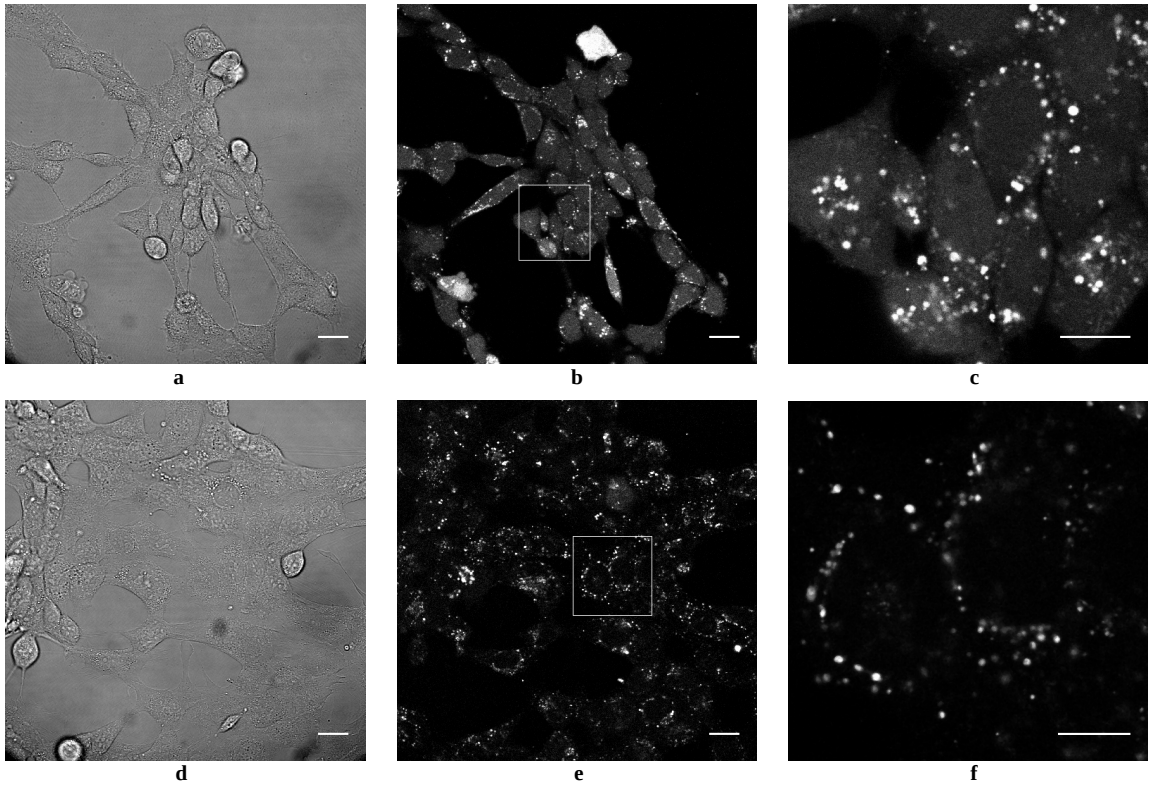

Fig. 4.8.5. Distribution of TAMRA-DADEYL-AM$_3$ in living MEF cells. Cells were incubated with a 45 µM (**b**) or 30 µM (**e**) solution of TAMRA-DADEYL-AM$_3$ in imaging medium for 30 min at room temperature. The peptide showed a diffused distribution only at the higher concentration (**c**). Pictures ***a***, ***d*** represent transmitted light images. Pictures ***c*** and ***f*** represent an enlarged view of the marked area in pictures ***b*** and ***e*.** Scale bar = 20 µm (**a, b, d, e**); 10 µm (**c, f**) (Material and methods, sect. 3.15).

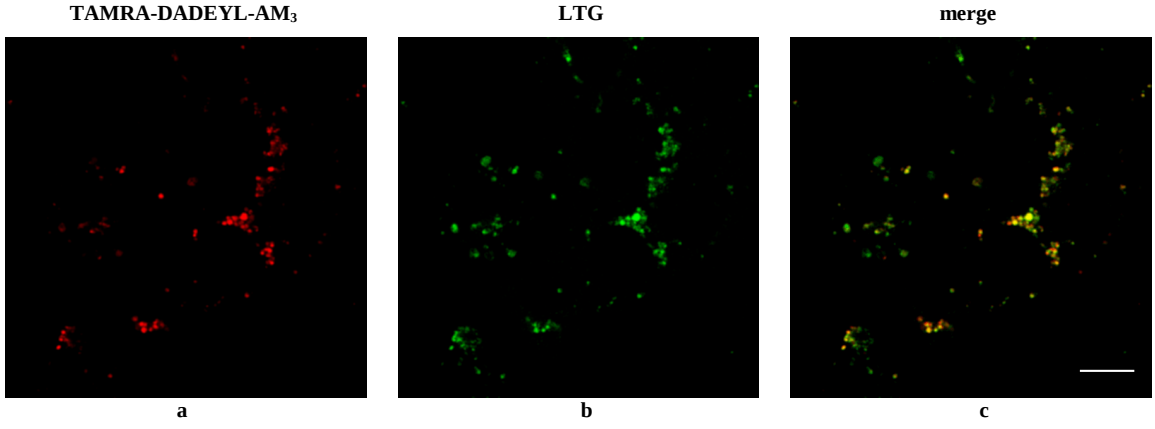

Fig. 4.8.6. TAMRA-DADEYL-AM$_3$ co-localized with LysoTracker® Green (LTG) in living MEF cells. Cells were incubated with a mixture of TAMRA-DADEYL-AM$_3$ and LTG (30 µM + 5 µM, pict. **a, b**) in imaging medium for 45 min at 37°C. The overlay picture shows co-localization in late endosomes (**c**). Scale bar = 10 µm (Material and methods, sect. 3.15).

To study the modality of uptake of the TAMRA-DADEYL-AM_3 peptide, time lapse recordings were made in HeLa Kyoto and MCF-7 cells (sect. 3.16). A plane of observation was selected where the cell body appeared dark with respect to the fluorescent surroundings: by doing so, the accumulation of the peptide over time could be easily followed and differences between a cytoplasmic or nuclear distribution could be assessed.

HeLa Kyoto and MCF-7 cells were incubated with a 10 μM solution of the peptide, as previously described (Material and methods, sect. 3.15). The acquisition revealed cytoplasmic and nuclear staining in both cell types already after 5 min (Fig. 4.8.7 *b* and 4.8.8 *b*). At the end of the incubation time (15 min for Kyoto, 20 min for MCF-7) the fluorescence signals from cytoplasm and nucleus of the cells were clearly distinguishable from the background (Fig. 4.8.7 *c* and 4.8.8 *c*). The scenario was particularly striking when the excess of peptide was rinsed from the support. The fluorescence appeared evenly distributed in the cytoplasm, but at the same time small dark vesicles were detectable: these regions of exclusion added further evidence of a real cytoplasmic distribution of the peptide (Fig. 4.8.7 *d* and 4.8.8 *d*).

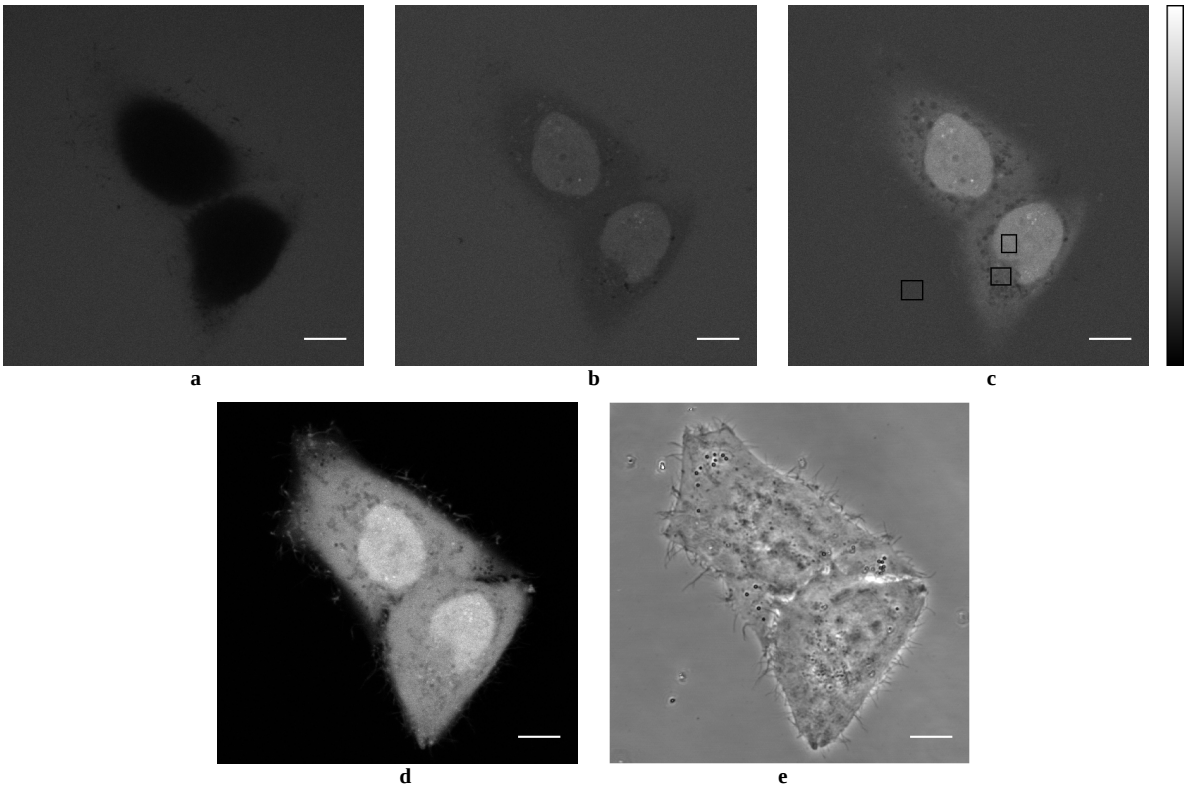

Fig. 4.8.7. Accumulation of TAMRA-DADEYL-AM_3 in living HeLa Kyoto cells as revealed by time-lapse microscopy. Cells were incubated with a 10 μM solution of TAMRA-DADEYL-AM_3 in imaging medium for 15 min at room temperature. Acquisitions were recorded at 6.5 sec intervals. The pictures represent the uptake at t = 0 (**a**), t = 5 (**b**) and t = 15 min (**c**) from the addition of the peptide. The areas marked in picture ***c*** were used to quantify the level of fluorescence over time, as reported in the graph below (Fig. 4.8.9). (**d**) Fluorescent image of the specimen after rinsing. (**e**) The specimen imaged under transmitted light (phase contrast). Scale bar = 10 μm (Material and methods, sect. 3.16).

More importantly, this analysis clearly showed that distribution of the TAMRA-DADEYL-AM_3 peptide in the cytoplasm (and nucleus) did not result from a "vesicle uptake and release" mechanism, but more likely from free diffusion through membranes. The presence of bright vesicles appeared to be a result of staining by diffusion of the free peptide from within the cytoplasm.

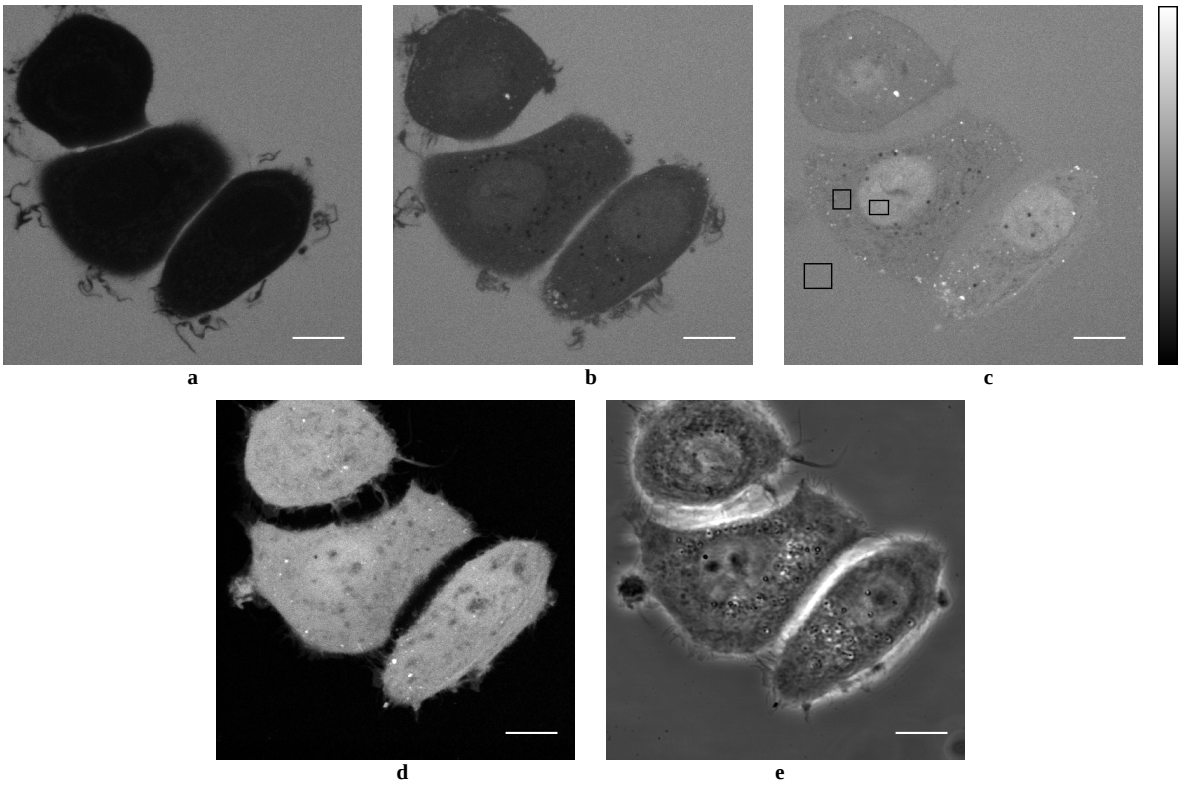

Fig. 4.8.8. Accumulation of TAMRA-DADEYL-AM_3 in living MCF-7 cells as revealed by time-lapse microscopy. Cells were incubated with a 10 μM solution of TAMRA-DADEYL-AM_3 in imaging medium (+ 1% FBS) for 20 min at room temperature. Acquisitions were recorded at 15 sec intervals. The pictures represent the uptake at t = 0 (**a**), t = 5 (**b**) and t = 15 min (**c**) from the addition of the peptide. The areas marked in picture ***c*** were used to quantify the level of fluorescence over time, as reported in the graph below (Fig. 4.8.9). (**d**) Fluorescent image of the specimen after rinsing. (**e**) The specimen imaged under transmitted light (phase contrast). Scale bar = 10 μm (Material and methods, sect. 3.16).

In order to shred light on the dynamics of the uptake process in these two cell types, a single cell was chosen and three different regions of interest (ROIs) were picked: nucleus, cytoplasm and background (Fig. 4.8.7 *c* and 4.8.8 *c*). Care was taken to choose those cellular regions where the peptide distribution was the most uniform. Calculations were made as previously described (Material and methods, sect. 3.16) and the resulting graphs are plotted in Fig. 4.8.9 and Fig. 4.8.10.

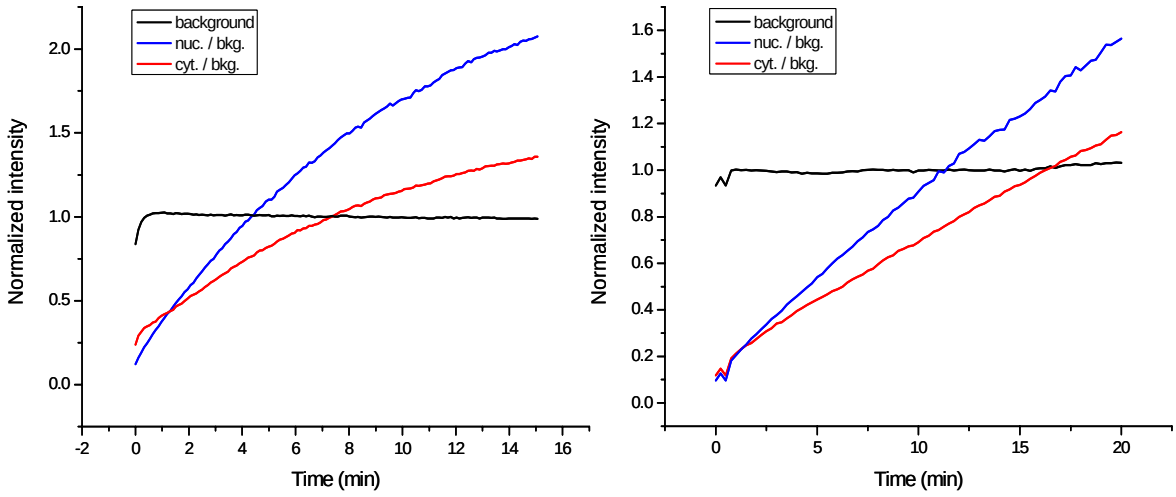

Fig. 4.8.9. Trend of accumulation of the TAMRA-DADEYL-AM$_3$ peptide in living HeLa Kyoto and MCF-7 cells. HeLa Kyoto and MCF-7 cells were incubated with a 10 µM solution of TAMRA-DADEYL-AM$_3$ in imaging medium, as described (Material and methods, sect. 3.16). Variation of fluorescence over time was measured in ROIs within a single cell (Fig. 4.8.7 and 4.8.8) where the intensity distribution appeared homogeneous. The curves represent the fluorescence intensity values normalized against the background (black line) in the nucleus (blue line) and the cytoplasm (red line) of a single HeLa Kyoto (graph **a**) and MCF-7 cell (graph **b**). Note the different ratio of peptide accumulation in the two cell lines (nuc.= nucleus, cyt. = cytoplasm, bkg. = background).

These data suggested differences in the behavior of Kyoto cells compared to MCF-7 cells, although the peptide accumulated in the nucleus at a faster rate compared to the cytoplasm in both cell types (Fig. 4.8.9, blue curves in graphs ***a, b***). In the Kyoto cells the fluorescence intensity in the nucleus reached the background level (here used as a reference value) shortly after 4 min and doubled after 15 min; the intensity in the cytoplasm reached the background level after about 7 min ending in a final value of about 1.3-fold the reference after 15 min. In MCF-7 cells the intensity in the nucleus equalled the background after more than 10 minutes, while the one in the cytoplasm took about 16 min. After 20 min the overall intensity in the nucleus and cytoplasm was about 1.6- and 1.1-fold the reference value, respectively.

Analysis of the plots suggested an exponential trend for uptake in Kyoto cells, reminiscent of a “saturation-like” mechanism. Nevertheless, a similar experiment performed in this cell line using a 5 µM peptide concentration and extending the incubation time to 1 h (room temp.) showed a more linear behaviour (Fig. 4.8.10), comparable to MCF-7 uptake where the correlation appeared mostly linear both in nucleus and cytoplasm (Fig. 4.8.9 *b*). Whether these conclusions could be extended to all MCF-7 cells is not clear, because different cells of the same specimen internalized the peptide to a different level, as showed (Fig. 4.8.1).

Nevertheless, these findings would support a free diffusion mechanism of cellular import of the AM-esterified peptide.

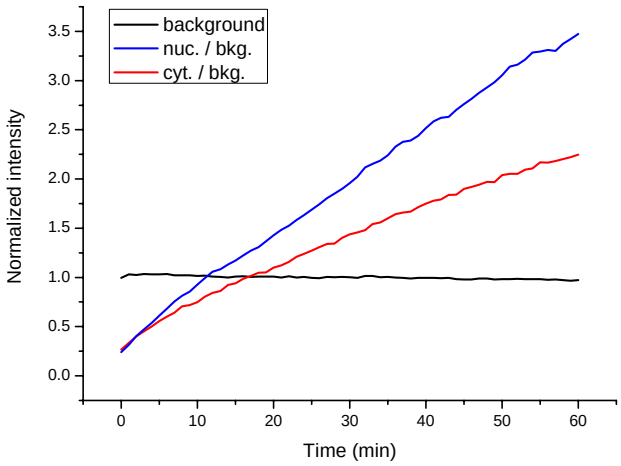

Fig. 4.8.10. Accumulation of the TAMRA-DADEYL-AM$_3$ peptide in living HeLa Kyoto cells appeared linear at a reduced concentration. Cells were incubated with a 5 µM solution of TAMRA-DADEYL-AM$_3$ in imaging medium, as described (Material and methods, sect. 3.16). The acquisition was made every minute for a total of 60 min of incubation. Variation of fluorescence over time was measured in ROIs within a single cell as done previously (Fig. 4.8.9). The curves represent the fluorescence intensity values normalized against the background (black line) in the nucleus (blue line) and the cytoplasm (red line) of a single cell. In these conditions the uptake appeared to be more linear in both cytoplasm and nucleus and matched that observed in MCF-7 cells (Fig. 4.8.9 *b*) at higher peptide concentration (nuc.= nucleus, cyt. = cytoplasm, bkg. = background) (Material and methods, sect. 3.16).

4.9 Influence of the number of AM esters on the cellular uptake

The synthesis of a short tri-peptide equipped with the TAMRA fluorophore and a single AM ester (TAMRA-EYL-AM$_1$, Fig. 4.9.1) was performed on a small scale using synthetic conditions described earlier (sect. 3.11). The use of this small fragment revealed interesting observations:

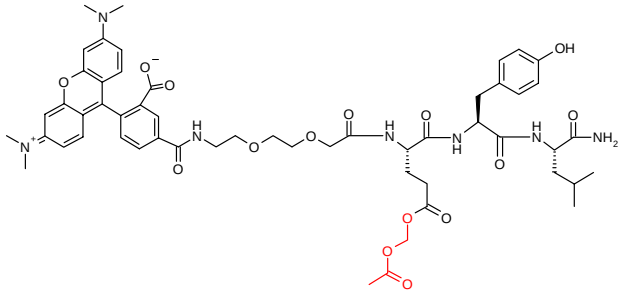

Fig 4.9.1. The TAMRA-EYL-AM$_1$ peptide. The proposed structure with the AM ester on the Glu residue coloured in red (MW 1051.16).

a) the separation of the TAMRA conjugates by HPLC, not performed on the longer peptide, afforded the two products with an overall yield of about 52% (Fig. 4.9.2). The use of

only one isomer in the AM esterification reaction allowed a straightforward identification of the products by LC/MS analysis: the presence of an additional AM ester on the molecule was confirmed and the TAMRA-EYL-AM_1 and TAMRA-EYL-AM_2 peptides could be isolated by semi-preparative HPLC (Fig. 4.9.3).

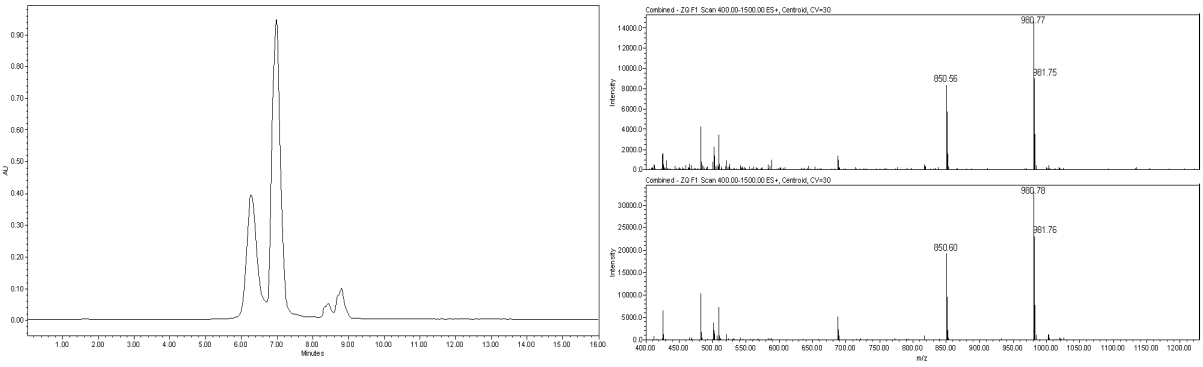

a **b**

Fig. 4.9.2. The TAMRA-EYL peptide. (**a**) HPLC analysis performed on the crude mixture following conjugation with 5(6)-TAMRA SE showed the expected two regioisomers, which in this case where separated by preparative chromatography before performing the AM esterification reaction. (**b**) ESI-MS confirmed both regioisomers as [M+H^+] (m/z 980.7) species (Material and methods, sect. 3.11).

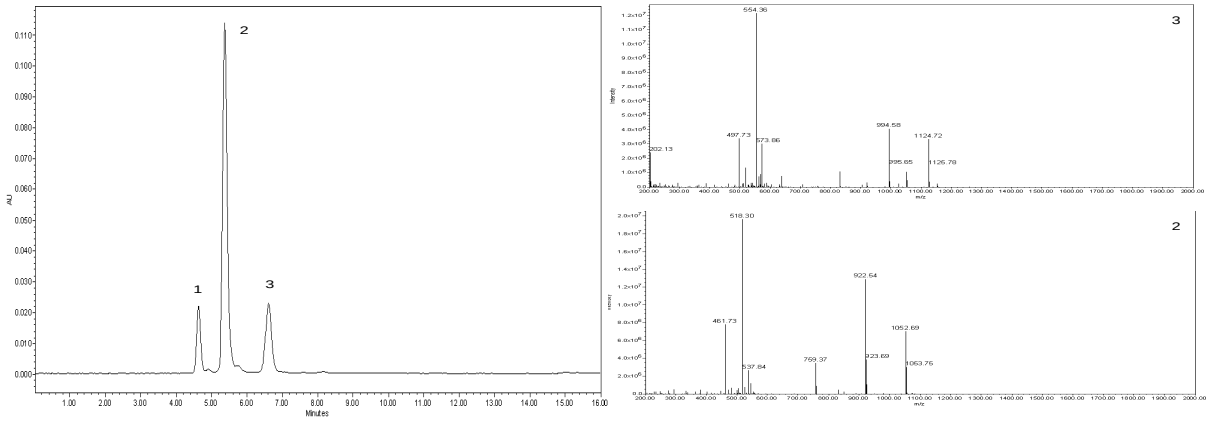

a **b**

Fig. 4.9.3. The TAMRA-EYL-AM_1 and TAMRA-EYL-AM_2 peptides. (**a**) In the alkylation reaction only one isomer was used, facilitating the analysis and separation of the products. The peak appearing at 4.7 min (n.1, 11%) corresponded to unreacted starting material, the one at 5.3 min (n. 2) was the peptide carrying one AM ester (69%), while the last one at 6.7 min (n. 3) was a peptide carrying two AM esters (17%). (**b**) The two peptides were characterized by ESI-MS as [M+H^+] species (TAMRA-EYL-AM_1, m/z 1052.69, spectrum n.2; TAMRA-EYL-AM_2, m/z 1124.82, spectrum n.3. Material and methods, sect. 3.11).

b) ESI-MS/MS analysis on the fragments obtained from the TAMRA-EYL-AM_2 peptide inferred the presence of the second AM ester functionality on the carboxylic group of the TAMRA. Nevertheless, the presence of an esterified tyrosine could not be excluded (Tab. 4.9 *a*).[17]

	AM at C-terminus		AM at N-terminus (TAMRA)	
	expected	observed 563.74	expected	observed 563.74
N-terminal	558.6	558.3 (background)	631.7	-
	759.8	759.3	832.8	831.3
C-terminal	365.4	-	292.4	292.95
	566.6	-	493.5	493.3

Tab. 4.9 a. ESI-MS/MS analysis of the TAMRA-EYL-AM_2 peptide. Fragmentation products obtained from the species with m/z 563.74 (corresponding to the double-charged peptide). The signals observed would be compatible with peptides carrying one AM ester either on the TAMRA (m/z 831.3, 292.9. 493.3) or at the C-terminus, likely on the Tyr residue (m/z 759.3). Only the signal at m/z 831.3 was nevertheless intense enough to be recorded unambiguously.

c) Incubation of HeLa Kyoto cells with TAMRA-EYL-AM_1 and TAMRA-EYL-AM_2 peptides in the same experimental conditions used for the TAMRA-DADEYL-AM_3 surprisingly revealed no or negligible cellular uptake (Fig. 4.9.4). This finding may suggest the need of a minimal number of three AM esters on this peptidic substrate in order to get an efficient translocation in cells. Of course, this speculation requires a more careful verification (the presence of different fluorophores on the peptide may also play a role).

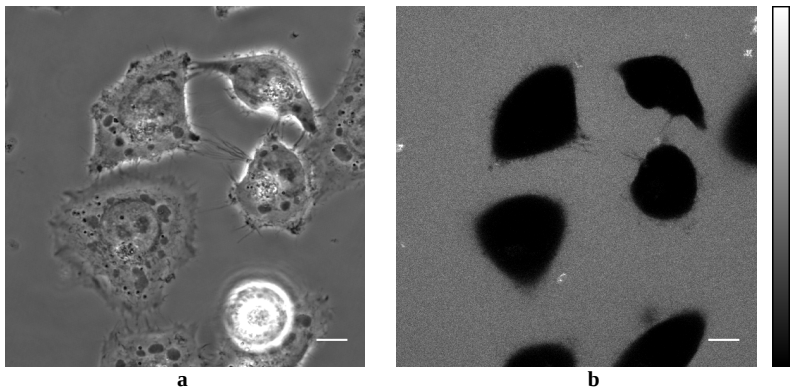

a **b**

[17] It must be stressed the fact that the instrumentation used for ESI-MS/MS at the EMBL Proteomic Core Facility is not designed for the analysis of low molecular weight species. Hence, the results here reported have a certain grade of uncertainty and cannot be considered conclusive.

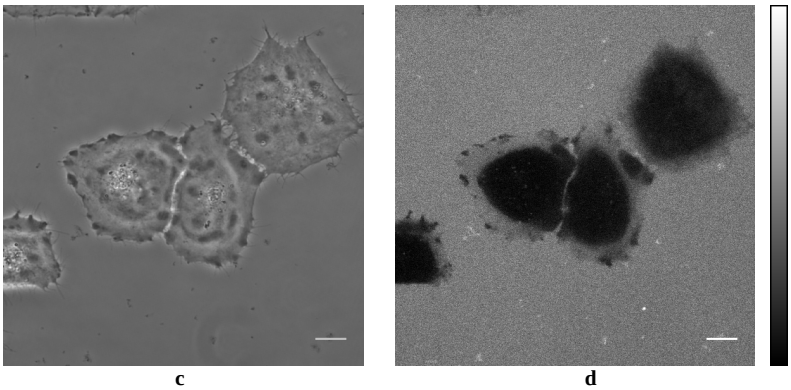

c d

Fig. 4.9.4. Incubation of living HeLa Kyoto cells with TAMRA-EYL-AM$_1$ or TAMRA-EYL-AM$_2$ revealed a lack of or poor peptide uptake. Cells were incubated with a 10 μM solution of TAMRA-EYL-AM$_1$ or TAMRA-EYL-AM$_2$ in imaging medium for 20 min at room temperature. In these conditions there was either a lack of staining with the TAMRA-EYL-AM$_1$ peptide (**a, b**) or a very faint one with the TAMRA-EYL-AM$_2$ peptide (**c, d**). Pictures *a* and *c* represent transmitted light (phase contrast) images. Scale bar = 10 μm (Material and methods, sect. 3.15).

4.10 Analysis of interaction between TAMRA-DADEYL-AM_3 peptide and EGFR assayed by FLIM/FRET microscopy

The translocation properties of the TAMRA-DADEYL-AM_3 peptide (sect. 4.8) formed the basis for its use as a probe to monitor the activity of the receptor tyrosine-kinase EGFR. To verify the possibility of monitoring this interaction in living cells, a series of experiments based on Förster Resonance Energy Transfer (FRET) were performed.

In the system proposed here the FRET event would only occur upon the specific interaction between the enzyme (equipped with a donor fluorophore) and its substrate (equipped with an acceptor fluorophore. See Fig. 2.1.2). This approach has already been validated as a tool for the study of an enzyme-substrate interaction *in vivo* [153]. A Green Fluorescent Protein (GFP) or a Yellow Fluorescent Protein (YFP) are well suited to act as donors toward the acceptor rhodamine, because of the favourable overlap between the emission spectra of GFP or YFP and the excitation spectrum of rhodamine (Fig. 2.1.1)

In a fluorescence lifetime imaging (FLIM) experiment, the FRET event is recorded as a decrease of the fluorescence donor's lifetime. Via the so-called *global analysis* of the FLIM image, the fractions of molecules undergoing FRET can be evaluated, affording temporal and spatial resolution for the observed phenomena [17, 160]. Despite the fact that only one fluorophore is observed, this kind of assay requires more specialized instrumentation with respect to a conventional FRET setup: the donor is repeatedly excited with a pulsed laser of a suitable wavelength, and the exponential decay of its fluorescence is recorded and analyzed. The experiments reported here have been made possible thanks to the availability of a confocal FLIM microscope at the laboratories of Prof. Philippe Bastiaens (Max Plank Institute of Molecular Physiology, Dortmund, Germany).

HeLa Kyoto cells stably transfected with a construct YFP-EGFR were incubated with a 10 μM solution of TAMRA-DADEYL-AM_3 for 20 min and stimulated with EGF (100 ng/mL). Lifetime images were recorded starting from 5 min after EGF addition and every 10 min (Fig. 4.10.2). Despite the presence of peptide in the cells, FLIM analysis did not show a variation of the YFP lifetime value, which remained constant around its average value of ca. 3.0 ns throughout the observation period (1 h). A rise in the background signal in the rhodamine channel indicated leakage of fluorescent product from the cells, which nevertheless continued to appear brightly stained (Fig. 4.10.2 *c*). An apparent delay of

internalization of the EGFR was noticed and considered as a possible effect of the probe. Nevertheless, further experiments revealed that the peptide did not impair EGFR internalization when used in the same experimental conditions, and the previous findings were attributed to physiological variations between different cell batches (observations by Dr. Vibor Laketa, EMBL, results not shown).

In order to reinforce the FLIM observations, an "acceptor photobleaching" experiment was performed next. In this assay the acceptor is bleached by high power laser illumination and the fluorescence intensity of the donor is recorded and compared to the original value before the bleaching. If the two fluorophores are part of an effective FRET pair, an increase of the donor fluorescence (unquenching) is normally observed as a direct result of a decrease in FRET.

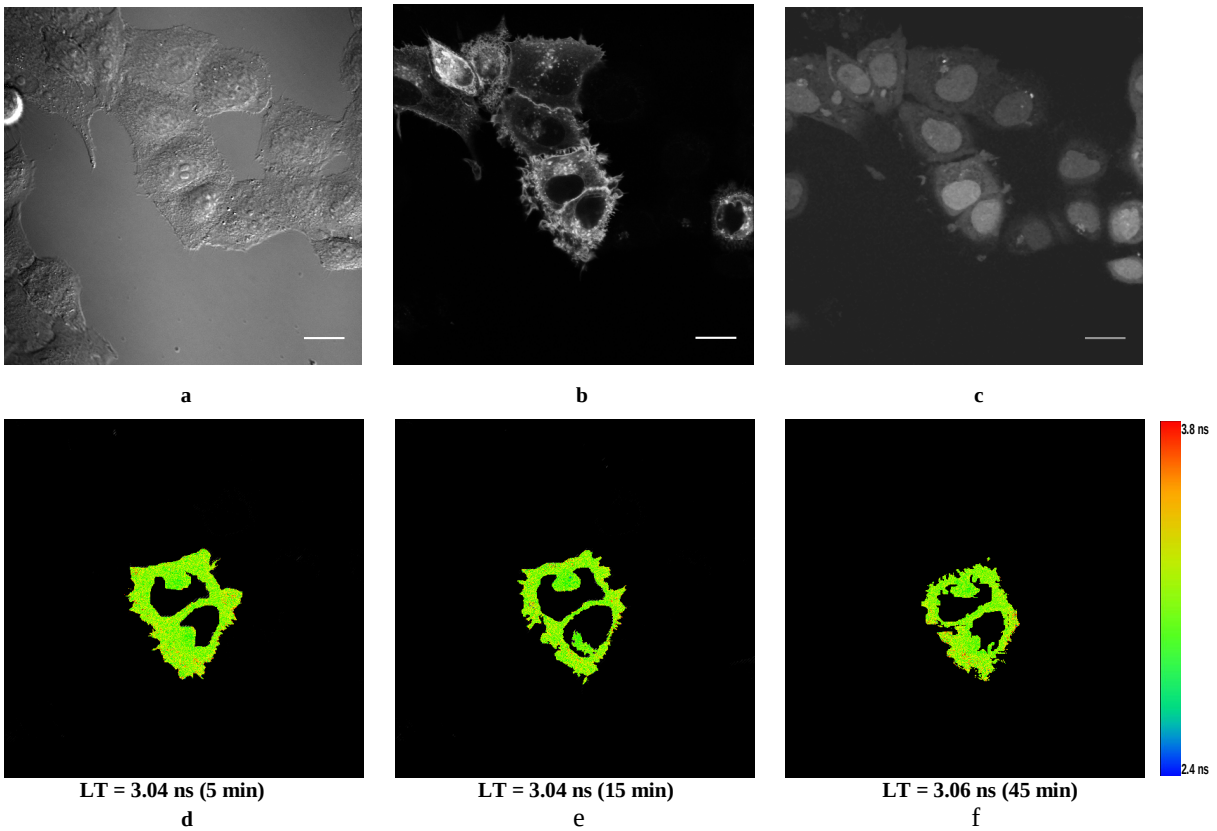

Fig. 4.10.2. Lifetime of YFP did not show reduction in HeLa Kyoto cells stably transfected with YFP-EGFR upon incubation with the TAMRA-DADEYL-AM$_3$ peptide. Cells were incubated with TAMRA-DADEYL-AM$_3$ peptide at 10 µM in imaging medium (20 min, room temp.), washed and incubated with EGF (100 ng/mL). (**a**) Trasmitted light image (phase contrast) of the cells. (**b**) YFP-EGFR. (**c**) TAMRA-DADEYL-AM$_3$ peptide. (**d, e, f**) Lifetime of YFP was recorded starting 5 min after EGF addition and every 10 min up to 1 h. Pictures represent a colour-coded average value for the YFP lifetime measured after 5, 15 and 45 min, respectively (the analysis was restricted only to the two cells present in the centre of the field). Fluorescence signal from the peptide was clearly detectable in the cells throughout the experiment, although a rise of the background signal indicated possible leakage (**c**). LT = lifetime. Scale bar = 20 µm. (Material and methods, sect. 3.17).

HeLa Kyoto cells were transiently transfected with a GFP-EGFR construct and incubated with the TAMRA-DADEYL-AM_3 peptide at 5 µM for 45 min. The extended incubation time was to verify whether hydrolysis of AM ester groups *in vivo* would have required a longer period of time. Cells were then stimulated with EGF (100 ng/mL) for 15 min, fixed and the acceptor photobleaching experiment was performed. Nevertheless, GFP fluorescence did not significantly vary after bleaching of the rhodamine, indicating a lack of FRET between the peptide and GFP-EGFR (Fig. 4.10.3).

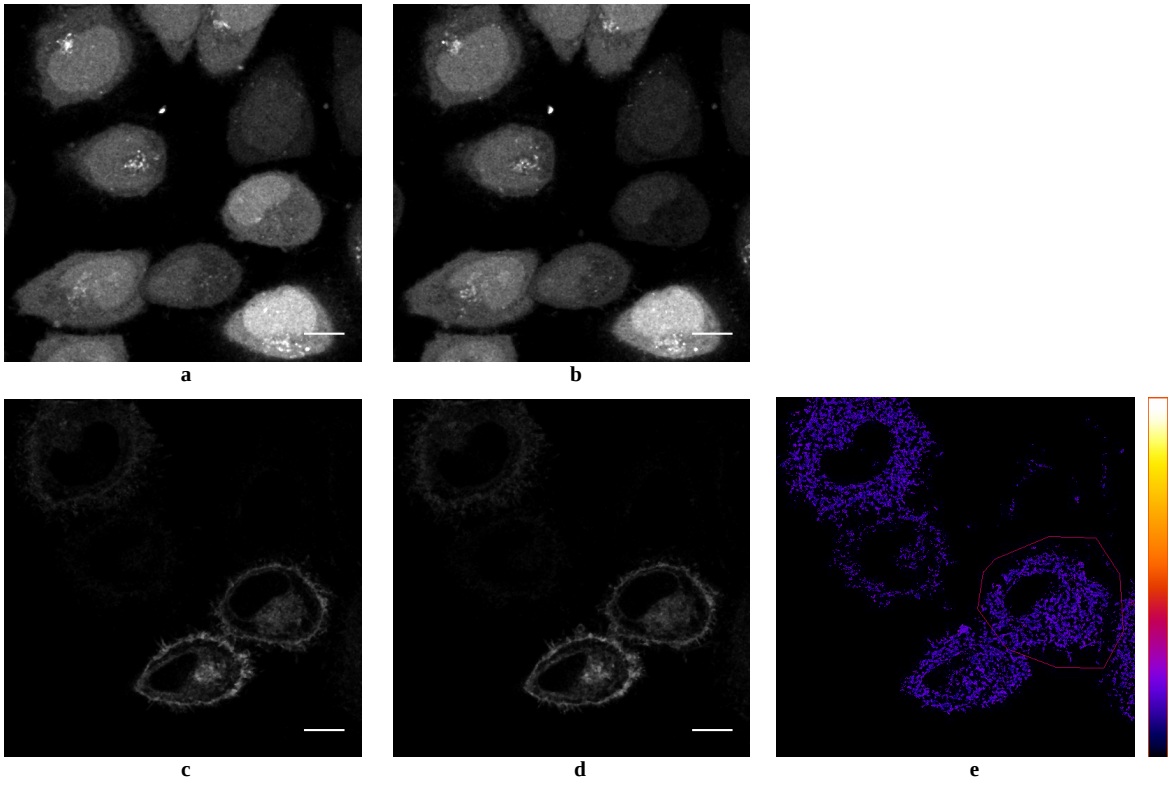

Fig. 4.10.3. Acceptor photobleaching of the TAMRA-DADEYL-AM_3 peptide did not reveal unquenching of GFP-EGFR in HeLa Kyoto cells. Cells transiently transfected with GFP-EGFR were incubated with a 5 µM solution of TAMRA-DADEYL-AM_3 peptide in imaging medium (45 min, room temp.), washed, incubated with EGF (100 ng/mL) for 15 min and finally fixed (3.7% PFA). The upper panel shows the cells imaged in the red channel before (**a**) and after the bleaching of one single cell. The lower panel shows the cells imaged in the green channel before (**c**) and after the bleaching (**d**). (**e**) Colour-coded picture expressing values of FRET efficiency. As illustrated, the cell which underwent bleaching (circled with the red line) showed intensity values identical to the unbleached neighbouring cells, indicating lack of FRET. Scale bar = 10 µm (Material and methods 3.18).

4.11 In vitro assessment of esterase activity over the TAMRA-DADEYL-AM_3 peptide

The outcome of the FRET-based experiments reported above suggested a lack of interaction between the peptide and the receptor, perhaps due to inefficient hydrolysis of the AM ester groups *in vivo*. To verify this hypothesis, the stability of the TAMRA-DADEYL-AM_3 peptide toward esterase activity was assessed *in vitro*.

Cell lysates were produced from HeLa Kyoto, MEF and MCF-7 cells (sect. 3.19). Their esterase activity was confirmed by means of a colorimetric test which used α-naphthyl acetate as a model substrate (Fig. 4.11.1). Commercial Porcine Liver Esterase (PLE, a known member of cellular carboxylesterases) mouse and fetal bovine serum were also tested for comparison. In this assay, the α-naphthol produced by enzymatic hydrolysis of α-naphthyl acetate reacts with an *o*-dianisidine derivative (named Fast Blue B) to produce a highly absorbing substance at 620 nm [161]. The amount of the latter correlates directly with the amount of α-naphthol produced, providing a qualitative readout of esterase activity contained in the sample.

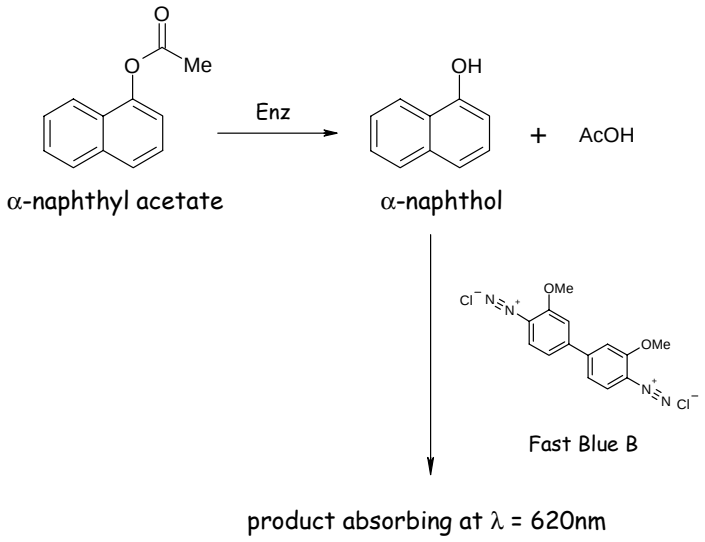

Fig. 4.11.1. The colorimetric esterase assay based on α-naphthyl acetate and Fast Blue B.

HeLa Kyoto, MEF and MCF-7 cell lysates showed high levels of esterase activity (85 to 95% of the substrate was converted to α-naphthol), which was not affected by protease inhibitors but was sensitive to heat: following incubation at 56°C for 45 min, a 71% reduction in activity was observed for the Kyoto lysate, 48% for the MEF lysate and 65% for the MCF-7 lysate (Fig. 4.11.2).

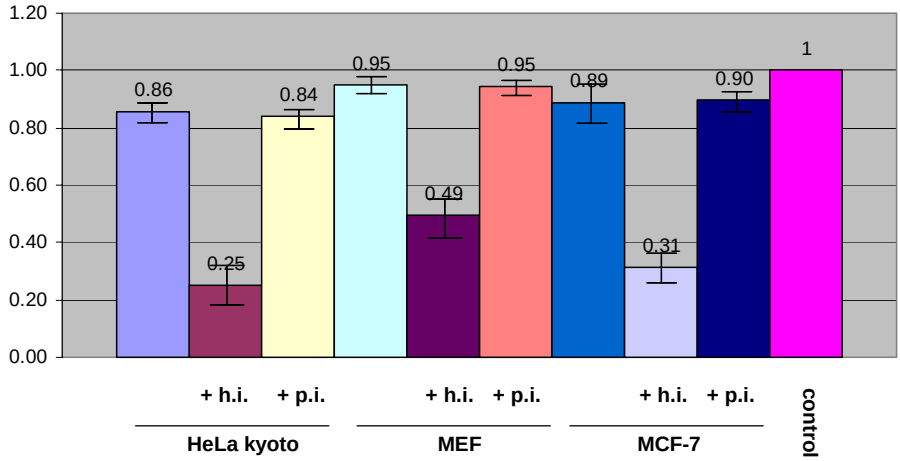

Fig. 4.11.2. Esterase assay of cell lysates using α-naphthyl acetate. A 0.2 mM solution of α-naphthyl acetate in HEPES (20 mM, pH 7.4) was incubated for 30 min at room temperature with 3% lysate (2 µg/µL protein content) obtained from HeLa Kyoto, MEF and MCF-7 cells. After addition of Fast Blue B, absorbance was measured at 620 nm. Each value represents the average of three independent measurements, normalized against the absorbance of a 0.2 mM solution of α-naphthol used as a control. All cell lysates showed high esterase activity against α-naphthyl acetate, which was reduced after heat treatment (56°C, 45 min) but remained insensitive to the presence of protease inhibitors. H.i. = heat inactivation; p.i. = protease inhibitors cocktail (Material and methods, sect. 3.20).

Mouse serum also showed potent esterase activity, but its value was reduced both by heat treatment (ca. 55% reduction) and protease inhibitors (ca. 35% reduction) (Fig. 4.11.3 *a*). Lower levels of activity were found for PLE and FBS, with the latter showing a 26% reduction following heat treatment (Fig. 4.11.3 *b*).

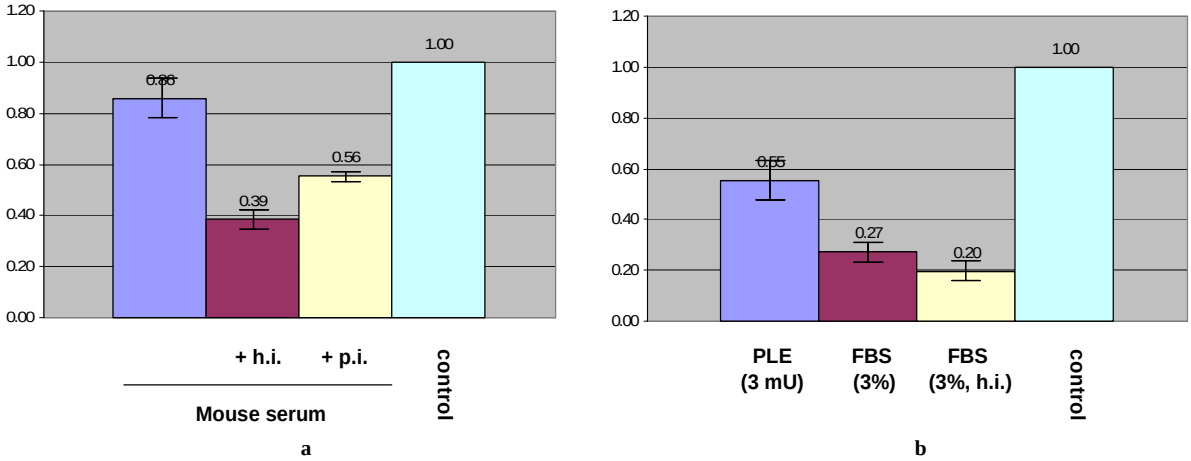

Fig. 4.11.3. Esterase assay of mouse serum, porcine liver esterase (PLE) and fetal bovine serum (FBS) using α-naphthyl acetate. A 0.2 mM solution of α-naphthyl acetate in Hepes 20 mM (pH 7.4) was incubated with 3% mouse serum (**a**) or with 3 mU PLE, 3% FBS and 3% heat-inactivated FBS (**b**) for 10 min at room temperature. After addition of Fast Blue B, absorbance was recorded at 620 nm. Each value represents the average of three independent measurements, normalized against the absorbance of a 0.2 mM solution of α-naphthol used as a control. Mouse serum showed high esterase activity which was reduced both by heat and protease inhibitors (55% and 35% reduction, respectively). Lower levels of activity were shown by PLE and FBS. H.i. = heat inactivation; p.i. = protease inhibitors cocktail (Material and methods, sect. 3.20).

The stability of the TAMRA-DADEYL-AM_3 peptide to the various esterase sources was then tested: first, a solution of the probe was incubated with mouse serum, PLE or HeLa Kyoto cell lysate, then the mixture was transferred to living cells and the translocating capability of the peptide was assessed by direct observation. A 10 min exposure to mouse serum was sufficient to dramatically affect the peptide, which proved no longer able to penetrate the cells (Fig. 4.11.4 *a*). Pre-incubation with cell lysate produced a similar situation, with fluorescence detectable in cells only at a very low level (Fig. 4.11.4 *b*). Surprisingly, the peptide resisted PLE action: a 10 min exposure to this enzyme did not affect translocation, which was not impaired even after a prolonged incubation of 1 h (Fig. 4.11.4 *c*). From these indirect observations it was concluded that both cell lysate and mouse serum were able to process the peptide in a relatively short time, thereby abolishing its penetrating capability, presumably via the hydrolysis of its AM groups. Conversely, PLE was found to have a less dramatic effect, if any.

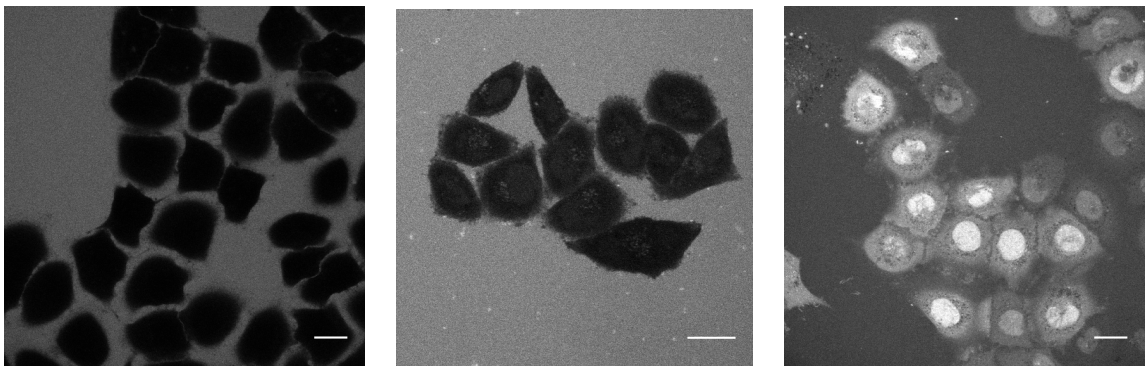

a **b** **c**

Fig. 4.11.4. Pre-exposure to mouse serum or to cell lysate, but not to PLE, impaired cell translocation of the TAMRA-DADEYL-AM_3 peptide. A 5 μM solution of TAMRA-DADEYL-AM_3 peptide in imaging medium was incubated with 3% mouse serum (10 min, room temp.), 3% HeLa Kyoto cell lysate (30 min, 37°C) or 3 mU PLE (1 h, 37°C). HeLa Kyoto cells were afterwards incubated with the three mixtures for 30 min at 37°C. While pre-incubation with mouse serum (**a**) and cell lysate (**b**) markedly abolished the penetration of the peptide into cells, PLE on the contrary did not affect this capability (**c**). Scale bar = 20 μm**.**

In order to further probe these observations, mass spectrometric analyses on the products of the esterase activity were performed (sect. 3.21). Incubation of the TAMRA-DADEYL-AM_3 peptide with both mouse serum and cell lysates afforded unexpected results: the major signals – m/z 1245.4, 1317.4, 1335.6, 1407.5 – appeared to correspond to peptides which retained up to two AM esters while featuring a concomitant dehydration. In both experiments equal species were observed, but the peptide corresponding to the complete hydrolysis of the AM groups could not be detected (Fig. 4.11.5, top & centre panels).

Proteolytic activity could also be excluded, because samples treated with heat-inactivated cell lysates or mouse serum, or with protease inhibitors, gave spectra identical to those here reported (see *Appendix*, Fig. A2). Moreover, the TAMRA-DADEYL peptide (without AM esters), tested as a control with cell lysates or mouse serum, proved to be stable (Fig. 4.11.5, bottom panel).

The mass spectrum of the products obtained from an overnight incubation of the TAMRA-DADEYL-AM_3 peptide with PLE gave additional pieces of information (Fig. 4.11.6): in this case a peptide which underwent a complete hydrolysis of all the AM ester groups could be detected (m/z 1281.44). Notably, a product retaining one AM ester was also visible (m/z 1353.46), despite the long period of incubation with the enzyme.

Following MALDI-MS, the same sample was subjected to ESI-MS/MS analysis: the fragmentation products originating from the peptide with m/z 1353.46 (Fig. 4.11.6) proved to be compatible with the presence of a single AM ester on Glu-3, Asp-4 or Asp-6 (Fig. 4.11.7). Interestingly, the single AM ester present in the TAMRA-EYL-AM_1 peptide (MW 1051.45) largely resisted hydrolysis when incubated with cell lysates, while was fully hydrolyzed after incubation with mouse serum (Fig. 4.11.8). This would provide some evidence for a differential esterase activity of cell lysate and mouse serum toward a Glu(AM)-Tyr-Leu tripeptide *in vitro*.

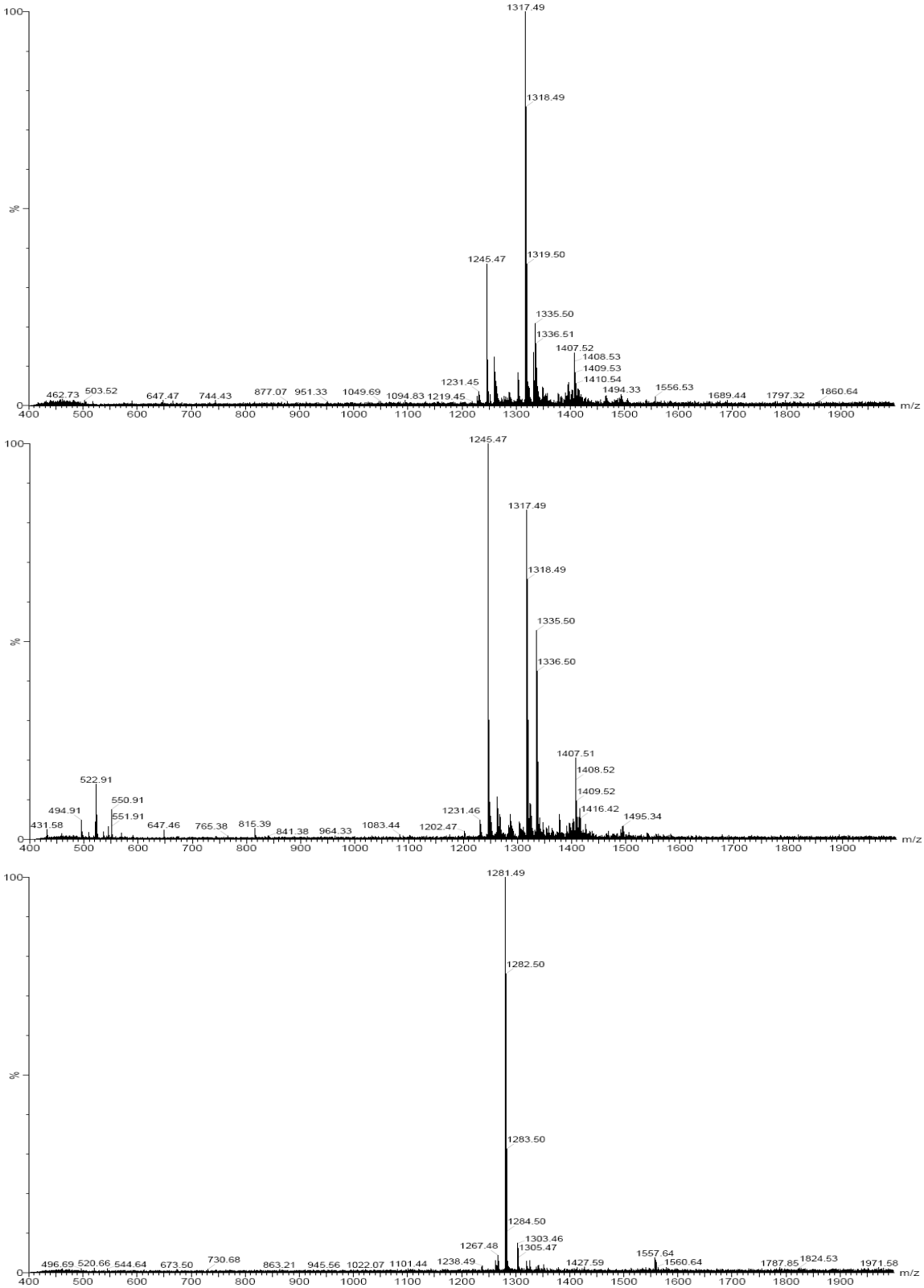

Fig. 4.11.5. TAMRA-DADEYL-AM$_3$ and TAMRA-DADEYL peptides incubated with cell lysate or mouse serum. MALDI mass spectra relative to the products of the incubation of the TAMRA-DADEYL-AM$_3$ peptide (5 μM) with 3% cell lysate (top panel) or 3% mouse serum (centre panel) for 30 min at room temperature. In both experiments equal species were produced. Under similar conditions the TAMRA-DADEYL peptide did not yield any relevant product (bottom panel, mouse serum incubation). The products that may have originated the masses recorded in these spectra are represented in Fig. 4.11.9 (Material and methods, sect. 3.21).

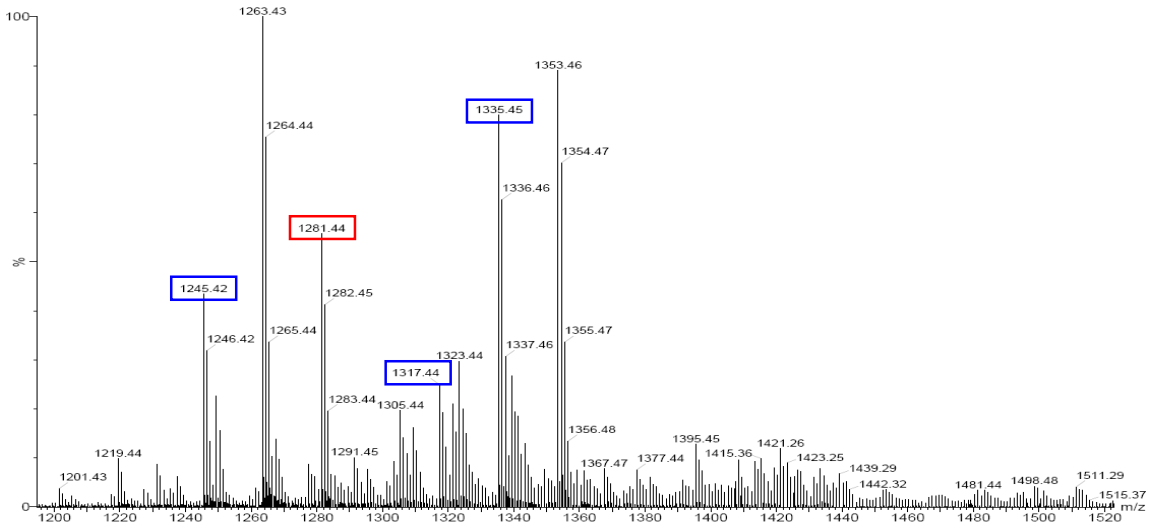

Fig. 4.11.6. The TAMRA-DADEYL-AM$_3$ peptide incubated with PLE. MALDI mass spectrum relative to the products of the incubation of the TAMRA-DADEYL-AM$_3$ peptide (5 µM) with 3 mU PLE at 37°C overnight. A product without residual AM esters (m/z 1281.44) is marked in red, while species matching those recorded after incubation of the peptide with cell lysates or mouse serum are marked in blue (see Fig. 4.11.5) (Material and methods, sect. 3.21).

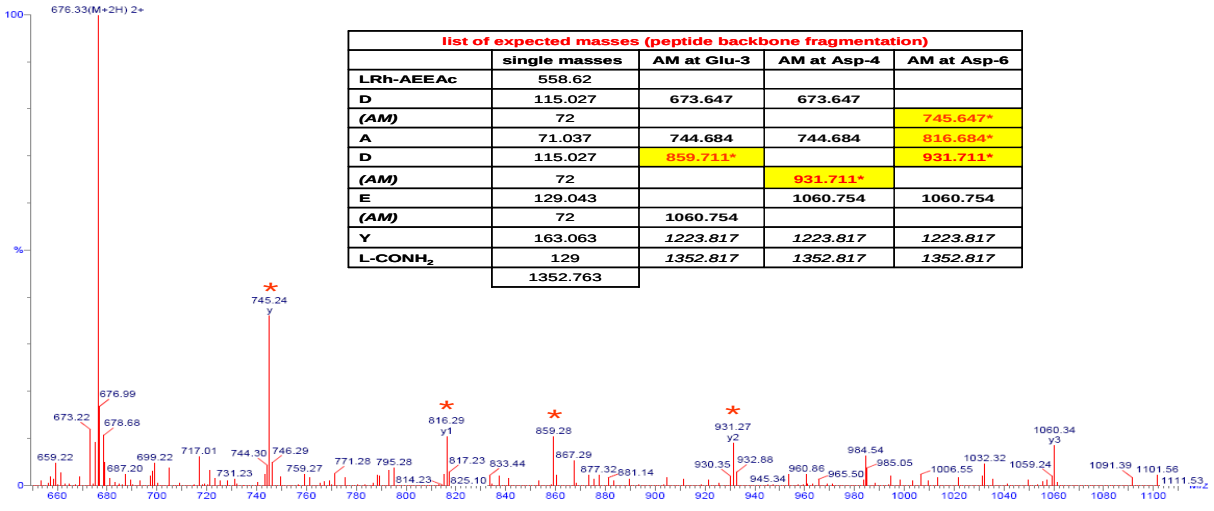

list of expected masses (peptide backbone fragmentation)				
	single masses	**AM at Glu-3**	**AM at Asp-4**	**AM at Asp-6**
LRh-AEEAc	558.62			
D	115.027	673.647	673.647	
(AM)	72			745.647*
A	71.037	744.684	744.684	816.684*
D	115.027	859.711*		931.711*
(AM)	72		931.711*	
E	129.043		1060.754	1060.754
(AM)	72	1060.754		
Y	163.063	*1223.817*	*1223.817*	*1223.817*
L-CONH$_2$	129	*1352.817*	*1352.817*	*1352.817*
	1352.763			

Fig. 4.11.7. ESI-MS/MS analysis on the product with m/z 1353.46 originating from incubation of the TAMRA-DADEYL-AM$_3$ peptide with PLE (see Fig. 4.11.6)**.** The table reports the calculated m/z values relative to the fragments originating at the level of the peptide backbone, with the observed species written in bold. The fragments compatible with the presence of one residual AM group on Glu-3, Asp-4 or Asp-6 are marked with a red asterisk.

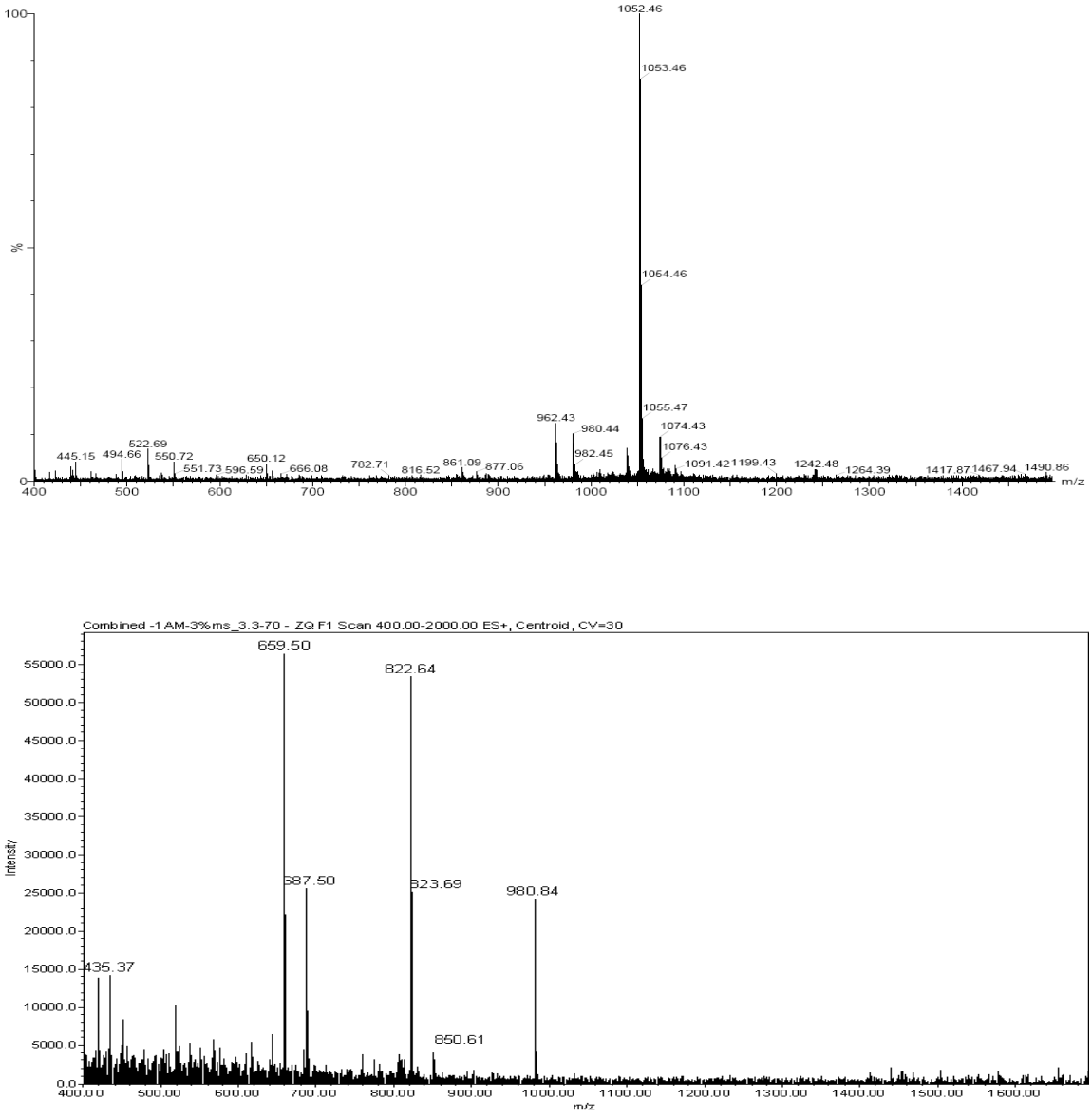

Fig. 4.11.8. The AM ester on Glu-3 in the TAMRA-EYL-AM$_1$ peptide largely resisted hydrolysis when incubated with cell lysate, while was fully hydrolyzed after incubation with mouse serum. Mass spectra relative to the products of the incubation of the TAMRA-EYL-AM$_1$ peptide (5 μM, MW 1051.45) with 3% cell lysate (top panel, MALDI mass spectrum) or 3% mouse serum (bottom panel, ESI-MS mass spectrum) for 30 min in HEPES 20 mM (pH 7.4) and at room temperature. While incubation with cell lysate produced little hydrolysis of the single AM ester (m/z 980.44, [M+H$^+$]), complete hydrolysis was observed after incubation with mouse serum (the two species with m/z 659.50 and 822.64 visible in the ESI-MS spectrum derived from those with m/z 687.50 and 850.61, respectively, which were fragmentation products of the peptide backbone) (Material and methods, sect. 3.21).

Various models may be proposed to explain the species observed in the mass analyses given in Fig. 4.11.5 and Fig. 4.11.6. One may envisage a process triggered by the presence of the AM esters: for instance, the different peptides may have originated via cyclization of the aspartate residues to the aspartimide, followed by their spontaneous hydrolysis (Figs. 4.11.9, 4.11.10). The latter event would justify the additional products observed in the mass spectrum given in Fig. 4.11.6, which may have formed during the extended incubation time. The spontaneous loss of water from peptides at higher mass appears less likely, since as shown in Fig. 4.11.5, the peptide without AM esters did not undergo any modification under the same experimental conditions.

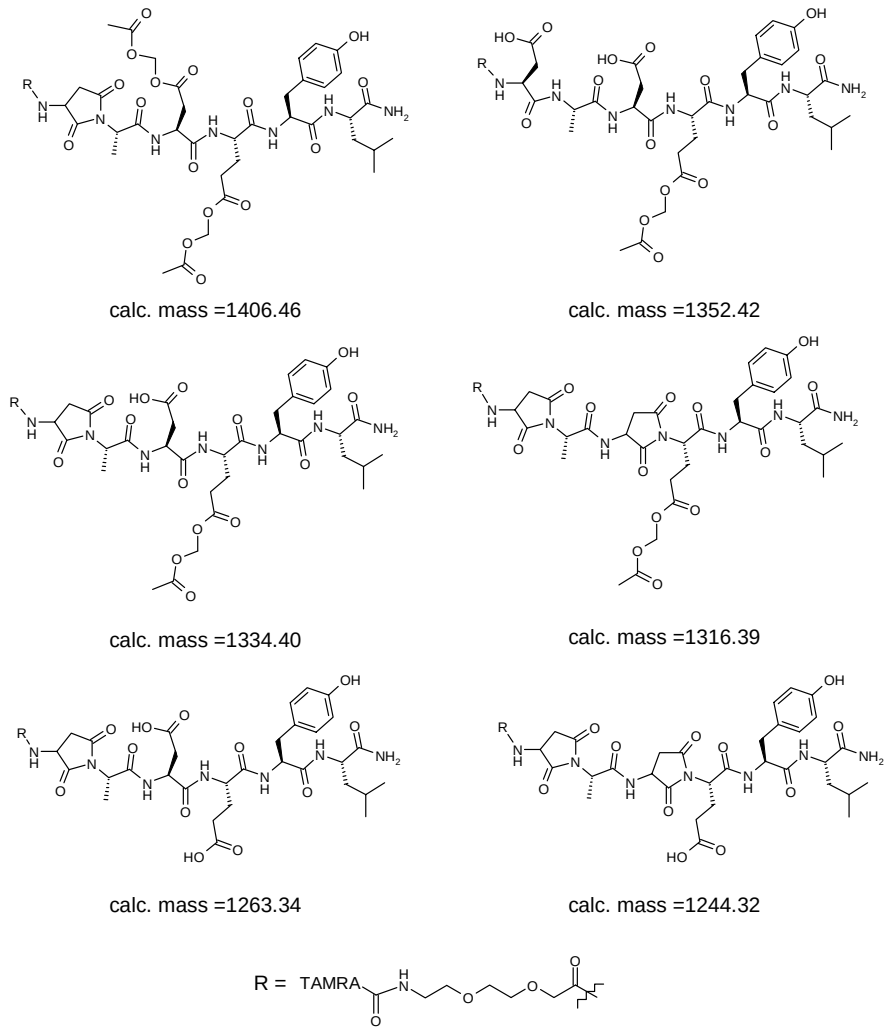

Fig. 4.11.9. Possible products originating from the TAMRA-DADEYL-AM$_3$ peptide after incubation with cell lysate, mouse serum or PLE. Cyclization of aspartate residues remains speculative and would require additional experimental evidence to be proved.

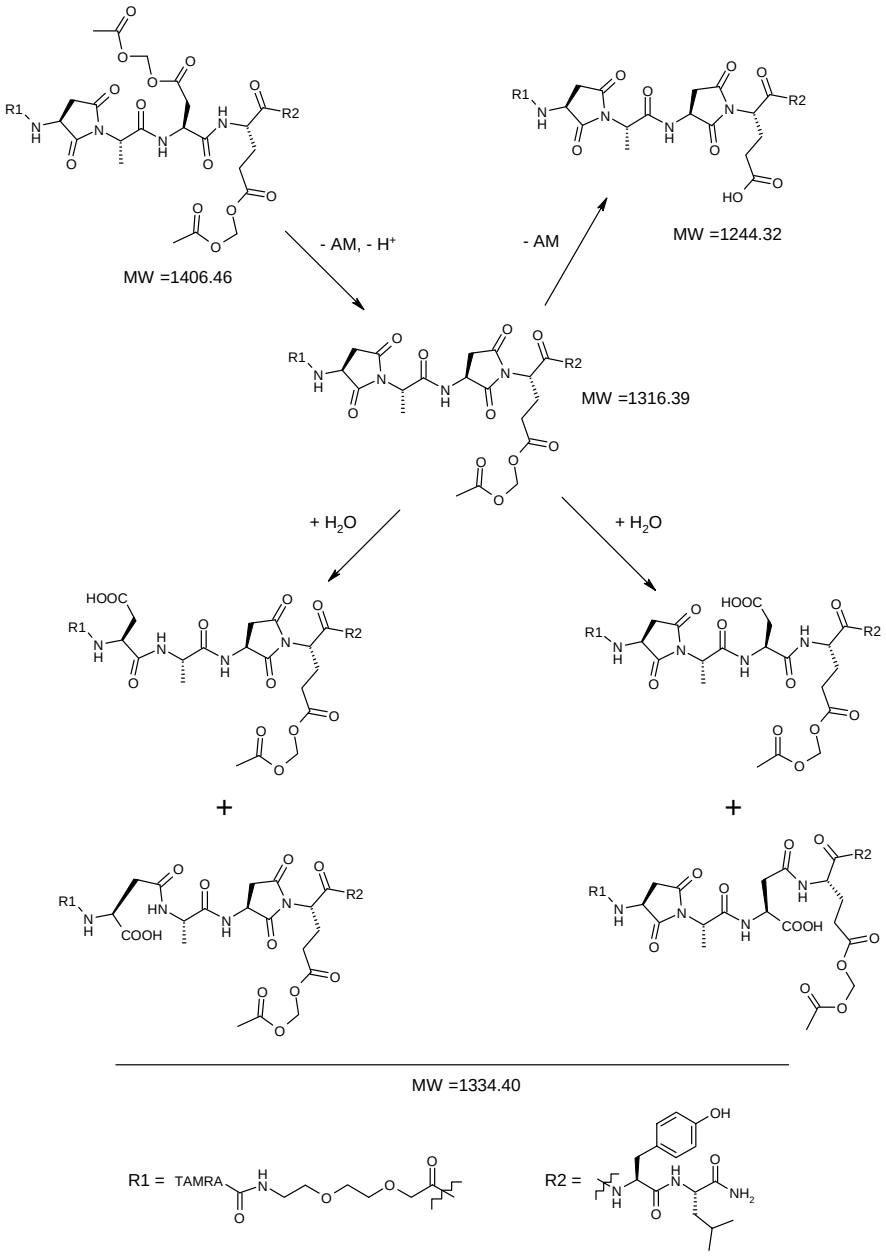

Fig. 4.11.10. A possible route to the products derived from the incubation of the TAMRA-DADEYL-AM$_3$ peptide with cell lysate or mouse serum. The hydrolysis of a single aspartimide residue would lead to a total of four products having the same observed mass (m/z 1335.50, [M+H$^+$], Fig. 4.11.5).

4.12 Effects of the Glu/Asp substitution in the DADEYL probe: *in vitro* and *in vivo* evaluation of the TAMRA-EAEEYL-AM$_3$ peptide

To verify possible differences in the pattern of AM ester hydrolysis, the synthesis of the TAMRA-EAEEYL-AM$_3$ peptide was performed, in which all the Asp residues were exchanged to Glu (Fig. 4.12.1).

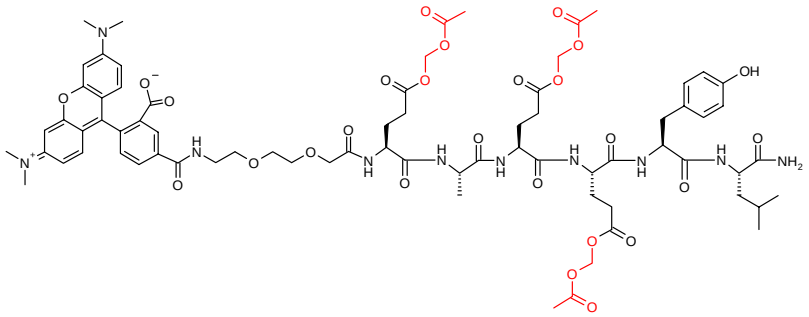

Fig 4.12.1. The TAMRA-EAEEYL-AM$_3$ peptide. The proposed structure with the AM esters on the Glu residues coloured in red (MW 1524.62).

Similarly to what was described earlier (sect. 4.9), care was taken to separate the products of the condensation of the 5(6)-TAMRA SE dye. By using only one of the two regioisomers, alkylation and subsequent purification could be accomplished easily. Along with the desired product, the reaction afforded in low yield also a peptide bearing four AM esters (Fig. 4.12.2).

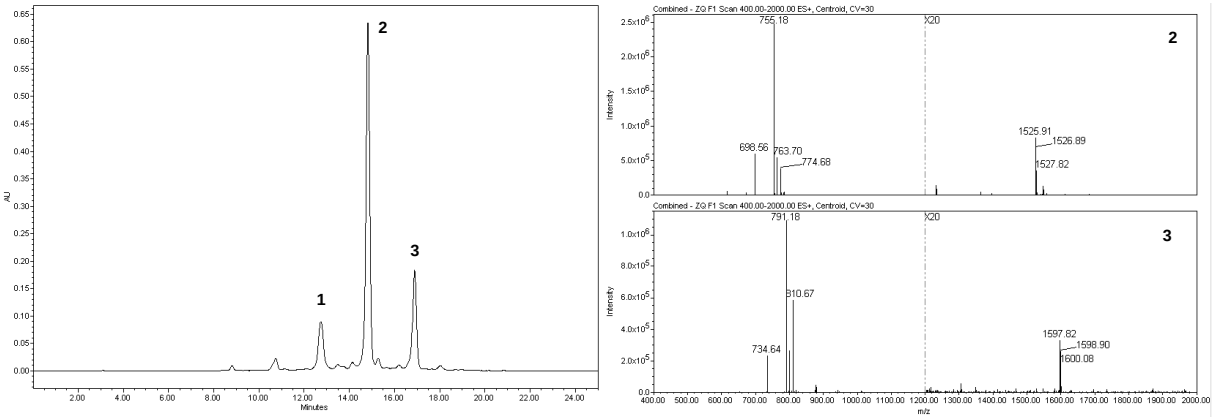

Fig. 4.12.2. LC/MS analysis of the crude from the AM-esterification reaction. The product eluting at 12.7 min (peak n.1, 11.5%) carried two AM esters, the one eluting at 14.8 min (peak n.2, 59%) three (TAMRA-EAEEYL-AM$_3$, m/z 1525.91 [M+H$^+$], mass n. 2, top right), the one eluting at 16.8 min (18%) four (TAMRA-EAEEYL-AM$_4$, m/z 1597.82 [M+H$^+$], mass n. 3, bottom right). See Material and methods, sect. 3.12.

In order to verify the location of the four AM moieties on the molecule, the latter peptide was subjected to ESI-MS/MS analysis. Unfortunally, low intensity signals were obtained from this sample, with an overall lack of accuracy and since the result could not be

confidently interpreted, it will not be reported here. Nevertheless, the penetrating capability of both peptides was tested in living HeLa Kyoto cells. The TAMRA-EAEEYL-AM_3 peptide distributed intracellularly in cytoplasm, nucleus and cytoplasmic structures resembling vacuoles (Fig. 4.12.3 *a, b*). Surprisingly, the TAMRA-EAEEYL-AM_4 peptide stained the cells only to a very limited extent (Fig. 4.12.3 *c, d*).

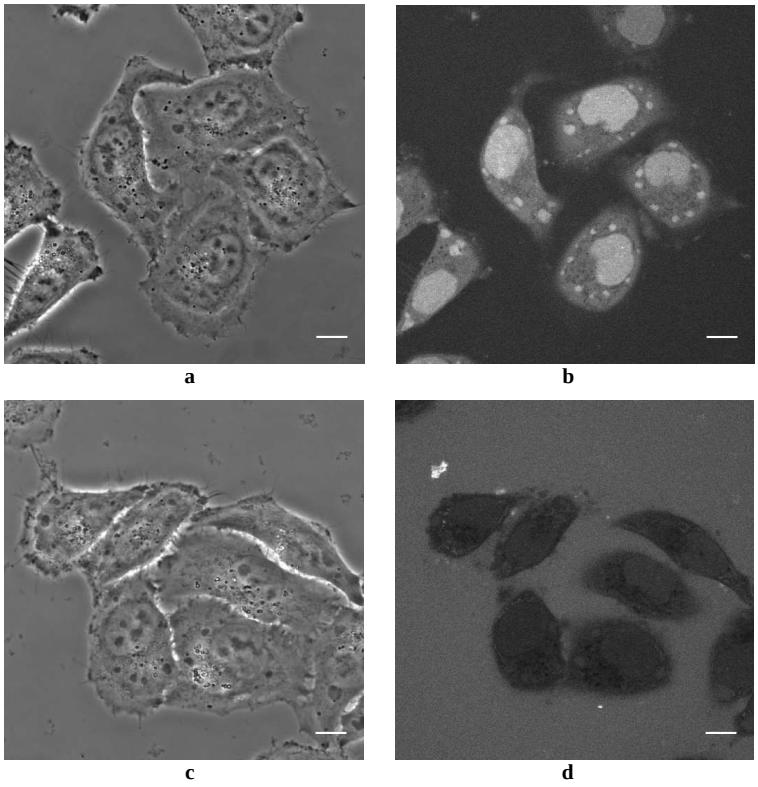

Fig. 4.12.3. The TAMRA-EAEEYL-AM_3 peptide distributed intracellularly, while the TAMRA-EAEEYL-AM_4 peptide did not translocate efficiently in living HeLa Kyoto cells. Cells were incubated with a 10 µM solution of TAMRA-EAEEYL-AM_3 (**a, b**) and TAMRA-EAEEYL-AM_4 (**c, d**) in imaging medium for 20 min at room temperature. Under these conditions the -AM_3 peptide distributed in the cell body, nucleus and other cytoplasmic structures resembling vacuoles. The -AM_4 peptide was detected in cells only to a very limited extent. Images were acquired without prior removal of peptide solutions. Pictures ***a*** and ***c*** represent transmitted light (phase contrast) images. Scale bar = 20 µm (Material and methods, sect. 3.15).

The reasons underlying this difference are still unclear. The possibility that alkylation of the carboxylic group of the TAMRA molecule (already speculated in sect. 4.9) negatively affects cell penetration requires additional analytical evidence, in order to be clarified unambiguously.

Similarly to previous *in vitro* experiments (sect. 4.11), the TAMRA-EAEEYL-AM_3 peptide was incubated with cell lysate and mouse serum to verify AM ester hydrolysis. The mass analysis revealed that, when incubated with cell lysate (Fig. 4.12.4), this alkylated peptide possessed a higher resistance compared to the corresponding TAMRA-DADEYL-

AM_3 peptide (Fig. 4.11.5). Nevertheless, the loss of one or two AM ester moieties was detectable, along with species which may have originated through cyclization (loss of 90 a.m.u.). This speculation would imply a phenomenon which, under the conditions tested, would extend also to glutamate residues. The product corresponding to a complete hydrolysis of the AM esters was on the contrary not detectable. In addition, species with lower mass indicated possible degradation not observed in the case of the TAMRA-DADEYL-AM_3 peptide (Fig. 4.11.5).

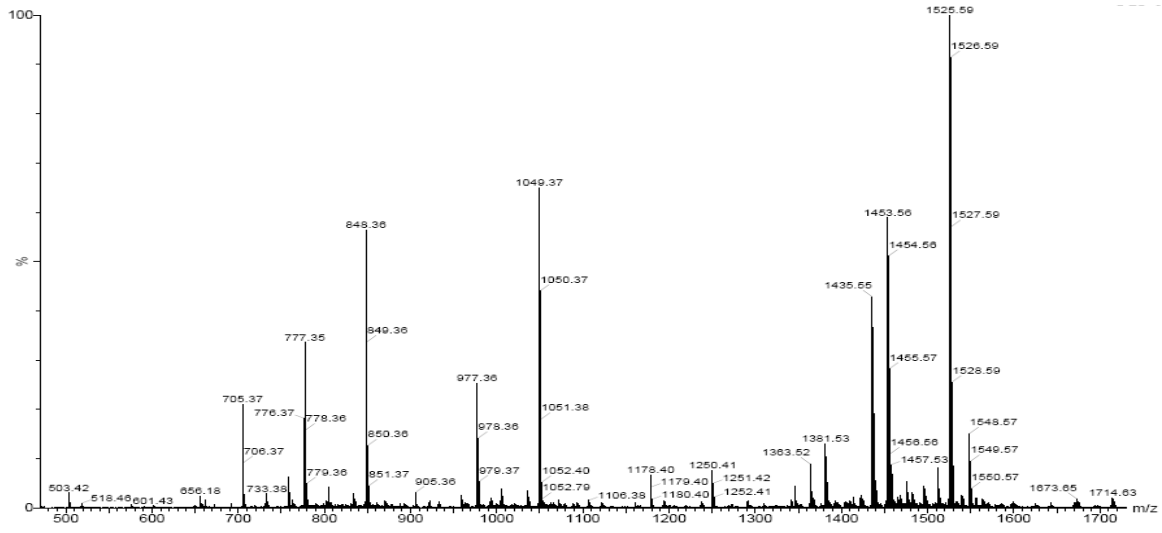

Fig. 4.12.4. The TAMRA-EAEEYL-AM_3 incubated with cell lysate. MALDI mass spectrum relative to the products of the incubation of the TAMRA-EAEEYL-AM_3 peptide (5 μM) with 3% cell lysate for 30 min in HEPES (20 mM, pH 7.4) and at room temperature. Along with the starting material carrying three AM esters (m/z 1525.59, $[M+H^+]$) peptides with two AM esters (m/z 1453.56, $[M+H^+]$) were detected. From these two species may have originated, via a speculative cyclization and elimination of the AM moiety (– 90 a.m.u.), the products with m/z 1435.55 and 1363.52, respectively. Peptides displaying one AM ester (m/z 1381.53, $[M+H^+]$) were also visible, but no product deriving from a complete AM esters hydrolysis. The presence of signals at m/z value < 1300 may prove additional degradation. Compare with Fig. 4.11.5 (Material and methods, sect. 3.21).

Following incubation with mouse serum, products corresponding to the hydrolysis of one (m/z 1453.61, $[M+H^+]$), two (m/z 1381.58, $[M+H^+]$) and three AM esters (m/z 1309.55, $[M+H^+]$) could be found. Interestingly, additional products observed in the previous experiment were not detected, while the starting material (m/z 1526.63, $[M+H^+]$) was present only in traces (Fig. 4.12.5).

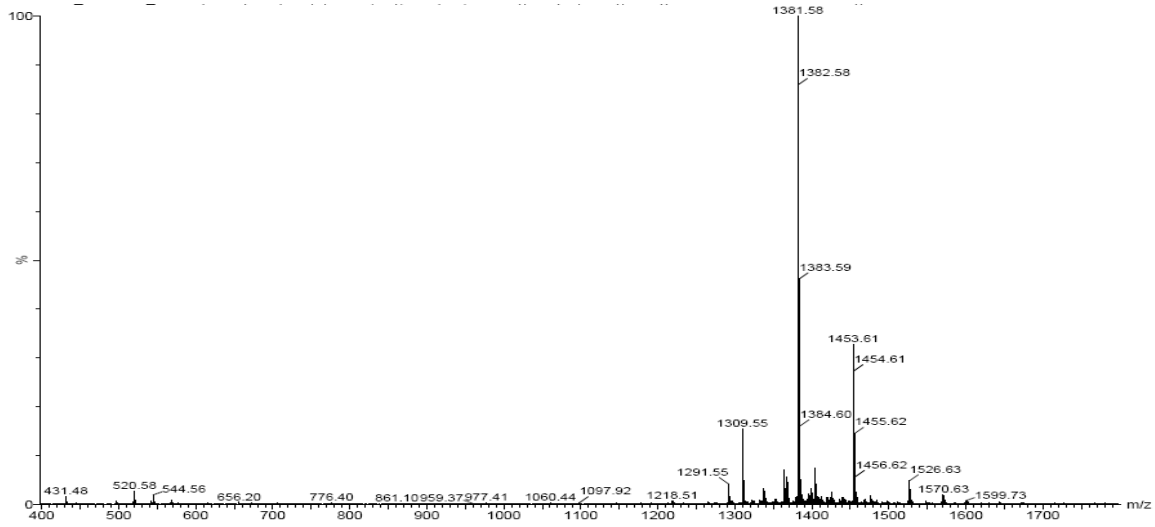

Fig. 4.12.5. The TAMRA-EAEEYL-AM$_3$ incubated with mouse serum. MALDI mass spectrum relative to the products of the incubation of the TAMRA-EAEEYL-AM$_3$ peptide (5 μM) with 3% mouse serum for 30 min in HEPES (20 mM, pH 7.4) and at room temperature. In these conditions traces of the starting material were detected (m/z 1526.63, [M+H$^+$]), along with products of hydrolysis of one AM ester (m/z 1453.61, [M+H$^+$]), two AM esters (m/z 1381.58, [M+H$^+$]) and three AM esters (m/z 1309.55, [M+H$^+$]). No secondary by-products were detectable. Compare with Figs. 4.11.5 and 4.12.4 (Material and methods, sect. 3.21).

Altogether, these findings provide evidence for a differential susceptibility of γ-glutamyl-AM esters toward hydrolysis compared to β-aspartyl-AM esters, when exposed to the esterase activity of cell lysate or mouse serum *in vitro.* Whether this situation is also reflected *in vivo* awaits confirmations. The TAMRA-EAEEYL-AM$_3$ peptide is currently under investigation in the laboratories of Prof. Bastiaens (MPI Molecular Physiology, Dortmund, Germany).

4.13 AM ester derivative of a phosphorylated DADEYL probe: a brief summary

During the course of this experimental work the synthesis of an AM ester derivative of a phosphorylated, rhodamine-labelled DADEYL probe was attempted. A peptide with a *caged* phosphate group was designed, *i.e.* a phosphate bearing a particular masking group removable via photolysis. Generally, caged compounds are inactive until irradiated (*decaged*) with light of a suitable wavelength (near-UV for the *o*-nitrobenzyl caging groups). The activation can be conveniently performed using standard microscope equipment. From a caged precursor introduced in the cell (for instance, by means of microinjection), the active molecule can be produced in an effective concentration to elicit a specific biological response, affording great temporal and spatial resolution. Clearly, cell-permeable derivatives expand remarkably the versatility of caged compounds, which have already been used in a large number of investigations and have proved to be essential components of the toolbox available to modern

cell biology [162, 163]. In particular, a caged phosphorylated, rhodamine-labelled DADEYL peptide has been recently used to monitor activity of Protein Tyrosine Phosphatase 1B (PTP1B) in living cells in a FLIM-based study [153]. The intention was to produce a cell-permeable derivative similar to the described TAMRA-DADEYL-AM_3 peptide (sect. 4.8).

As mentioned previously (sect. 4.7), the incorporation of a Tyr(Cl-Trt) into the sequence allowed phosphorylation of the Tyr residue on the resin, following selective removal of the Cl-Trt group. This was achieved by swelling the resin-bound peptide with a 1% (v/v) solution of TFA in DCM (sect. 3.1). Phosphorylation was accomplished in two steps, in analogy to published procedures [164]: 1) phosphitylation of the phenolic -OH group of the tyrosine with O-*t*-butyl-O'-(4,5-dimethoxy-2-nitrobenzyl)-N,N-diisopropylphosphoramidite;[18] 2) P^{III} to P^{V} oxidation using *t*-butyl hydroperoxide. These two steps are summarized in Fig. 4.13.1. The caged phosphorylated peptide was obtained with a purity of 89% as assessed by HPLC and its identity was confirmed by ESI-MS (Fig. 4.13.2). Following Fmoc deprotection from the N-terminus, the peptide was conjugated to the 5(6)-TAMRA SE fluorophore, then cleaved from the support and purified by preparative HPLC, affording 13.2 mg (yield = 45%) of the rhodamine-labelled, caged phosphorylated peptide, obtained with an overall purity of 98% (mixed isomers). Next, an alkylation reaction was performed to produce the AM ester derivative (sect. 3.13). Although MS analysis revealed the presence of the desired compound in the crude mixture (m/z 1845.15, $[M+H^+]$, Fig. 4.13.3), its isolation via HPLC was not successful. TFA was omitted throughout the chromatographic process to avoid premature hydrolysis of the ester on the phosphate moiety. By doing so, nevertheless, the detection of peaks became difficult, due to the overall poor resolution of the spectrum. Collection of various fractions was attempted, but the highest m/z value obtained by MS analysis was eventually 1738.2, thus differing by 107 a.m.u. from that expected. Other strategies were attempted to achieve the isolation of the desired product, including ion exchange and reverse-phase chromatography on SPE mini-columns, or solvent extraction (by using anhydrous ethyl acetate or toluene) but all these procedures were unsuccessful. Given these difficulties, further efforts in this direction were not pursued.

[18] The compound was a synthesized by Dr. Sirus Zarbakhsh (Schultz group alumnus, EMBL-Heidelberg, Germany) according to published protocols [169].

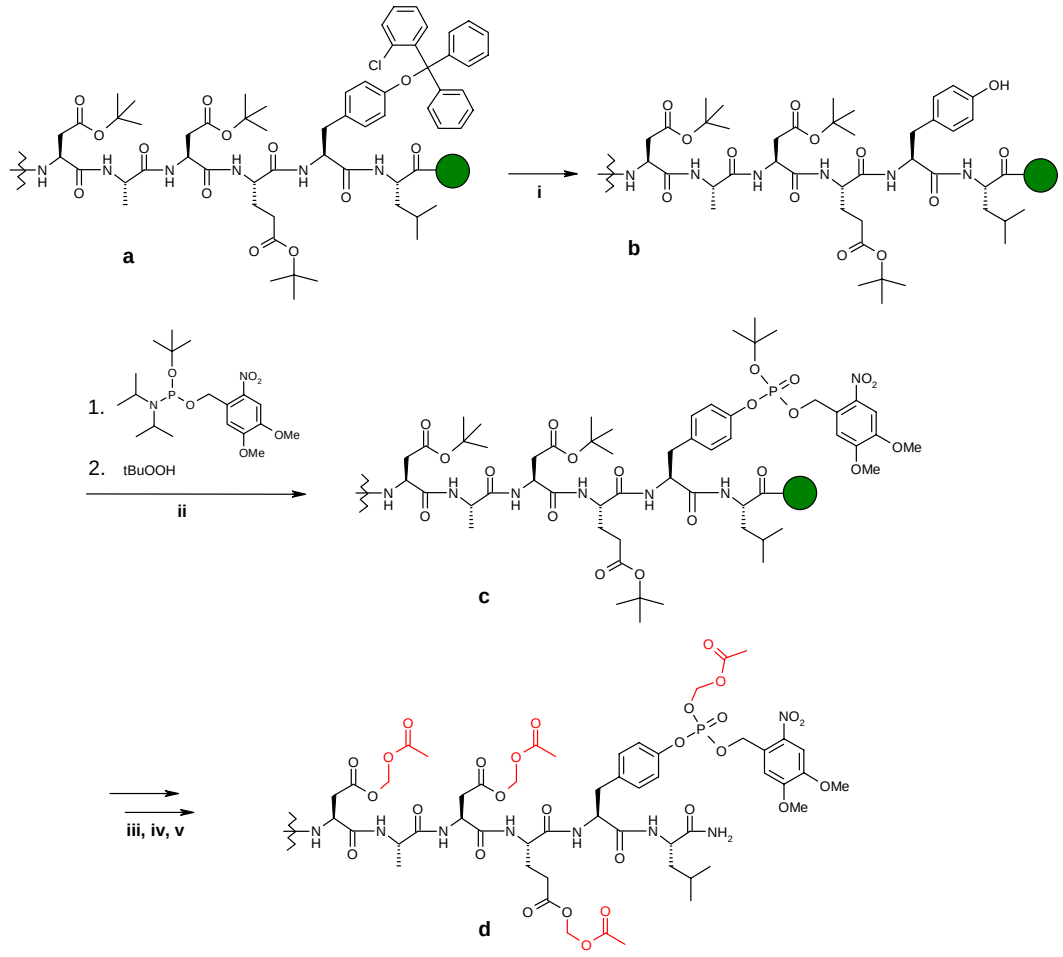

Conditions:
i. 1% TFA (v/v) in DCM
ii. 1. O-t-butyl-O'-(4,5-dimethoxy-2-nitrobenzyl)-N,N-diisopropyl phosphoramidite (10 eq), DCI (10 eq) / anh. DCM, overnight
2. tbuOOH (ca. 0.5M) in NMP, 2 x 1h
iii. 5(6)-TAMRA SE (1.1 eq) / NMP : DCM (1:1, v/v), 4h (dark)
iv. TFA/TIS/water (95:2.5:2.5, v/v/v), 3 h
v. Bromomethyl acetate (12 eq), DIPEA (12 eq)/ anh. DMF, 30 min

Fig. 4.13.1. Synthetic route to the caged phosphorylated, rhodamine-labelled, AM-esterified DADEYL peptide. The resin-bound peptide (**a**) was treated with a 1% TFA solution in DCM to remove the orthogonal group Cl-Trt from the Tyr residue (**b**). Treatment with *O-t*-butyl-*O'*-(4,5-dimethoxy-2-nitrobenzyl)-N,N-diisopropyl phosphoramidite followed by oxidation with *t*-butyl hydroperoxide afforded the caged phosphate group on Tyr (**c**). Following labelling with 5(6)-TAMRA SE, cleavage and purification, the peptide was alkylated with the intention of synthesising the AM ester derivative (d). Although MS analysis confirmed the product, every attempt to isolate the compound failed (**note:** the AEEAc spacer and the TAMRA fluorophore are omitted from the drawing). (Material and methods, sect. 3.13.)

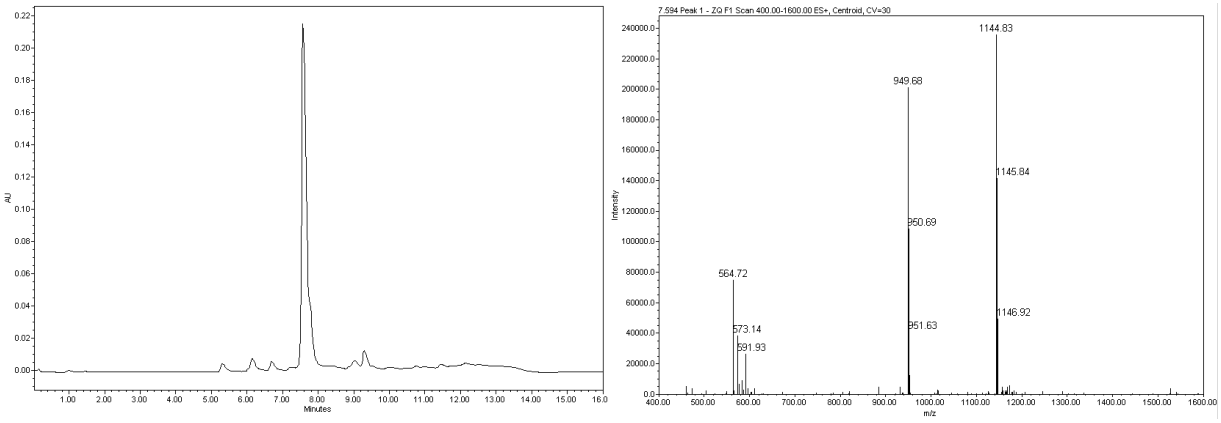

a **b**

Fig. 4.13.2. The caged phosphate on the Tyr side chain in the DADEYL peptide. (**a**) HPLC analysis showing the caged phosphorylated peptide eluting after 7.6 min in 89% purity. (**b**) ESI-MS identified the product as a $[M+H^+]$ (m/z 1144.83) species (Material and methods, sect. 3.13).

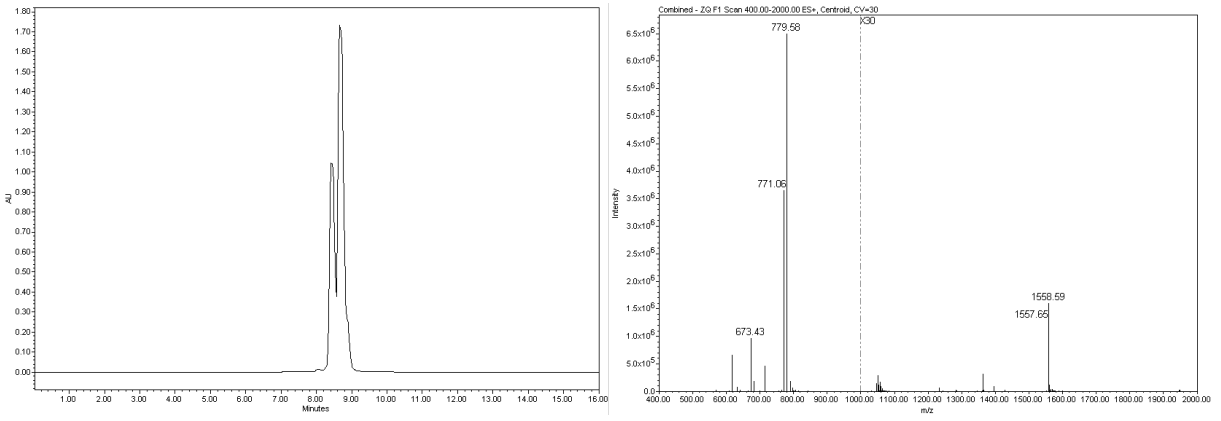

a **b**

Fig. 4.13.3. The rhodamine labelled, caged phosphorylated DADEYL peptide. (**a**) HPLC analysis showing the peptide as a mixture of partially resolved regioisomer eluting after 8.5 and 8.7 min in 98% overall purity. (**b**) ESI-MS identified the product as a $[M+H^+]$ (m/z 1557.65) and $[M+2H^+/2]$ (m/z 779.58) species (Material and methods, sect. 3.13).

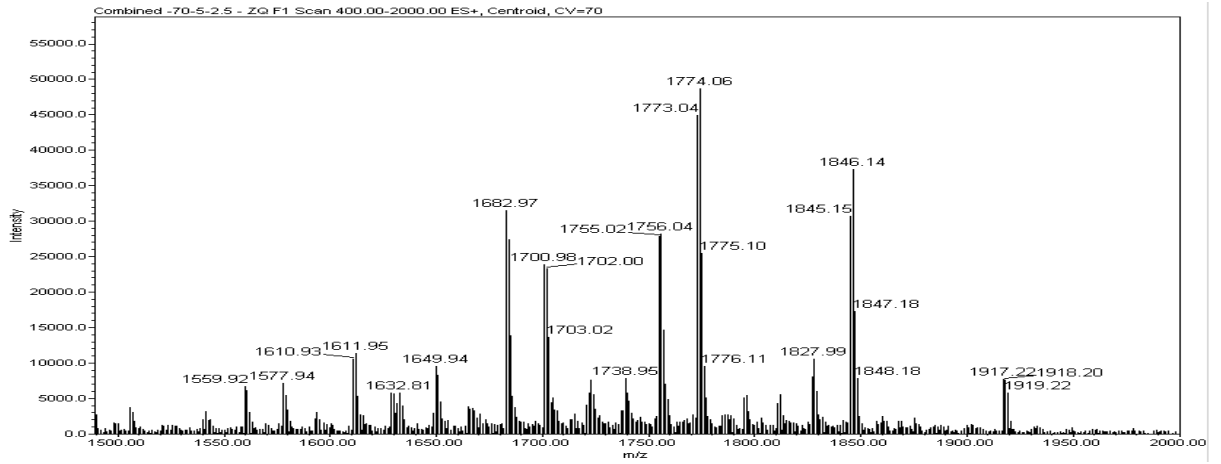

Fig. 4.13.4. ESI-MS analysis on the crude mixture from the AM esterification reaction. The $-AM_4$ ester product is visible with m/z 1845.15 ($[M+H^+]$), along with the $-AM_5$ ester species, m/z 1917.22 ($[M+H^+]$). Every attempt performed to purify the desired peptide was unfortunally unsuccessful (Material and methods, sect. 3.13).

5. Discussion

The goal of this thesis was the evaluation of the most suitable strategy aimed at the delivery to the cytoplasm of different cell types of synthetic peptide-based probes for the detection of enzyme activity in fluorescence-based (FRET) assays. In particular, we explored the possibility to confer cell-permeant properties to highly charged peptides like, for instance, the sequence DADEYL which comprises the residues 988-993 of the epithelial grow factor receptor (EGFR), and mimics one of the autophosphorylation domains. This sequence is known to be phosphorylated on the tyrosine residue *in vitro* [139, 140]. Based on this peptide, we intended to design a fluorescent probe to monitor the kinase activity of the EGFR in living cells. This probe was synthesized via the SPPS technique (sect. 3.1, 4.2) and equipped with a red fluorescent dye (rhodamine) in order to establish an ideal FRET pair with a GFP- or YFP-tagged EGFR construct (sect. 2.1). Moreover, a previous study indicated how this same sequence, when displaying a phosphorylated tyrosine, served as a probe of the protein tyrosine phosphatase 1B (PTP1B) [153]. Ideally, this substrate would serve interchangeably as a sensor for a GFP(YFP)-EGFR construct, or for a GFP(YFP)-PTP1B construct in EGFR-expressing cells.

This sequence, presenting a net negative charge at physiological pH, is poorly permeable to cell membranes. To achieve the task of a non-invasive intracellular delivery of this reporter, two possibilities have been considered: 1) the conjugation to a vector belonging to the family of the cell-penetrating peptides (CPPs) (sect. 1.2); 2) the modification of its Asp and Glu residues in order to enhance hydrophobicity and to allow its diffusion through the plasma membrane.

Two rhodamine derivatives of the cell-penetrating TAT peptide [137], termed LRh-TAT_{49-57} and TAT(K-LRh) have been synthesized (LRh = Lissamine™-rhodamine, fig 3.1.2 *a*) and analyzed regarding their translocating properties in living cells (sect. 4.1). TAT(K-LRh) is a novel fluorescent variant which, to the best of our knowledge, has remained so far undocumented. Initial observations on living HeLa Kyoto cells were performed using these compounds with a low grade of purity. Uptake into vesicles was observed, enough to initially judge the limitation of these peptides as potential vectors for the probe (Fig. 4.1.2). A diffused distribution in the cytoplasm was unfortunately the result of fixation procedures, and as such

could not be hailed as a valuable property of the TAT vectors (Fig. 4.1.3). This observation underlined the importance of performing experiments in living, unfixed cells only. Nevertheless, a new set of experiments using a highly purified preparation of the TAT peptides revealed a different scenario and reinforced the significance of a proper purification procedure. The vectors were still internalized in membrane-bound compartments, and although the nature of these has not been clarified, they appeared to be different from the endosomal vesicles initially observed (Fig. 4.1.6). The final localization may have been the result of the affinity of the Lissamine™-rhodamine dye for a specific cell compartment, but the lack of endosomal vesicles may have been denoted a different mode of cell entry. Time-lapse microscopy experiments will help to address this point. Moreover, the use of known fluorescent markers will be instrumental in revealing a possible co-localization in a specific organelle. A fluorescein-labelled 16-mer peptide containing the fragment TAT_{47-57} (YGRKKRRGRRR) has been found to penetrate and accumulate in different proportions in cytoplasm and nucleus of living fibroblasts, in about 50% of the cells within the sample [101]. In another study, a similar fluorescein-TAT_{47-57} derivative appeared to access also the nuclei of HeLa cells [99]. Here it has been shown how a large number of living mouse embryonic fibroblasts picked up the LRh-TAT_{49-57} peptide, but clearly without nuclear or endosomal accumulation (Fig. 4.1.8). This observation put emphasis on how different fluorophores may contribute to the final localization of a cell-penetrating peptide in live cells. Of particular interest in this study was the finding that the derivative TAT(K-LRh) (Fig. 4.1.1) retained the capability to permeate cells and accumulate, apparently, in compartments similar to those stained by the linear LRh-TAT_{49-57} peptide (Fig. 4.1.6). This confirmed the results of an earlier study, in which the authors described how a fluorescent Gln54Ala variant of the TAT_{49-57} domain was still capable of penetrating into cells, as measured by flow cytometry. Indeed, the Gln54Ala substitution appeared to be the only one permissive within the polycationic sequence [81]. It is surprising, nevertheless, to note how this old observation has fuelled little further research: in this respect, the new Tat(K-LRh) variant may serve as a novel, branched polycationic vector (see sect. 6). A concern regarding the TAT peptides may be their potential cytotoxicity. Nevertheless, this issue appeared to be cell specific – some cell types were more tolerant than others (MEF *vs.* HeLa Kyoto and MCF-7, sect. 4.1) and must determined in each case.

While the TAT peptides were analyzed only with respect to their translocation properties, a commercial activated Penetratin preparation was conjugated via a disulfide

bridge to the DADEYL probe and the uptake was evaluated in living MEF and MCF-7 cells (sect. 4.2, 4.3). The results appeared disappointing: the construct was internalized in endosomal vesicles in MEF cells (Fig. 4.3.1), while no uptake was recorded in MCF-7 cells under the same experimental conditions (Fig. 4.3.2). The use of two red and green fluorescent derivatives of Penetratin (RR-PEN1 and OG-PEN1), synthesized *ad hoc* (sect. 4.4), displayed a different uptake and distribution behaviour. In particular, MEF cells internalized the red Penetratin at room temperature, while uptake of the green Penetratin occurred only at 37°C, suggesting a possible role of additional components in the uptake process (Fig. 4.5.3). Despite both Penetratins appearing to concentrate in vesicles, co-localization with endosomal markers was evident only for the red Penetratin, indicating the possibility that the vesicles which entrapped the two Penetratins were not of the same nature. On the contrary, MCF-7 cells showed accumulation of the red and green Penetratins in the same compartments at 37°C, which nevertheless may have differed from the late acidic endosomes (Fig. 4.6.2). These results demonstrated how the response of a single cell toward variants of the same vector can vary, here simulated by the presence of two different fluorophores. Such comparative studies, surprisingly, has been rarely conducted in the area of fluorescent CPPs [165].

When used in large excess, (100 μM) Penetratin did not substantially change its distribution, while it compromised the membrane integrity of MEF cells as probed by the nuclear stain propidium iodide (PI), a dye membrane-impermeable to intact cells (Fig. 4.5.4). Cell morphology appeared visibly altered under transmitted light (refer to picture A1 in *Appendix* and compare nucleus and cell shape with Figs. 4.5.1 *a* – *e*). Moreover, the concentrated pattern of the PI staining could have reflected compaction of chromatin, thus indicating an on-going apoptotic process (Andrew Riddel, Flow Cytometry Core Facility, EMBL-Heidelberg, Germany, *personal communication*). Previous studies in K562 cells indicated a toxic level for Penetratin of about 30 μM, above which cell membrane permeabilization was assessed by flow cytometry with a calcein leakage test [85]. Membrane permeabilization is usually considered a sign of altered cell physiology and compromised viability: for example, cells that display PI fluorescence are normally excluded from quantification analyses during flow cytometry [166]. Finally, it was shown that the light-induced endosomal release of a fluorescent Penetratin in MCF-7 cells was characterized by evident photo-toxicity damage (Fig. 4.6.3) and clearly illustrated the limits of this kind of approach [159].

The sequestration in membrane-bound compartments of the TAT and Penetratin vectors, either alone or in conjugation with the probe of interest, appeared the major limitation for the scopes of this work. To overcome this fact, a different approach was devised. The negatively-charged Asp and Glu residues of the DADEYL fluorescent reporter were equipped with bioactivatable protecting groups in the form of acetoxymethyl (AM) esters (sect. 4.7). The rationale for this was to enhance the hydrophobic character of the molecule, thus allowing a direct diffusion through cell membranes. Once inside the cells, the probe would have been restored to its original condition by the action of non-specific ubiquitous esterases. Although successfully applied in the case of other molecules (sect. 1.1), the use of AM esters on flurescently-labelled peptides has not been extensively documented. The modification was performed after the complete synthesis, including the fluorophore 5(6)-TAMRA SE conjugation (sect. 4.7). This work demonstrated that the side-chain esterification of aspartate or glutamate residues with acetoxymethyl groups is a feasible process. Yields of the desired products increased and purifications were easily accomplished when the peptides bearing the two regioisomers of the TAMRA dye were separated by chromatography prior to the alkylation reaction (sect. 4.9, 4.12).

Remarkably the peptide with three AM esters (TAMRA-DADEYL-AM_3) distributed uniformly in the cytoplasm and nucleus of living HeLa Kyoto, and virtually in any cell present in the sample (Fig. 4.8.1 *a*). MCF-7 cells were also stained in a high number, although the intracellular concentration appeared to vary (Fig. 4.8.1 *b*). Accumulation in the cell nuclei may be attributed to the affinity of the TAMRA dye for chromatin. The modified peptide was well tolerated up to 25 μM, but a concentration as low as 5 μM was sufficient to give a noticeable signal (the peptide was routinely used at 10 μM concentration). The distribution was also effective in the presence of serum (Fig. 4.8.2) and in cells either transiently or stably transfected (Figs. 4.8.3, 4.8.4): this was an important achievement, because the Penetratin conjugate was often found to be less prone to distribute in transfected cells.

Time lapse microscopy enabled the internalization process of the TAMRA-DADEYL-AM_3 peptide to be followed, showing differences in the uptake ratio between HeLa Kyoto and MCF-7 cells (Figs. 4.8.9, 4.8.10). Nevertheless, the kinetics would be consistent with free diffusion through membranes. The difference observed may be due, for instance, to a different membrane composition between the two cell lines. This hypothesis could be eventually extended to MEF cells, which conversely showed uptake in vesicles and some diffuse

fluorescence only at a high peptide concentration (50 μM) (Fig. 4.8.5). Unexpectedly, a tripeptide displaying only one or two AM esters (TAMRA-EYL-AM_1 and -AM_2, sect. 4.9), could not translocate efficiently (Fig. 4.9.4). There are no good explanations for such behaviour, and the hypothesis of a minimal number of modified residues to produce an effective translocation needs more experimental support. Mass spectrometry analyses on the TAMRA-EYL-AM_2 peptide suggested the carboxylic group of the TAMRA dye as the additional alkylation site, although the involvement of the phenolic side chain of tyrosine could not be excluded (Tab. 4.9 *a*).

Despite the important goal of a cytoplasmic distribution of the chemically-modified DADEYL probe being achieved, fluorescence-based studies to probe the peptide-enzyme interaction failed (sect 4.10). To investigate the possible reasons, a series of *in vitro* experiments were designed. First, esterase sources were chosen (cell lysate, mouse serum, FBS, PLE) and their activity tested using the model compound α-naphthyl acetate. A high esterase activity was confirmed for cell lysates and mouse serum, a medium grade for PLE and a low grade for FBS (Figs. 4.11.2, 4.11.3). Next, the TAMRA-DADEYL-AM_3 peptide was incubated with the various esterase sources and the products analyzed via mass spectrometry (sect. 4.11). The results revealed how, along with incomplete AM ester hydrolysis, the peptide likely underwent secondary modifications which may have included cyclization of aspartate residues to form aspartimide moieties (Figs. 4.11.5, 4.11.6, 4.11.9); these, in turn, may have undergone spontaneous hydrolysis, with the consequence of the formation of β-amino acid residues (Fig. 4.11.10). At this stage it is not possible to claim whether the supposed modifications also occurred in the cell environment, but if so, they would contribute significantly to the loss of affinity of the substrate and the lack of a specific response. Clearly, the hypotheses formulated from these *in vitro* data need further investigations to be tested, with the help of additional analytical techniques. To assess possible differences in the hydrolysis of the AM esters, a mimic of the DADEYL peptide containing only glutamate residues in place of the aspartate (TAMRA-EAEEYL-AM_3), was synthesized (sect. 4.12). Its penetration into cells appeared equally efficient (Fig. 4.12.3). Mass spectrometry analysis following incubation with cell lysate showed also in this case an incomplete hydrolysis of AM esters, probably accompanied by the formation of additional degradation products (Fig. 4.12.4). Interestingly, the same peptide underwent a “clean”

hydrolysis of the AM groups when incubated with mouse serum (Fig. 4.12.5). This may reflect a differential esterase activity present in cell lysates and mouse serum.

Finally, the chemical synthesis of a caged phosphorylated, AM-esterified peptide (TAMRA-DADEY(cgdP)L-AM_4, sect. 4.13) was successful as indicated by mass spectrometry, while its isolation failed, probably due to a higher propensity to hydrolyse than the TAMRA-DADEYL-AM_3 peptide.

6. Conclusions

This work reported the following observations:

a) despite its use in numerous applications (sect.1.2), the vector Penetratin appeared unsuitable for the delivery of the designed DADEYL probe. Both the conjugate LRh-DADEYL-PEN and two different fluorescence derivatives of the vector showed a constant entrapment in vesicles, some of which are of lysosomal origin.

b) TAT(K-LRh), a novel branched derivative of the TAT_{49-57} domain appeared to distribute in different membrane bound compartments from the endosomal vesicles, and as such it may be used as a novel vector for delivery of probes in specific cell locations (see sect. 7).

c) Direct modification of the negatively-charged residues of the DADEYL peptide in the form of acetoxymethyl esters allowed a straightforward, highly efficient penetration in the cytoplasm and nucleus of two different cell types (HeLa Kyoto and MCF-7 cells). Unfortunally, no activity of the probe could be detected in fluorescent-based assays, likely because of secondary modifications which could have reduced its affinity for the target enzyme (EGFR). Understanding the exact nature of these modifications (so far only postulated on the basis of *in vitro* data) will help eventually to modify the strategy regarding the esterification step. Different kind of esters could in fact reveal themselves more suited for this temporary protection and less prone to deleterious side reactions. This may be usefully extended to the synthesis of alkyl-protected, phosphorylated peptides in order to achieve a better stability of these compounds.

7. Outlook

The family of the polycationic cell-penetrating peptides largely catalyzes nowadays the attention of the investigators [75, 125, 137, 167]. In this work a novel TAT variant – TAT(K-LRh) – has been presented. Equipped with a Lissamine™-rhodamine dye, this peptide gained access to the intracellular environment without apparent distribution in endosomal vesicles. Further studies will need to be performed in order to assess the influence of different fluorophores to the intracellular localization. Moreover, the co-incubation with known fluorescent markers will help to identify the cellular organelle(s) involved in its accumulation. Particularly interesting will be to verify whether the peptide localizes in mitochondria, since this possibility has so far been disputed for the TAT peptide or its protein conjugates [168-171]. The accumulation in a different compartment from the endosome, if confirmed, will provide the interesting perspective of redirecting conjugates with cargoes of interest specifically to that compartment. Alternatively, for a more general use of the vector, an activated thiol group could be inserted into the sequence to enable conjugation via disulfides [172]. Hence, the construct would have the advantage to undergo spontaneous hydrolysis in the reducing environment of the cell. The branched TAT(Q54K) peptide would look as represented in Fig. 7.1.

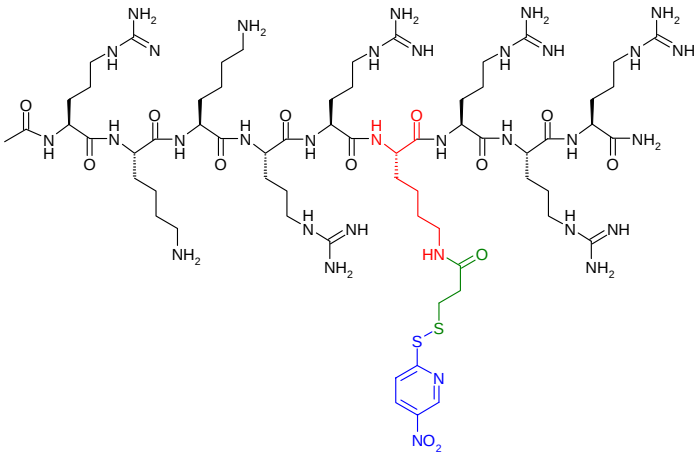

Fig. 7.1. A branched TAT(Q54K) peptide as a novel TAT-based cargo. The Lys residue (red) would be introduced with an orthogonal protecting group such the Mtt group (sect. 4.1). Insertion of 3,3'-dithiodipropionic acid followed by reduction (e.g. mercaptoethanol) would further elongate the chain (green). Last, activation of the free thiol group with dithio-bis(5-nitropyridine) (DTNP, blue) would permit conjugation to a cargo via disulfide bridge formation.

Poly-arginine peptides having a minimal number of six to nine residues (Arg_6 – Arg_9) are synthetic TAT analogues known to translocate into cells [118, 167, 173]. In previous

studies tryptophan residues were shown to be important for the internalization process of Penetratin [79]. These residues may be eventually combined in novel peptides comprised of modules such as $[Trp\text{-}Arg\text{-}Trp\text{-}Arg]_n$ or $[Gly\text{-}Arg\text{-}Trp\text{-}Arg]_n$ (n = 3 or 4). These peptides may display interesting characteristics in terms of cell translocation. Eventually, an activated terminal thiol group would enable conjugation to a cargo via a disulfide bridge (Fig. 7.2).

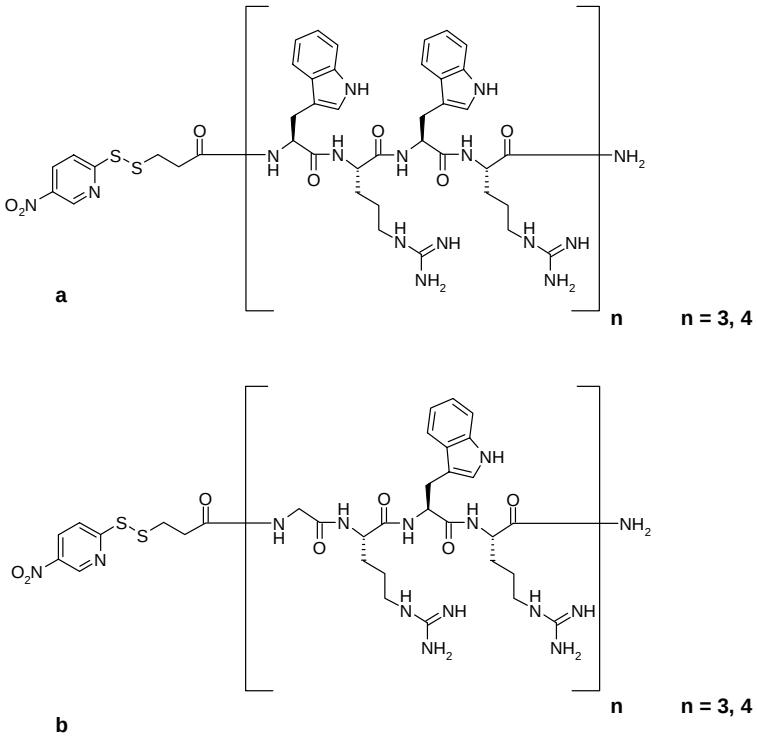

Fig. 7.1. Novel poly-arginine analogues. Would peptides comprised of modules such as $[Trp\text{-}Arg\text{-}Trp\text{-}Arg]_n$ or $[Gly\text{-}Arg\text{-}Trp\text{-}Arg]_n$ (n = 3 or 4) mimic and improve upon the features of both TAT and Penetratin vectors?

The AM-esterified DADEYL peptide has shown excellent translocating properties, with the capability of diffusing evenly through the cytoplasm and nucleus of cells. Unfortunately, the peptide seemed to favour secondary modifications which altered the structure and properties of the probes. Nevertheless, short oligopeptides bearing acetoxymethyl (or other) esters may yet serve as good candidates for the role of vector. The experience obtained with the TAMRA-DADEYL-AM_3 peptide may pave the way to the use of a vector built upon the sequence $[Asp(O\text{-}AM)\text{-}X]_n$ (n = 3) where X would be, for instance, Ala or another small hydrophobic/ uncharged amino acid. In this case, the conjugation via disulphide to a cargo would be performed preferably prior the alkylation step, since the free sulfhydryl group would likely compete for the alkylating reagent or be the cause of cross-reactions. The possibility of using different alkyl moieties should also be evaluated, having in mind that bulky or longer

chain esters may be detrimental to the solubility. A vector such as the one depicted in Fig. 7.3 may be usefully exploited, for instance, for the internalization of small, cell-impermeable compounds.

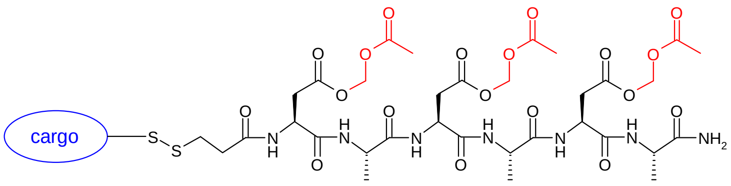

Fig. 7.3. Proposed vector based on AM ester-protected oligopeptide. A sequence based on the module [Asp(O-AM)-X]$_n$ (X = Ala; n = 3) linked to a cargo via disulphide bridge may be potentially useful for cytoplasmic delivery.

Appendix

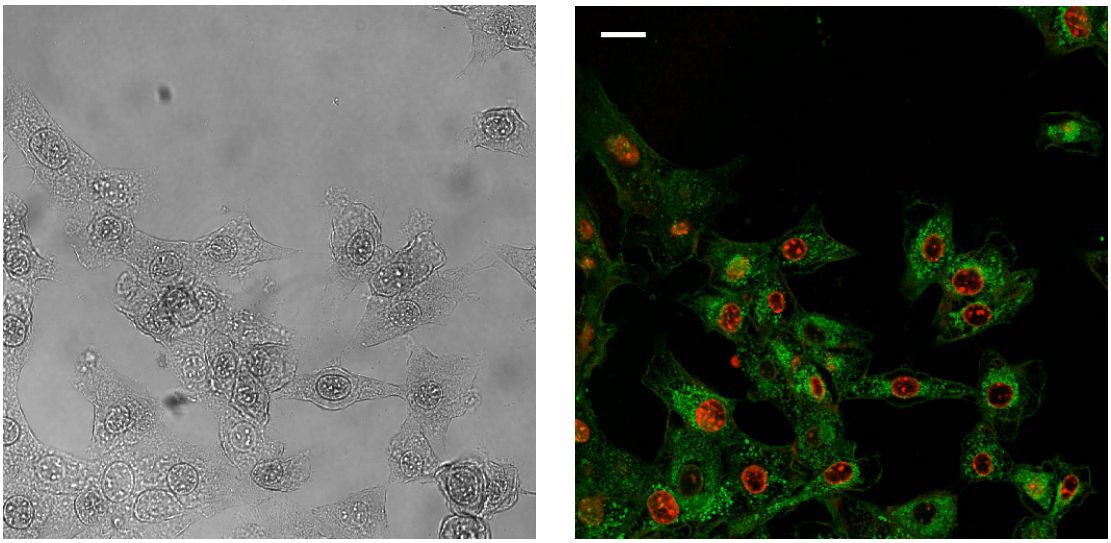

Fig. A1. (**left**) A transmitted light image showing MEF cells after the pulse with 100 µM OG-PEN1 peptide. Severe changes in the morphology of the cells are evident. (**right**) The fluorescent image as reported in fig. 4.5.4 *c*. Scale bar = 20 µm.

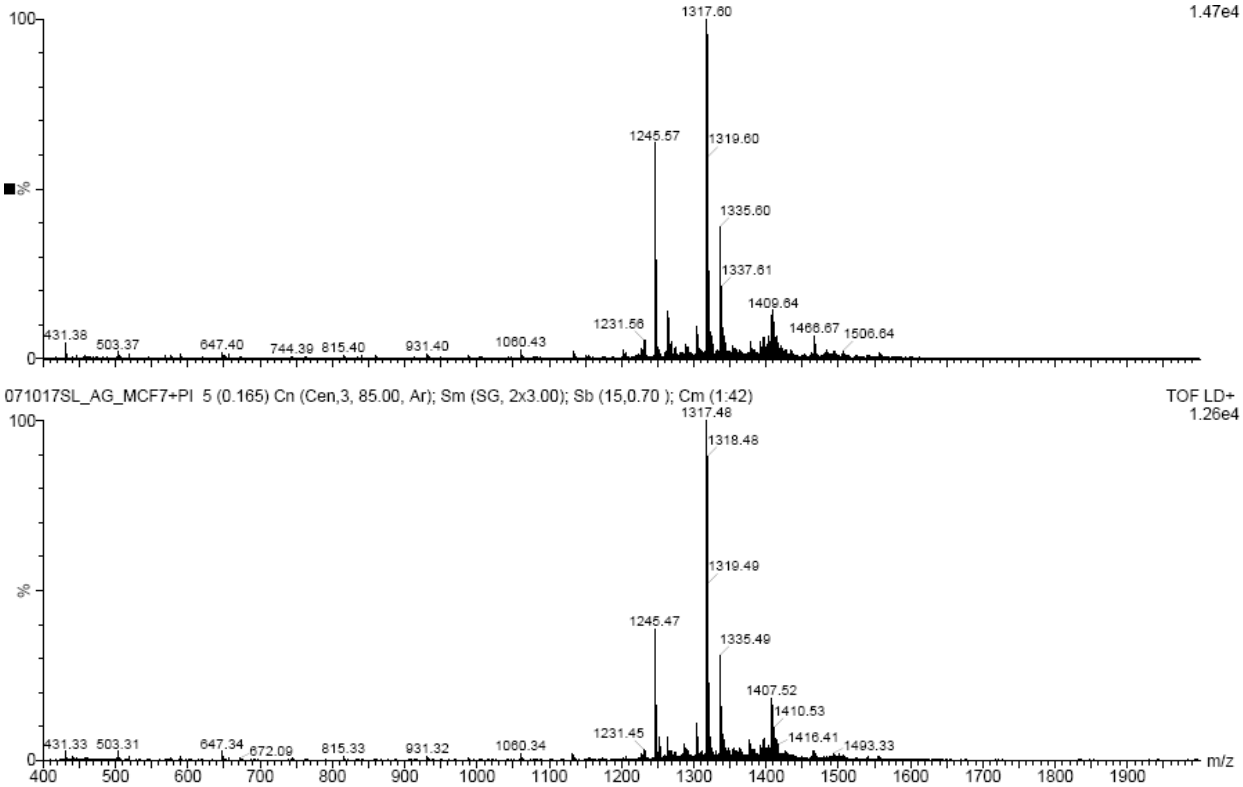

Fig. A2. Products of the incubation of the peptide TAMRA-DADEYL-AM_3 with heat-inactivated (56°C, 45 min) cell lysate (top panel), or with cell lysate in the presence of proteases inhibitors (bottom panel).

Acknowledgments

My years at EMBL made me discover how fascinating microscopy can be, which I probably consider now as the “real” job for any biologist, despite its complicated features and all the unexpected difficulties (...those that pop up in the middle of the night, when you are doing your ultimate experiment, and nobody is around to save your soul!). I am very thankful to my friend and labmate Alen Piljic, and to Dr. Stefan Terjung (from EMBL - ALMF group) for their help and their willingness to share “tricks and tips” regarding all the *hands-on* and image processing topics.

I am much in debt to my friend and labmate Adrian Neal, who with patience and care “smoothed” my english and helped me to make this thesis – hopefully – a pleasant reading.

A big “goodbye” and “hug” to all present and past members of the Schultz group, in particular Alen, Adrian, Amanda, Sirus, Gregor, Christiane and Shannon with whom I shared thoughts, advice, support and tons of “cheeky cheeky coffees”!

A warm thankyou to the components of my TAC, Dr. Carsten Schultz (EMBL), Dr. Lars Steinmetz (EMBL), Dr. Michael Knop (EMBL), Prof. Andres Jäschke (Heidelberg University) and to Prof. Jennifer Reed (Heidelberg University), who promptly accepted to join the committee for my *defence.*

Un saluto particolare a tutta la “comunità” italiana all’EMBL, presente e passata, ed un grazie di cuore a Fabiana, Barbara, Antonino, Max, Tiziana per il loro supporto e sostegno nei momenti difficili...anche se vi siete sparpagliati chi di qua, chi di là, siete sempre con me!

E, per finire, un pensiero particolare alla mia famiglia, per la sua costante vicinanza.

References

1. Gurtu, V., S.R. Kain, and G. Zhang, *Fluorometric and colorimetric detection of caspase activity associated with apoptosis.* Anal Biochem, 1997. **251**(1): p. 98-102.
2. Nishikata, M., et al., *A phosphotyrosine-containing quenched fluorogenic peptide as a novel substrate for protein tyrosine phosphatases.* Biochem J, 1999. **343 Pt 2**: p. 385-91.
3. Baruch, A., D.A. Jeffery, and M. Bogyo, *Enzyme activity--it's all about image.* Trends Cell Biol, 2004. **14**(1): p. 29-35.
4. Shaner, N.C., P.A. Steinbach, and R.Y. Tsien, *A guide to choosing fluorescent proteins.* Nat Methods, 2005. **2**(12): p. 905-9.
5. Sameni, M., J. Dosescu, and B.F. Sloane, *Imaging proteolysis by living human glioma cells.* Biol Chem, 2001. **382**(5): p. 785-8.
6. Sameni, M., K. Moin, and B.F. Sloane, *Imaging proteolysis by living human breast cancer cells.* Neoplasia, 2000. **2**(6): p. 496-504.
7. Mook, O.R., et al., *In situ localization of gelatinolytic activity in the extracellular matrix of metastases of colon cancer in rat liver using quenched fluorogenic DQ-gelatin.* J Histochem Cytochem, 2003. **51**(6): p. 821-9.
8. Hirata, H., et al., *Caspases are activated in a branched protease cascade and control distinct downstream processes in Fas-induced apoptosis.* J Exp Med, 1998. **187**(4): p. 587-600.
9. Komoriya, A., et al., *Assessment of caspase activities in intact apoptotic thymocytes using cell-permeable fluorogenic caspase substrates.* J Exp Med, 2000. **191**(11): p. 1819-28.
10. Blum, G., et al., *Dynamic imaging of protease activity with fluorescently quenched activity-based probes.* Nat Chem Biol, 2005. **1**(4): p. 203-9.
11. Wichmann, O., J. Wittbrodt, and C. Schultz, *A small-molecule FRET probe to monitor phospholipase A2 activity in cells and organisms.* Angew Chem Int Ed Engl, 2006. **45**(3): p. 508-12.
12. Murakami, M. and I. Kudo, *Phospholipase A2.* J Biochem, 2002. **131**(3): p. 285-92.
13. Funk, C.D., *Prostaglandins and leukotrienes: advances in eicosanoid biology.* Science, 2001. **294**(5548): p. 1871-5.
14. Lackowicz, J.R., *Principles of Fluorescence Spectroscopy*. 1983, New York: Plenum.
15. Förster, V.T., *Zwischenmolekulare Energiewanderung und Fluoreszenz.* Ann. Phys., 1948: p. 54-75.
16. Cardullo, R.A. and V. Parpura, *Fluorescence resonance energy transfer microscopy: theory and instrumentation.* Methods Cell Biol, 2003. **72**: p. 415-30.
17. Wouters, F.S., P.J. Verveer, and P.I. Bastiaens, *Imaging biochemistry inside cells.* Trends Cell Biol, 2001. **11**(5): p. 203-11.
18. Zlokarnik, G., et al., *Quantitation of transcription and clonal selection of single living cells with beta-lactamase as reporter.* Science, 1998. **279**(5347): p. 84-8.
19. Rudolf, M.T., et al., *Antagonists of myo-inositol 3,4,5,6-tetrakisphosphate allow repeated epithelial chloride secretion.* Bioorg Med Chem, 2003. **11**(15): p. 3315-29.
20. Jiang, T., et al., *Membrane-permeant esters of phosphatidylinositol 3,4,5-trisphosphate.* J Biol Chem, 1998. **273**(18): p. 11017-24.
21. Dinkel, C., et al., *Membrane-Permeant 3-OH-Phosphorylated Phosphoinositide Derivatives.* Angew Chem Int Ed Engl, 2001. **40**(16): p. 3004-3008.
22. Schultz, C., *Prodrugs of biologically active phosphate esters.* Bioorg Med Chem, 2003. **11**(6): p. 885-98.

23. Wermuth, C.G., *Designing Prodrugs and Bioprecursors,* in *The Practice of Medicinal Chemistry*. 2003, Elsevier.
24. Bodor, N., et al., *A strategy for delivering peptides into the central nervous system by sequential metabolism.* Science, 1992. **257**(5077): p. 1698-700.
25. Borchardt, R.T., *Optimizing oral absorption of peptides using prodrug strategies.* J Control Release, 1999. **62**(1-2): p. 231-8.
26. Oliyai, R. and V.J. Stella, *Prodrugs of peptides and proteins for improved formulation and delivery.* Annu Rev Pharmacol Toxicol, 1993. **33**: p. 521-44.
27. Wang, W., et al., *Prodrug approaches to the improved delivery of peptide drugs.* Curr Pharm Des, 1999. **5**(4): p. 265-87.
28. Lee, C.L., et al., *Localized measurement of kinase activation in oocytes of Xenopus laevis.* Nat Biotechnol, 1999. **17**(8): p. 759-62.
29. Frankel, A.D. and C.O. Pabo, *Cellular uptake of the tat protein from human immunodeficiency virus.* Cell, 1988. **55**(6): p. 1189-93.
30. Green, M. and P.M. Loewenstein, *Autonomous functional domains of chemically synthesized human immunodeficiency virus tat trans-activator protein.* Cell, 1988. **55**(6): p. 1179-88.
31. Joliot, A., et al., *Antennapedia homeobox peptide regulates neural morphogenesis.* Proc Natl Acad Sci U S A, 1991. **88**(5): p. 1864-8.
32. Vives, E., P. Brodin, and B. Lebleu, *A Truncated HIV-1 Tat Protein Basic Domain Rapidly Translocates through the Plasma Membrane and Accumulates in the Cell Nucleus.* J. Biol. Chem., 1997. **272**(25): p. 16010-16017.
33. Vives, E., et al., *Structure–activity relationship study of the plasma membrane translocating potential of a short peptide from HIV-1 Tat protein.* Lett Peptide Sci, 1997. **4**(4-6): p. 429-436.
34. Derossi, D., et al., *The third helix of the Antennapedia homeodomain translocates through biological membranes.* J. Biol. Chem., 1994. **269**(14): p. 10444-10450.
35. Langel, U., ed. *Cell-penetrating peptides. Processes and Applications*. Pharmacology and Toxicology: Basic and Clinical Aspects. 2002, CRC Press: Boca Raton, FL (USA). 406.
36. Fischer, R., et al., *Break on through to the other side-biophysics and cell biology shed light on cell-penetrating peptides.* Chembiochem, 2005. **6**(12): p. 2126-42.
37. Zorko, M. and U. Langel, *Cell-penetrating peptides: mechanism and kinetics of cargo delivery.* Advanced Drug Delivery Reviews, 2005. **57**(4): p. 529-545.
38. Lin, Y.Z., et al., *Inhibition of nuclear translocation of transcription factor NF-kappa B by a synthetic peptide containing a cell membrane-permeable motif and nuclear localization sequence.* J Biol Chem, 1995. **270**(24): p. 14255-8.
39. Rojas, M., S. Yao, and Y.Z. Lin, *Controlling epidermal growth factor (EGF)-stimulated Ras activation in intact cells by a cell-permeable peptide mimicking phosphorylated EGF receptor.* J Biol Chem, 1996. **271**(44): p. 27456-61.
40. Troy, C.M., et al., *The contrasting roles of ICE family proteases and interleukin-1beta in apoptosis induced by trophic factor withdrawal and by copper/zinc superoxide dismutase down-regulation.* Proc Natl Acad Sci U S A, 1996. **93**(11): p. 5635-40.
41. Taylor, C.T., et al., *Phosphorylation-dependent targeting of cAMP response element binding protein to the ubiquitin/proteasome pathway in hypoxia.* Proc Natl Acad Sci U S A, 2000. **97**(22): p. 12091-6.
42. Dostmann, W.R., et al., *Highly specific, membrane-permeant peptide blockers of cGMP-dependent protein kinase Ialpha inhibit NO-induced cerebral dilation.* Proc Natl Acad Sci U S A, 2000. **97**(26): p. 14772-7.

43. Chang, M., et al., *Dissecting G protein-coupled receptor signaling pathways with membrane-permeable blocking peptides. Endogenous 5-HT(2C) receptors in choroid plexus epithelial cells.* J Biol Chem, 2000. **275**(10): p. 7021-9.
44. Dunican, D.J. and P. Doherty, *Designing cell-permeant phosphopeptides to modulate intracellular signaling pathways.* Biopolymers, 2001. **60**(1): p. 45-60.
45. Bonny, C., et al., *Cell-permeable peptide inhibitors of JNK: novel blockers of beta-cell death.* Diabetes, 2001. **50**(1): p. 77-82.
46. Lu, J., et al., *TAP-independent presentation of CTL epitopes by Trojan antigens.* J Immunol, 2001. **166**(12): p. 7063-71.
47. Pooga, M., et al., *Cell penetrating PNA constructs regulate galanin receptor levels and modify pain transmission in vivo.* Nat Biotechnol, 1998. **16**(9): p. 857-61.
48. Astriab-Fisher, A., et al., *Conjugates of antisense oligonucleotides with the Tat and antennapedia cell-penetrating peptides: effects on cellular uptake, binding to target sequences, and biologic actions.* Pharm Res, 2002. **19**(6): p. 744-54.
49. Simeoni, F., et al., *Insight into the mechanism of the peptide-based gene delivery system MPG: implications for delivery of siRNA into mammalian cells.* Nucleic Acids Res, 2003. **31**(11): p. 2717-24.
50. Muratovska, A. and M.R. Eccles, *Conjugate for efficient delivery of short interfering RNA (siRNA) into mammalian cells.* FEBS Lett, 2004. **558**(1-3): p. 63-8.
51. Chaubey, B., et al., *A PNA-transportan conjugate targeted to the TAR region of the HIV-1 genome exhibits both antiviral and virucidal properties.* Virology, 2005. **331**(2): p. 418-28.
52. Tripathi, S., et al., *Anti-HIV-1 activity of anti-TAR polyamide nucleic acid conjugated with various membrane transducing peptides.* Nucleic Acids Res, 2005. **33**(13): p. 4345-56.
53. Turner, J.J., et al., *Cell-penetrating peptide conjugates of peptide nucleic acids (PNA) as inhibitors of HIV-1 Tat-dependent trans-activation in cells.* Nucl. Acids Res., 2005. **33**(21): p. 6837-6849.
54. Bendifallah, N., et al., *Evaluation of Cell-Penetrating Peptides (CPPs) as Vehicles for Intracellular Delivery of Antisense Peptide Nucleic Acid (PNA).* Bioconjugate Chem., 2006. **17**(3): p. 750-758.
55. Turner, J.J., et al., *RNA targeting with peptide conjugates of oligonucleotides, siRNA and PNA.* Blood Cells, Molecules, and Diseases, 2007. **38**(1): p. 1-7.
56. Singh, D., et al., *Peptide-based intracellular shuttle able to facilitate gene transfer in mammalian cells.* Bioconjug Chem, 1999. **10**(5): p. 745-54.
57. Gratton, J.P., et al., *Cell-permeable peptides improve cellular uptake and therapeutic gene delivery of replication-deficient viruses in cells and in vivo.* Nat Med, 2003. **9**(3): p. 357-62.
58. Ignatovich, I.A., et al., *Complexes of plasmid DNA with basic domain 47-57 of the HIV-1 Tat protein are transferred to mammalian cells by endocytosis-mediated pathways.* J Biol Chem, 2003. **278**(43): p. 42625-36.
59. Moy, P., et al., *Tat-mediated protein delivery can facilitate MHC class I presentation of antigens.* Molecular Biotechnology, 1996. **6**(2): p. 105-113.
60. Elliott, G. and P. O'Hare, *Intercellular trafficking and protein delivery by a herpesvirus structural protein.* Cell, 1997. **88**(2): p. 223-33.
61. Rojas, M., et al., *Genetic engineering of proteins with cell membrane permeability.* Nat Biotechnol, 1998. **16**(4): p. 370-5.
62. Stein, S., et al., *A disulfide conjugate between anti-tetanus antibodies and HIV (37-72)Tat neutralizes tetanus toxin inside chromaffin cells.* FEBS Lett, 1999. **458**(3): p. 383-6.

63. Schwarze, S.R., et al., *In vivo protein transduction: delivery of a biologically active protein into the mouse.* Science, 1999. **285**(5433): p. 1569-72.
64. Morris, M.C., et al., *A peptide carrier for the delivery of biologically active proteins into mammalian cells.* Nat Biotechnol, 2001. **19**(12): p. 1173-6.
65. Fittipaldi, A., et al., *Cell Membrane Lipid Rafts Mediate Caveolar Endocytosis of HIV-1 Tat Fusion Proteins.* J. Biol. Chem., 2003. **278**(36): p. 34141-34149.
66. Futaki, S., et al., *Arginine carrier peptide bearing Ni(II) chelator to promote cellular uptake of histidine-tagged proteins.* Bioconjug Chem, 2004. **15**(3): p. 475-81.
67. Saalik, P., et al., *Protein cargo delivery properties of cell-penetrating peptides. A comparative study.* Bioconjug Chem, 2004. **15**(6): p. 1246-53.
68. Wadia, J.S. and S.F. Dowdy, *Transmembrane delivery of protein and peptide drugs by TAT-mediated transduction in the treatment of cancer.* Adv Drug Deliv Rev, 2005. **57**(4): p. 579-96.
69. Myrberg, H., M. Lindgren, and U. Langel, *Protein Delivery by the Cell-Penetrating Peptide YTA2.* Bioconjugate Chem., 2007. **18**(1): p. 170-174.
70. Lewin, M., et al., *Tat peptide-derivatized magnetic nanoparticles allow in vivo tracking and recovery of progenitor cells.* Nat Biotechnol, 2000. **18**(4): p. 410-4.
71. Eguchi, A., et al., *Protein Transduction Domain of HIV-1 Tat Protein Promotes Efficient Delivery of DNA into Mammalian Cells.* J. Biol. Chem., 2001. **276**(28): p. 26204-26210.
72. Torchilin, V.P., et al., *TAT peptide on the surface of liposomes affords their efficient intracellular delivery even at low temperature and in the presence of metabolic inhibitors.* Proc Natl Acad Sci U S A, 2001. **98**(15): p. 8786-91.
73. Gupta, B., T.S. Levchenko, and V.P. Torchilin, *TAT peptide-modified liposomes provide enhanced gene delivery to intracranial human brain tumor xenografts in nude mice.* Oncol Res, 2007. **16**(8): p. 351-9.
74. Prochiantz, A., *Peptide nucleic acid smugglers.* Nat Biotechnol, 1998. **16**(9): p. 819-20.
75. Joliot, A. and A. Prochiantz, *Transduction peptides: from technology to physiology.* Nat Cell Biol, 2004. **6**(3): p. 189-96.
76. Vives, E., *Present and future of cell-penetrating peptide mediated delivery systems: "Is the Trojan horse too wild to go only to Troy?"* Journal of Controlled Release, 2005. **109**(1-3): p. 77-85.
77. Futaki, S., *Arginine-rich peptides: potential for intracellular delivery of macromolecules and the mystery of the translocation mechanisms.* Int J Pharm, 2002. **245**(1-2): p. 1-7.
78. Mitchell, D.J., et al., *Polyarginine enters cells more efficiently than other polycationic homopolymers.* J Pept Res, 2000. **56**(5): p. 318-25.
79. Drin, G., et al., *Physico-chemical requirements for cellular uptake of pAntp peptide. Role of lipid-binding affinity.* Eur J Biochem, 2001. **268**(5): p. 1304-14.
80. Derossi, D., et al., *Cell Internalization of the Third Helix of the Antennapedia Homeodomain Is Receptor-independent.* J. Biol. Chem., 1996. **271**(30): p. 18188-18193.
81. Wender, P.A., et al., *The design, synthesis, and evaluation of molecules that enable or enhance cellular uptake: Peptoid molecular transporters.* Proceedings of the National Academy of Sciences, 2000. **97**(24): p. 13003-13008.
82. Yang, Y., et al., *HIV-1 TAT-mediated protein transduction and subcellular localization using novel expression vectors.* FEBS Lett, 2002. **532**(1-2): p. 36-44.
83. Richard, J.P., et al., *Cell-penetrating Peptides. A reevaluation of the mechanism of cellular uptake.* J. Biol. Chem., 2003. **278**(1): p. 585-590.

84. Olsnes, S., O. Klingenberg, and A. Wiedlocha, *Transport of exogenous growth factors and cytokines to the cytosol and to the nucleus.* Physiol Rev, 2003. **83**(1): p. 163-82.
85. Drin, G., et al., *Studies on the Internalization Mechanism of Cationic Cell-penetrating Peptides.* J. Biol. Chem., 2003. **278**(33): p. 31192-31201.
86. Thoren, P.E.G., et al., *Uptake of analogs of penetratin, Tat(48-60) and oligoarginine in live cells.* Biochemical and Biophysical Research Communications, 2003. **307**(1): p. 100-107.
87. Letoha, T., et al., *Membrane translocation of penetratin and its derivatives in different cell lines.* J Mol Recognit, 2003. **16**(5): p. 272-9.
88. Nakase, I., et al., *Cellular uptake of arginine-rich peptides: roles for macropinocytosis and actin rearrangement.* Mol Ther, 2004. **10**(6): p. 1011-22.
89. Fotin-Mleczek, M., R. Fischer, and R. Brock, *Endocytosis and cationic cell-penetrating peptides--a merger of concepts and methods.* Curr Pharm Des, 2005. **11**(28): p. 3613-28.
90. Kaplan, I.M., J.S. Wadia, and S.F. Dowdy, *Cationic TAT peptide transduction domain enters cells by macropinocytosis.* J Control Release, 2005. **102**(1): p. 247-53.
91. Conner, S.D. and S.L. Schmid, *Regulated portals of entry into the cell.* Nature, 2003. **422**(6927): p. 37-44.
92. Mousavi, S.A., et al., *Clathrin-dependent endocytosis.* Biochem J, 2004. **377**(Pt 1): p. 1-16.
93. Anderson, R.G., *The caveolae membrane system.* Annu Rev Biochem, 1998. **67**: p. 199-225.
94. Rejman, J., et al., *Size-dependent internalization of particles via the pathways of clathrin- and caveolae-mediated endocytosis.* Biochem J, 2004. **377**(Pt 1): p. 159-69.
95. Nichols, B.J. and J. Lippincott-Schwartz, *Endocytosis without clathrin coats.* Trends Cell Biol, 2001. **11**(10): p. 406-12.
96. Wadia, J.S., R.V. Stan, and S.F. Dowdy, *Transducible TAT-HA fusogenic peptide enhances escape of TAT-fusion proteins after lipid raft macropinocytosis.* Nat Med, 2004. **10**(3): p. 310-5.
97. Christiaens, B., et al., *Membrane interaction and cellular internalization of penetratin peptides.* Eur J Biochem, 2004. **271**(6): p. 1187-97.
98. Richard, J.P., et al., *Cellular Uptake of Unconjugated TAT Peptide Involves Clathrin-dependent Endocytosis and Heparan Sulfate Receptors.* J. Biol. Chem., 2005. **280**(15): p. 15300-15306.
99. Potocky, T.B., A.K. Menon, and S.H. Gellman, *Cytoplasmic and Nuclear Delivery of a TAT-derived Peptide and a {beta}-Peptide after Endocytic Uptake into HeLa Cells.* J. Biol. Chem., 2003. **278**(50): p. 50188-50194.
100. Fischer, R., et al., *A Stepwise Dissection of the Intracellular Fate of Cationic Cell-penetrating Peptides.* J. Biol. Chem., 2004. **279**(13): p. 12625-12635.
101. Ziegler, A., et al., *The Cationic Cell-Penetrating Peptide CPP^{TAT} Derived from the HIV-1 Protein TAT Is Rapidly Transported into Living Fibroblasts: Optical, Biophysical, and Metabolic Evidence.* Biochemistry, 2005. **44**(1): p. 138-148.
102. Duchardt, F., et al., *A comprehensive model for the cellular uptake of cationic cell-penetrating peptides.* Traffic, 2007. **8**(7): p. 848-66.
103. Rothbard, J.B., et al., *Role of membrane potential and hydrogen bonding in the mechanism of translocation of guanidinium-rich peptides into cells.* J Am Chem Soc, 2004. **126**(31): p. 9506-7.
104. Rothbard, J.B., T.C. Jessop, and P.A. Wender, *Adaptive translocation: the role of hydrogen bonding and membrane potential in the uptake of guanidinium-rich transporters into cells.* Adv Drug Deliv Rev, 2005. **57**(4): p. 495-504.

105. Rusnati, M., et al., *Interaction of HIV-1 Tat protein with heparin - Role of the backbone structure, sulfation, and size.* Journal of Biological Chemistry, 1997. **272**(17): p. 11313-11320.
106. Hakansson, S., A. Jacobs, and M. Caffrey, *Heparin binding by the HIV-1 tat protein transduction domain.* Protein Science, 2001. **10**(10): p. 2138-2139.
107. Albini, A., et al., *HIV-tat protein is a heparin-binding angiogenic growth factor.* Oncogene, 1996. **12**(2): p. 289-97.
108. Mann, D.A. and A.D. Frankel, *Endocytosis and targeting of exogenous HIV-1 Tat protein.* Embo J, 1991. **10**(7): p. 1733-9.
109. Tyagi, M., et al., *Internalization of HIV-1 tat requires cell surface heparan sulfate proteoglycans.* J Biol Chem, 2001. **276**(5): p. 3254-61.
110. Console, S., et al., *Antennapedia and HIV Transactivator of Transcription (TAT) "Protein Transduction Domains" Promote Endocytosis of High Molecular Weight Cargo upon Binding to Cell Surface Glycosaminoglycans.* J. Biol. Chem., 2003. **278**(37): p. 35109-35114.
111. Nakase, I., et al., *Interaction of arginine-rich peptides with membrane-associated proteoglycans is crucial for induction of actin organization and macropinocytosis.* Biochemistry, 2007. **46**(2): p. 492-501.
112. Gerbal-Chaloin, S., et al., *First step of the cell-penetrating peptide mechanism involves Rac1 GTPase-dependent actin-network remodelling.* Biol Cell, 2007. **99**(4): p. 223-38.
113. Holinger, E.P., T. Chittenden, and R.J. Lutz, *Bak BH3 Peptides Antagonize Bcl-xL Function and Induce Apoptosis through Cytochrome c-independent Activation of Caspases.* J. Biol. Chem., 1999. **274**(19): p. 13298-13304.
114. Gallouzi, I.E. and J.A. Steitz, *Delineation of mRNA export pathways by the use of cell-permeable peptides.* Science, 2001. **294**(5548): p. 1895-901.
115. Stolzenberger, S., M. Haake, and A. Duschl, *Specific inhibition of interleukin-4-dependent Stat6 activation by an intracellularly delivered peptide.* Eur J Biochem, 2001. **268**(17): p. 4809-14.
116. Pouniotis, D.S., V. Apostolopoulos, and G.A. Pietersz, *Penetratin tandemly linked to a CTL peptide induces anti-tumour T-cell responses via a cross-presentation pathway.* Immunology, 2006. **117**(3): p. 329-39.
117. Apostolopoulos, V., et al., *Delivery of tumor associated antigens to antigen presenting cells using penetratin induces potent immune responses.* Vaccine, 2006. **24**(16): p. 3191-202.
118. Zaidi, N., et al., *A novel cell penetrating aspartic protease inhibitor blocks processing and presentation of tetanus toxoid more efficiently than pepstatin A.* Biochemical and Biophysical Research Communications, 2007. **364**(2): p. 243-249.
119. Tripathi, S., et al., *Anti HIV-1 virucidal activity of polyamide nucleic acid-membrane transducing peptide conjugates targeted to primer binding site of HIV-1 genome.* Virology, 2007. **363**(1): p. 91-103.
120. Rayne, F., et al., *The ability of chloroquine to prevent tat-induced cytokine secretion by monocytes is implicated in its in vivo anti-human immunodeficiency virus type 1 activity.* J Virol, 2004. **78**(21): p. 12054-7.
121. Caron, N.J., S.P. Quenneville, and J.P. Tremblay, *Endosome disruption enhances the functional nuclear delivery of Tat-fusion proteins.* Biochemical and Biophysical Research Communications, 2004. **319**(1): p. 12-20.
122. Michiue, H., et al., *The NH2 terminus of influenza virus hemagglutinin-2 subunit peptides enhances the antitumor potency of polyarginine-mediated p53 protein transduction.* J Biol Chem, 2005. **280**(9): p. 8285-9.

123. Snyder, E.L., et al., *Treatment of terminal peritoneal carcinomatosis by a transducible p53-activating peptide.* PLoS Biol, 2004. **2**(2): p. E36.
124. Mae, M. and U. Langel, *Cell-penetrating peptides as vectors for peptide, protein and oligonucleotide delivery.* Curr Opin Pharmacol, 2006. **6**(5): p. 509-14.
125. Gupta, B. and V.P. Torchilin, *Transactivating transcriptional activator-mediated drug delivery.* Expert Opin Drug Deliv, 2006. **3**(2): p. 177-90.
126. Pardridge, W.M., *Blood-brain barrier delivery of protein and non-viral gene therapeutics with molecular Trojan horses.* Journal of Controlled Release
Proceedings of the Thirteenth International Symposium on Recent Advances in Drug Delivery Systems, 2007. **122**(3): p. 345-348.
127. Wang, W. and W.S. El-Deiry, *Targeting p53 by PTD-mediated transduction.* Trends Biotechnol, 2004. **22**(9): p. 431-4.
128. Kim, C.H., et al., *Enhanced antitumour immunity by combined use of temozolomide and TAT-survivin pulsed dendritic cells in a murine glioma.* Immunology, 2007. **122**(4): p. 615-22.
129. Michiue, H., et al., *Ubiquitination-resistant p53 protein transduction therapy facilitates anti-cancer effect on the growth of human malignant glioma cells.* FEBS Lett, 2005. **579**(18): p. 3965-9.
130. Inagaki, K., et al., *Cardioprotection by epsilon-protein kinase C activation from ischemia: continuous delivery and antiarrhythmic effect of an epsilon-protein kinase C-activating peptide.* Circulation, 2005. **111**(1): p. 44-50.
131. Bright, R., G.K. Steinberg, and D. Mochly-Rosen, *DeltaPKC mediates microcerebrovascular dysfunction in acute ischemia and in chronic hypertensive stress in vivo.* Brain Res, 2007. **1144**: p. 146-55.
132. Choi, H.S., et al., *PEP-1-SOD fusion protein efficiently protects against paraquat-induced dopaminergic neuron damage in a Parkinson disease mouse model.* Free Radic Biol Med, 2006. **41**(7): p. 1058-68.
133. Choi, H.S., et al., *Transduced Tat-alpha-synuclein protects against oxidative stress in vitro and in vivo.* J Biochem Mol Biol, 2006. **39**(3): p. 253-62.
134. Kilic, E., U. Kilic, and D.M. Hermann, *TAT-GDNF in neurodegeneration and ischemic stroke.* CNS Drug Rev, 2005. **11**(4): p. 369-78.
135. Kilic, E., U. Kilic, and D.M. Hermann, *TAT fusion proteins against ischemic stroke: current status and future perspectives.* Front Biosci, 2006. **11**: p. 1716-21.
136. Bullok, K.E., et al., *Permeation peptide conjugates for in vivo molecular imaging applications.* Mol Imaging, 2006. **5**(1): p. 1-15.
137. Gump, J.M. and S.F. Dowdy, *TAT transduction: the molecular mechanism and therapeutic prospects.* Trends in Molecular Medicine, 2007. **13**(10): p. 443-448.
138. Meade, B.R. and S.F. Dowdy, *Exogenous siRNA delivery using peptide transduction domains/cell penetrating peptides.* Adv Drug Deliv Rev, 2007. **59**(2-3): p. 134-40.
139. Fan, Y.X., et al., *Ligand regulates epidermal growth factor receptor kinase specificity: activation increases preference for GAB1 and SHC versus autophosphorylation sites.* J Biol Chem, 2004. **279**(37): p. 38143-50.
140. Fan, Y.X., L. Wong, and G.R. Johnson, *EGFR kinase possesses a broad specificity for ErbB phosphorylation sites, and ligand increases catalytic-centre activity without affecting substrate binding affinity.* Biochem J, 2005. **392**(Pt 3): p. 417-23.
141. Hubbard, S.R. and W.T. Miller, *Receptor tyrosine kinases: mechanisms of activation and signaling.* Curr Opin Cell Biol, 2007. **19**(2): p. 117-23.
142. Blume-Jensen, P. and T. Hunter, *Oncogenic kinase signalling.* Nature, 2001. **411**(6835): p. 355-65.

143. Slamon, D.J., et al., *Human breast cancer: correlation of relapse and survival with amplification of the HER-2/neu oncogene.* Science, 1987. **235**(4785): p. 177-82.
144. Sawyers, C.L., *Chronic myeloid leukemia.* N Engl J Med, 1999. **340**(17): p. 1330-40.
145. Yarden, Y., *The EGFR family and its ligands in human cancer. signalling mechanisms and therapeutic opportunities.* Eur J Cancer, 2001. **37 Suppl 4**: p. S3-8.
146. Paez, J.G., et al., *EGFR mutations in lung cancer: correlation with clinical response to gefitinib therapy.* Science, 2004. **304**(5676): p. 1497-500.
147. Hynes, N.E. and H.A. Lane, *ERBB receptors and cancer: the complexity of targeted inhibitors.* Nat Rev Cancer, 2005. **5**(5): p. 341-54.
148. Wouters, F.S. and P.I. Bastiaens, *Fluorescence lifetime imaging of receptor tyrosine kinase activity in cells.* Curr Biol, 1999. **9**(19): p. 1127-30.
149. Verveer, P.J., et al., *Quantitative imaging of lateral ErbB1 receptor signal propagation in the plasma membrane.* Science, 2000. **290**(5496): p. 1567-70.
150. Ting, A.Y., et al., *Genetically encoded fluorescent reporters of protein tyrosine kinase activities in living cells.* Proc Natl Acad Sci U S A, 2001. **98**(26): p. 15003-8.
151. Reynolds, A.R., et al., *EGFR activation coupled to inhibition of tyrosine phosphatases causes lateral signal propagation.* Nat Cell Biol, 2003. **5**(5): p. 447-53.
152. Offterdinger, M., et al., *Imaging phosphorylation dynamics of the epidermal growth factor receptor.* J Biol Chem, 2004. **279**(35): p. 36972-81.
153. Yudushkin, I.A., et al., *Live-cell imaging of enzyme-substrate interaction reveals spatial regulation of PTP1B.* Science, 2007. **315**(5808): p. 115-9.
154. Mergler, M.a.D., J.P., *The BACHEM practice of SPPS*. 2000, BACHEM AG, Bubendorf, Switzerland.
155. Gius, D.R., et al., *Transduced p16INK4a peptides inhibit hypophosphorylation of the retinoblastoma protein and cell cycle progression prior to activation of Cdk2 complexes in late G1.* Cancer Res, 1999. **59**(11): p. 2577-80.
156. Okuyama, M., et al., *Small-molecule mimics of an alpha-helix for efficient transport of proteins into cells.* Nat Methods, 2007. **4**(2): p. 153-9.
157. Silhol, M., et al., *Different mechanisms for cellular internalization of the HIV-1 Tat-derived cell penetrating peptide and recombinant proteins fused to Tat.* Eur J Biochem, 2002. **269**(2): p. 494-501.
158. Yudushkin, I., *Imaging Enzyme Activity by Monitoring Dynamics of the Enzyme-Substrate Intermediate In Live Cells, PhD Thesis*. 2006, Heidelberg University. p. 108.
159. Maiolo, J.R., E.A. Ottinger, and M. Ferrer, *Specific Redistribution of Cell-Penetrating Peptides from Endosomes to the Cytoplasm and Nucleus upon Laser Illumination.* J. Am. Chem. Soc., 2004. **126**(47): p. 15376-15377.
160. Verveer, P.J., A. Squire, and P.I. Bastiaens, *Global analysis of fluorescence lifetime imaging microscopy data.* Biophys J, 2000. **78**(4): p. 2127-37.
161. Devonshire, A.L., *The properties of a carboxylesterase from the peach-potato aphid, Myzus persicae (Sulz.), and its role in conferring insecticide resistance.* Biochem J, 1977. **167**(3): p. 675-83.
162. Goeldner, M., Givens, R., ed. *Dynamic studies in Biology. Phototriggers, photoswitches and caged biomolecules*. 2005, Wiley-VCH: Weinheim (Germany). xxvii, 557.
163. Giordano, A., Zarbakhsh, S., Schultz, C., *Controlling protein function by caged compounds*, in *Chemical Biology - from small compounds to Systems Biology and drug design*, S.L. Schreiber, Kapoor, T.M., Wess, G., Editor. 2007, Wiley-VCH: Weinem (Germany). p. 1206.

164. Rothman, D.M., et al., *General method for the synthesis of caged phosphopeptides: tools for the exploration of signal transduction pathways.* Org Lett, 2002. **4**(17): p. 2865-8.
165. Fischer, R., et al., *A quantitative validation of fluorophore-labelled cell-permeable peptide conjugates: fluorophore and cargo dependence of import.* Biochim Biophys Acta, 2002. **1564**(2): p. 365-74.
166. Coder, D.M., *Assessment of Cell Viability*, in *Current Protocols In Cytometry*. 2001, John Wiley & sons, Inc.
167. Marshall, N.B., et al., *Arginine-rich cell-penetrating peptides facilitate delivery of antisense oligomers into murine leukocytes and alter pre-mRNA splicing.* Journal of Immunological Methods, 2007. **325**(1-2): p. 114-126.
168. Del Gaizo, V., J.A. MacKenzie, and R.M. Payne, *Targeting proteins to mitochondria using TAT.* Mol Genet Metab, 2003. **80**(1-2): p. 170-80.
169. Del Gaizo, V. and R.M. Payne, *A novel TAT-mitochondrial signal sequence fusion protein is processed, stays in mitochondria, and crosses the placenta.* Mol Ther, 2003. **7**(6): p. 720-30.
170. Ross, M.F. and M.P. Murphy, *Cell-penetrating peptides are excluded from the mitochondrial matrix.* Biochem Soc Trans, 2004. **32**(Pt 6): p. 1072-4.
171. Ross, M.F., et al., *Cell-penetrating peptides do not cross mitochondrial membranes even when conjugated to a lipophilic cation: evidence against direct passage through phospholipid bilayers.* Biochem J, 2004. **383**(Pt. 3): p. 457-68.
172. Galande, A.K., R. Weissleder, and C.H. Tung, *An effective method of on-resin disulfide bond formation in peptides.* J Comb Chem, 2005. **7**(2): p. 174-7.
173. Li, R., et al., *Targeting antiapoptotic Bcl-2 family members with cell-permeable BH3 peptides induces apoptosis signaling and death in head and neck squamous cell carcinoma cells.* Neoplasia, 2007. **9**(10): p. 801-11.